MODELING AND ANALYSIS OF REINFORCED GRANULAR LAYER OVERLAYING VERY SOFT SOIL

Dory Bitar

A Thesis

in

The Department

of

Building, Civil and Environmental Engineering

Presented in Partial Fulfillment of the Requirements
For the Degree of Doctor of Philosophy at
Concordia University
Montreal, Quebec, Canada

October 2007

Your file Votre référence
ISBN: 978-0-494-37742-0
Our file Notre référence
ISBN: 978-0-494-37742-0

ABSTRACT

MODELING AND ANALYSIS OF REINFORCED GRANULAR LAYER OVERLAYING VERY SOFT SOIL

Dory Bitar, Ph.D.
Concordia University, 2007

Many regions of lowlands contain areas of very soft soils where large settlements are observed. Placing a fill over these areas will lead to extensive differential settlements. For this reason, reclaiming such surfaces with the aid of reinforcements is very essential.

The proposed model is an elastic-plastic constitutive model derived from CANAsand model which uses a non-associated flow rule along with the concept of the state boundary surface possessing the critical and the compact state. The model is capable of simulating the surface profile of reinforced granular fill over very soft soil due to the immediate settlement. A primary ground deformation profile is evaluated prior to filling and is based on a parametric study involving variables such as the height and the spacing of the embankment fingers, the stiffness modulus of the reinforcement and the cohesion of the soft soil. The numerical results indicated that these parameters affect the performance of the system in many direct ways. The immediate and final settlement is based on the level the first deformation has attained and is estimated using a nonlinear and incremental stress-strain analysis. An integro-differential equation written in its finite difference form is developed to estimate the total displacement field of the system. The computer generated results showed that larger surface settlements were associated with high void ratios whereas smaller surface settlements were associated with low void ratios.

ACKNOWLEDGEMENTS

The author would like to express his sincere gratitude to Professor Hormoz B. Poorooshasb for his invaluable guidance, encouragement and continuous support throughout his Ph.D. studies at Concordia University. Without his valuable and critical research advice, this work could not have been accomplished.

The author would also like to express his sincere appreciation to Dr. Attila Zsaki for his infinite support and guidance throughout his studies. His help is gratefully acknowledged.

I would like to thank my parents for their endless patience, unconditional love and support, and understanding and without whom it could not have been possible to pursue graduate studies at Concordia University.

TABLE OF CONTENTS

	Page
LIST OF FIGURES	ix
LIST OF TABLES	xiii
Chapter	
1. INTRODUCTION	1
1.1 Introduction	1
1.2 Statement of the problem	2
1.3 Objective of the study	2
1.4 Structure of the thesis	4
2. LITERATURE REVIEW	6
2.1 Introduction	6
2.2 Review of reclamation techniques	7
2.2.1 The process and classification of deposition	7
2.2.2 Natural drying	10
2.2.3 Displacement and replacement	11
2.2.4 Removal and replacement	12
2.2.5 Near surface reinforcement or geosynthetic reinforcement	14

2.3 Geotextile description and properties 17

2.4 Unreinforced granular bed on soft soil 20

2.4.1 Bearing capacity of sand overlaying soft clay 21

2.4.2 Stress-strain behavior of soil and models 24

2.4.3 Foundation response 26

2.5 Reinforced granular bed on soft soil 30

2.5.1 Review of various analytical methods 31

2.5.2 Review of numerical methods 37

2.5.3 Laboratory and field testing results 38

2.5.4 Modeling of reinforced Foundation beds 41

3. MODELING THE NON-LINEAR BEHAVIOUR OF COHESIONLESS GRANULAR MEDIA 45

3.1 Introduction 45

3.2 Background on important concepts and laws 51

3.2.1 The concept of critical void ratio 51

3.2.2 The concept of critical state line 55

3.2.3 Steady state of deformation 58

3.2.4 Similarity laws 62

3.3 The CANAsand constitutive model 64

3.3.1 General features 64

3.3.2 Critical state surface 66

3.3.3 Compact state surface 67

3.3.4 The state boundary surface 69

3.4 Modeling the elastic-plastic response of soil 74

3.4.1 Stress-strain response of granular soil 74

3.4.2 Constitutive formulation of sand 79

4. MODELING OF THE REINFORCED EARTH PROBLEM OVERLAYING VERY SOFT SOIL 88

4.1 Introduction 88

4.2 The construction process of reinforcing a soft soil 88

4.3 Modeling of the reinforced earth problem 90

4.4 Results and discussion 101

4.5 Conclusion 106

5. NONLINEAR ANALYSIS OF THE REINFORCED GRANULAR LAYER 108

5.1 Introduction 108

5.2 Formulation of the constitutive equations 109

5.3 The integro-differential (ID) technique 118

5.4 Mathematical formulation of the problem 119

5.5 The numerical scheme 122

5.6 Stress loading the reinforcement 127

5.7 Characteristics of elastic-plastic response 129

5.8 Results and discussion 134

5.8.1 Results and discussion of the finite element model 143

5.9 Final Remarks 151

6. CONCLUSION 154

6.1 Concluding remarks 154

6.2 Recommendations for further research 157

LIST OF REFERENCES 158

LIST OF FIGURES

	Page
Figure 2.1 Surface piercing island and caisson retained island	8
Figure 2.2 Typical artificial island structure	8
Figure 2.3 Classification of hydraulic deposition	9
Figure 2.4 Phreatic surfaces	10
Figure 2.5 Sun drying effect	11
Figure 2.6 Forced displacement method	12
Figure 2.7 Removal and replacement method	13
Figure 2.8 Multiple geosynthetic reinforcement for reclaiming lagoons	15
Figure 2.9 Floating mat method	15
Figure 2.10 Geosynthetic with Cakar Ayam system	16
Figure 2.11 Sand replacement with geonet	17
Figure 2.12 Load spread through sand overlaying clay	21
Figure 2.13 Failure of soil below footing on dense sand above soft clay	22
Figure 2.14 Coefficient of punching shearing resistance	23
Figure 2.15 Models: Winkler, Filonenko-Borodich, Vlasov, and Kerr	27
Figure 2.16 Kerr model	29
Figure 2.17 Loading characteristics of piles strain controlled inclusion	32
Figure 2.18 Internal strain field	33
Figure 2.19 Zero extension lines characteristics	34

Figure 2.20 Pattern of reinforcement beneath footing 34

Figure 2.21 Stress condition in the reinforced region 36

Figure 3.1 Drucker-Prager yield surface 48

Figure 3.2 Bounding surface and yield surface 50

Figure 3.3 Casagrande C.V.R Line for Sacramento River Sand 53

Figure 3.4 The state space 55

Figure 3.5 The critical state line 56

Figure 3.6 Projection of the critical state line 56

Figure 3.7 Influence of density on undrained 57

Figure 3.8 Influence of initial confining pressure 58

Figure 3.9 Undrained stress-strain curves and stress 59

Figure 3.10 Critical and compact states for gravel 67

Figure 3.11 The compact void ratio line 68

Figure 3.12 A possible stress path 69

Figure 3.13 A state path in (τ, σ', e) space 70

Figure 3.14 State path followed and the state boundary surface 70

Figure 3.15 Critical, compact and state boundary surface 71

Figure 3.16 Shear stress at the state boundary surface 72

Figure 3.17 Schematic shear behaviour of sand 75

Figure 3.18 a) Volumetric behaviour, b) Change in volume in (e, ε) space 76

Figure 3.19 Angle of interlocking, δ 77

Figure 3.20 Angle of friction, ϕ 78

Figure 3.21 Stress-strain relationship 79

Figure 3.22 Plastic strain rate 81

Figure 3.23 Curves of constant φ 82

Figure 3.24 Yield loci, plastic potentials and plastic strain vectors 86

Figure 4.1 Sequence of reclamation using geosynthetic reinforcement 89

Figure 4.2 Sketch of a) Real model b) Idealized model 90

Figure 4.3 Forces acting on the system 91

Figure 4.4 Symmetric components of the system 92

Figure 4.5 Free body diagram of the reinforcement 93

Figure 4.6 The loading of pressure p 94

Figure 4.7 a) Characteristics of the stress field, b) Velocity field 95

Figure 4.8 Zone I 96

Figure 4.9 Zone III 97

Figure 4.10 Radial fan zone: Zone II 98

Figure 4.11 Settlement profile 101

Figure 4.12 Settlement profile for a 10 meter spacing 102

Figure 4.13 Settlement profile for a stiffness modulus of 4000 kN/m 103

Figure 4.14 Settlement profile for an 8 meter spacing 104

Figure 4.15 Settlement profile for a 12 meter spacing 104

Figure 4.16 Settlement profile for a height of 4 meters and loading of 80 kN/m^2 105

Figure 5.1 System under study and the coordinates system used in the analysis 111

Figure 5.2 Stress invariants used in the present study 113

Figure 5.3 Stress components on an element within the reinforced granular layer 119

Figure 5.4 Network used in this study 123

Figure 5.5 Loading of the geotextile reinforcement 127

Figure 5.6 Profile before the immediate settlement 135

Figure 5.7 The superposition of settlements 136

Figure 5.8 Settlement of a very dense fill 137

Figure 5.9 Settlement of a dense to medium fill 138

Figure 5.10 Settlement of a medium to loose fill 139

Figure 5.11 Settlement of a loose to very loose fill 140

Figure 5.12 Settlement of a very loose fill 140

Figure 5.13 Settlement vs. depth (e = 0.5 – 0.9) 142

Figure 5.14 FEM model 145

Figure 5.15 Settlement of a very dense fill 146

Figure 5.16 Settlement of a dense to medium fill 147

Figure 5.17 Settlement of a medium to loose fill 148

Figure 5.18 Settlement of a loose to very loose fill 149

Figure 5.19 Settlement of a very loose fill 150

Figure 5.20 FEM model with a refined mesh 150

LIST OF TABLES

	Page
Table 2.1 Classification of soft ground	10
Table 2.2 Conventional products used for reinforcing soil	18
Table 5.1 Settlement with respect to depth	141
Table 5.2 Results of refined mesh	151

1. INTRODUCTION

1.1 INTRODUCTION

Lowlands are defined as the areas wherein the resident populations are dealing with problems and disasters caused by the changes and fluctuations of water levels of sea, rivers and lakes. Many of the problems of lowlands are accentuated by the presence of soft ground underneath. A significant percentage of the world population either resides in or have activities, (agricultural, industrial, commercial or recreational) connected with these lowlands. In view of the relative sea level rise due to global warming, subsidence due to groundwater withdrawal, risks, dangers and the problems with lowland areas would be of increasing importance in the near future. There is an urgent need to bring together engineers, scientists, planners, and administrators into an organization to focus attention and to evolve solutions to the problems of lowlands.

The formed deposits on the surface in many lowlands areas are diverse. Vast regions of moderately capable ground may surround areas containing very soft soil and the material is much more compressible in comparison with its surroundings. If a fill is to be placed over such regions then large differential settlements are likely to occur on the surface of the fill duè to its self-weight. Hence, ground improvement techniques are required to ameliorate the performance of the ground. The use of reinforcements is effective along with the compaction of the granular fill in reducing the settlement of the fill layer. A reinforced granular layer over a very soft soil will improve the settlement profile of the fill and provide a competent surface for construction.

1.2 STATEMENT OF THE PROBLEM

The modeling and analysis of the reinforced granular layer over soft soil will provide a reasonable and analytical model to evaluate the settlement profile of such systems due to the immediate settlement. Constitutive and governing equations developed in this study will be able to present a practical model of the soil behavior by using an incremental elastic-plastic model. The developed model will be able to estimate different surface profile due to the immediate settlement of the fill. It is a simple model to use in comparison with other numerical models. CANAsand model which uses a non-associated flow rule and its developed equations is used to represent the stress-strain behavior of the soil. The performance of the system will depend on several parameters which play an important role such as the unit weight of the fill and the embankment fingers, the cohesion of the soft soil, the stiffness modulus of the reinforcement, the height of and the distance between the embankment fingers and the depth of the reinforced fill. Moreover, the model will be capable of predicting the settlement profile at different void ratios of the granular fill ranging from very dense to very loose fill.

1.3 OBJECTIVE OF THE STUDY

The objective of the present study is to investigate the surface profile of a reinforced granular layer overlaying very soft soil due to the immediate settlement. To study the above mentioned problem in a qualitative way, it is necessary:

- To evaluate a primary settlement profile of the system consisting of the reinforcement, the embankment fingers and the very soft soil prior to the spreading of the granular fill between the embankment fingers.

- To describe the non-linear behavior of the fill and the stress and strain relationship. Constitutive equations are derived from CANAsand model using the critical state, the compact state concept and the state boundary surface.

- To develop an elastic-plastic constitutive model to analyze the behavior of the reinforced granular layer and to describe a mathematical formulation to estimate the total displacement field of the system.

- To establish an efficient computational method capable of simulating the settlement profile of the system after the dispersal of the granular layer by incorporating the elastic-plastic model with the aid of the integro-differential equation referred to as the ID technique. The immediate settlement of the system is determined by superposition of the bulge due to the loading of the embankment fingers and the settlement due to the self-weight of the fill.

In order to obtain satisfactory results, the above described points need to be targeted concurrently. Taking into consideration the constraints and the complexities of the experimental assessment of the size of the stress-strain in a sample, the present study

focuses on information acquired from theoretical analysis and numerical trials to have a creditable idea of the developed model.

1.4 STRUCTURE OF THE THESIS

The material covered in this current research is divided into six chapters. Following the first chapter which explains the objective of the study, reviews of some previous works which have been achieved in this domain are presented in Chapter two.

Chapter three starts with a brief historical outline on the theory of plasticity and after that a background on important concepts and laws useful for this research. CANAsand model is presented and described along with the critical state, the compact state and the state boundary surface. The stress-strain relationship for the non-linear soil behavior along with the elastic and plastic components of strain is illustrated.

Chapter four focuses on estimating a primary settlement profile for the system under study. A description of the reclamation technique used for reinforcing a granular layer over soft soil is presented, followed by modeling and analyzing the system prior to the filling and the effect of the involved parameters is analyzed. Finally, results and some discussions are highlighted.

The formulation of the constitutive equations is presented in Chapter five. Constitutive equations are derived for the analysis and modeling of the elastic-plastic

behavior of the granular layer. The integro-differential technique with the mathematical formulation of the problem is discussed. It is followed by the numerical scheme employed to cover the solution region and the finite difference method used to solve the governing equation. The results of the numerical evaluations incorporating a range of void ratios of the fill layer are compared and discussed.

Finally, the main conclusions drawn from the present study are highlighted in Chapter 6 with the recommendations for future research in this field.

2. LITERATURE REVIEW

2.1 INTRODUCTION

One of the greatest challenges in the development of lowlands is the reclamation of ground consisting of very soft soils and affected by fluctuating water levels. In order to use these lands as construction facilities, they have to be reclaimed from the existing ground level to make it safe from inundation. If the subgrade is very soft, large settlements will occur and hence ground improvement techniques are required to ameliorate the performance of the ground against applied loads. One of the reclamation techniques is to spread a compacted granular bed over the soft subgrade soil. It reduces the surface settlements by spreading the applied loads through a wider area. With the advent of geosynthetics, the settlements can be reduced by placing a geosynthetic at the base or within the granular bed in one or more layers. This improvement increases the bearing capacity from the reinforcement action of the geosynthetic layer in the granular bed.

The reinforced earth concept was developed by Vidal (1966). Since then large number of attempts have been made to understand the behavior of the reinforcing element as well as the reinforced earth structures. Research in this area has been progressing a lot over the last few years especially in studying the mechanisms of reinforced soil. In addition to that, several model tests using various forms of reinforcing elements such as strips, bars, sheets, grids and nets have been conducted to obtain an approach into the reinforcing mechanisms of these materials. Finite element analysis has

helped in measuring the increase of the bearing capacity of reinforced foundation beds. Few models based on elastic theories and mechanical models are also available for representing the behavior of footings resting on unreinforced and on reinforced granular beds.

2.2 REVIEW OF RECLAMATION TECHNIQUES

This section reviews the process of deposition and the various methods of reclamation of soft deposits that are in vogue such as natural drying, displacement and replacement, removal and replacement and near surface reinforcement.

2.2.1 The Process and Classification of Deposition

Reclaimed ground consists of very soft soils with their water contents either close to or often somewhat higher than the liquid limit values. One of the earliest examples reported by Feld (1971) has been the work of Spezia Harbor, in Italy, by the Italian engineer Berberis. The soil at the site consisted of 32 m of very soft fluid mud. The site was dredged to a depth of 14.3 m below sea level and filled up with sand to a level of + 4.5 m for a dry dock. The settlement at the bottom of the sand layer was 0.9 m during 1912 to 1915 and 0.3 m from 1916 to 1927 and no intrusion of the mud into the sand blanket was observed over twenty years.

Artificial islands are a form of reclamation. The initial artificial islands were built with side slope of 10:1 to 15:1 for water depth less than 20 m. Subsequently, modern

form of island construction or reclamation with caisson rings had become very popular. Figure 2.1 shows two typical examples of a surface piercing island and a caisson retained island. Figure 2.2 shows the process of construction of a typical artificial island structure.

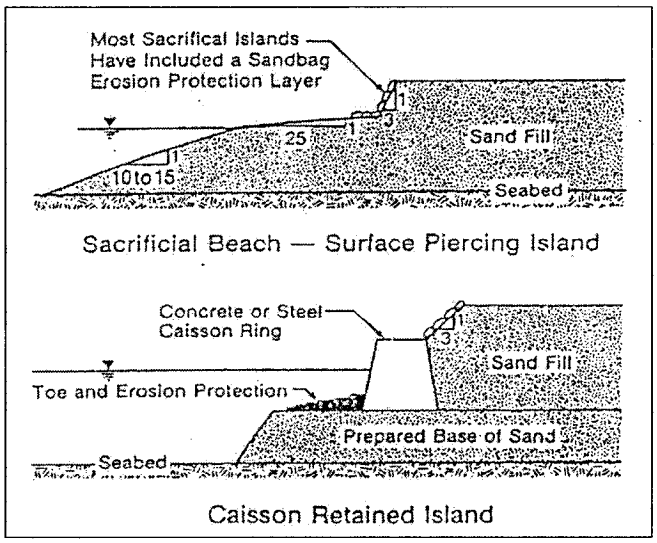

Figure 2.1 Surface piercing island and caisson retained wall (Mitchell (1988))

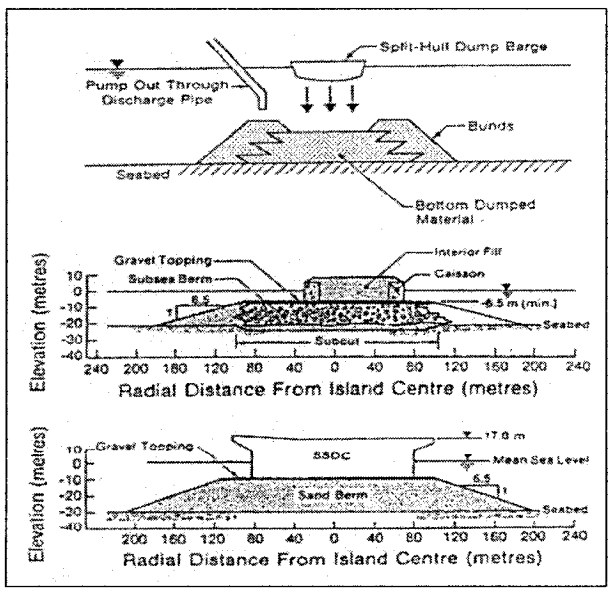

Figure 2.2 A typical artificial island structure (Mitchell (1988))

For the development of lowlands, one is normally concerned with sub-aqueous deposition either in the form of beach or non-beach deposition. The behavior of the ground is very much influenced by the process of deposition of the materials. Morgenstern and Kupper (1988) presented a report on hydraulic fills. The process of deposition has been classified according to the diagram shown in Figure 2.3.

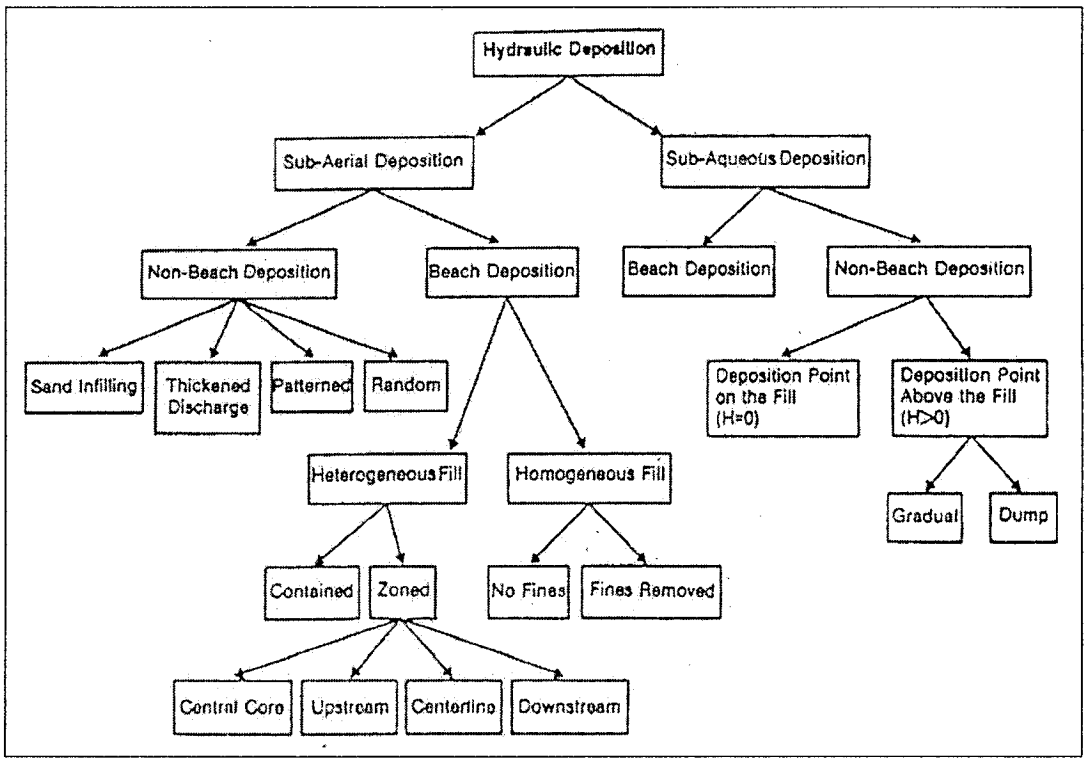

Figure 2.3 Classification of hydraulic deposition (Morgenstern and Kupper (1988))

The deposits that are often reclaimed are very young sediments that always require some engineering modification before the site can be developed for any use. They consist of either cohesionless fills of low relative density, low strength and high liquefaction potential or fine grained soils of high water content, high compressibility and low strength. The soil consisting of soft ground material may be classified as in Table 2.1.

Type of Borrow Material	Characteristics of Soft Ground
Clean sand (< 15% finer than No.200 sieve)	Uniform soil of low to medium density
Silty or clayey sand	Heterogeneous soil of large void ratio
Stiff cohesive soil	Clay balls with sand and clay matrix
Soft cohesive soil	Soft normally or under-consolidated clay

Table 2.1 Classification of soft ground (Whitman (1971))

2.2.2 Natural Drying

In many parts of the world, evaporation from the surface either seasonally or throughout the year, due to favorable climatic conditions, can be expected to dry out hydraulically deposited fine-grained material, either during placement or after complete deposition. With the drying process, the phreatic surface propagates downwards and continually falls down as shown in Figure 2.4.

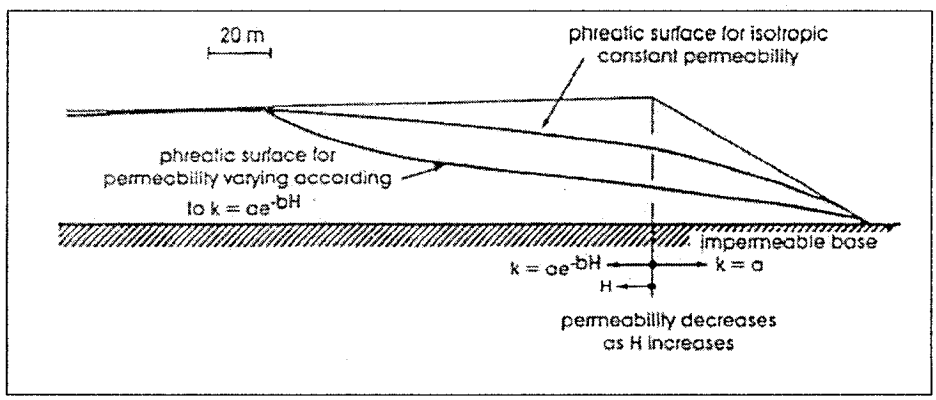

Figure 2.4 Phreatic surfaces (Blight (1988))

The increase in effective stress due to desiccation causes a reduction in the void ratio and could generate pseudo-preconsolidation effect (Blight (1988)). Figure 2.5 depicts the effect of desiccation on gold slimes fill. This method is very economical but requires considerable amount of time.

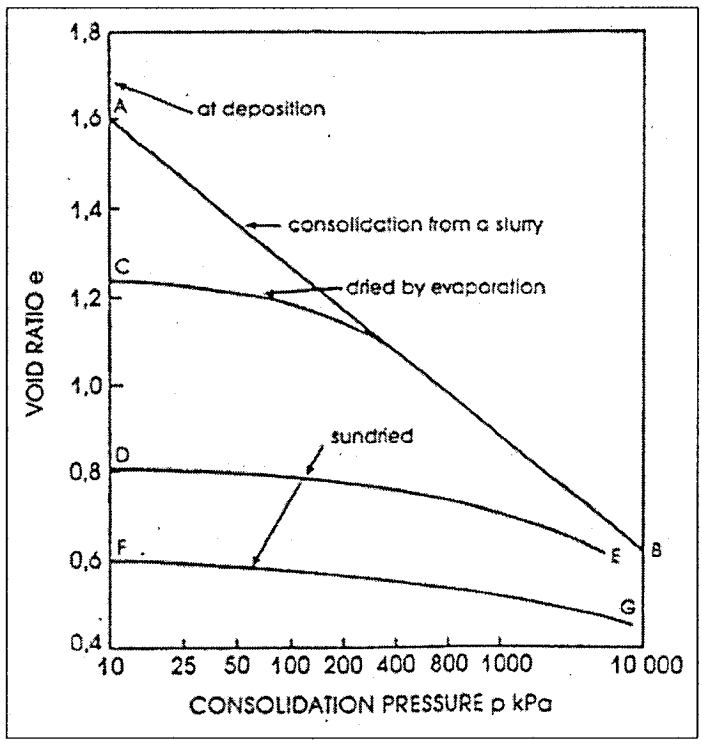

Figure 2.5 Sun drying effect (Blight (1988))

2.2.3 Displacement and Replacement

The soft soil is displaced and replaced by gradual dumping of a good quality of granular fill and the weight of the granular fill squeezes the soft soil out. The reclaimed ground gets stabilizes when the surrounding soft deposits resists the load from the fill. This method is commonly used for the construction of dykes for the development of

polders in Japan and breakwaters into the sea in most Asian countries. However, the disadvantage in the displacement technique is that it requires a huge amount of granular material. Figure 2.6 illustrates an example of the displacement method proposed by Azaraih et al. (1999).

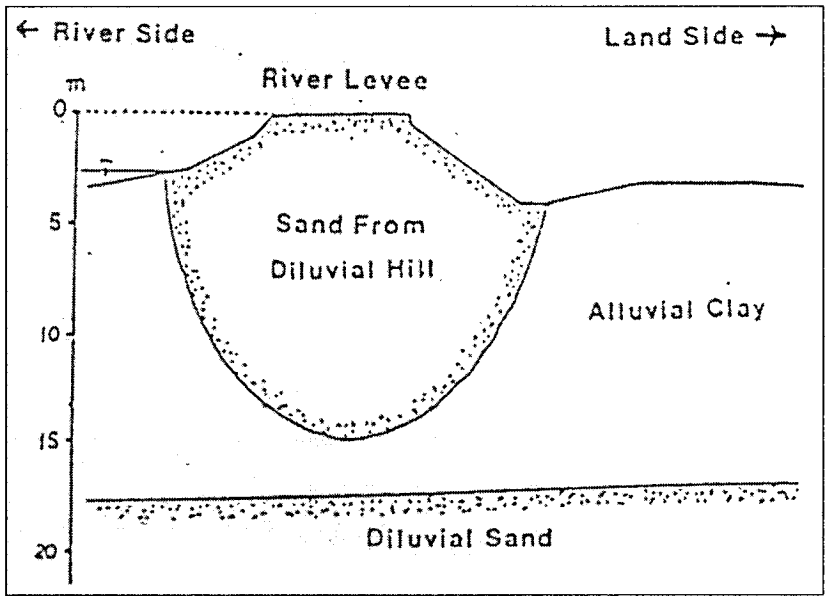

Figure 2.6 Forced displacement method (Azaraih et al. (1999))

2.2.4 Removal and Replacement

The replacement of original soil is extensively practiced all over the world before the advent of modern geotechnical practices. This technique has been used for the construction of embankments and sea revetments. The soft soil is excavated first and replaced by sands or sandy clay fills. Complete or partial replacement is achieved depending on the depth of the soft layer. Reclamation by the removal and replacement

method is depicted in Figure 2.7 where the sea bottom was excavated first with aid of dredger cutter.

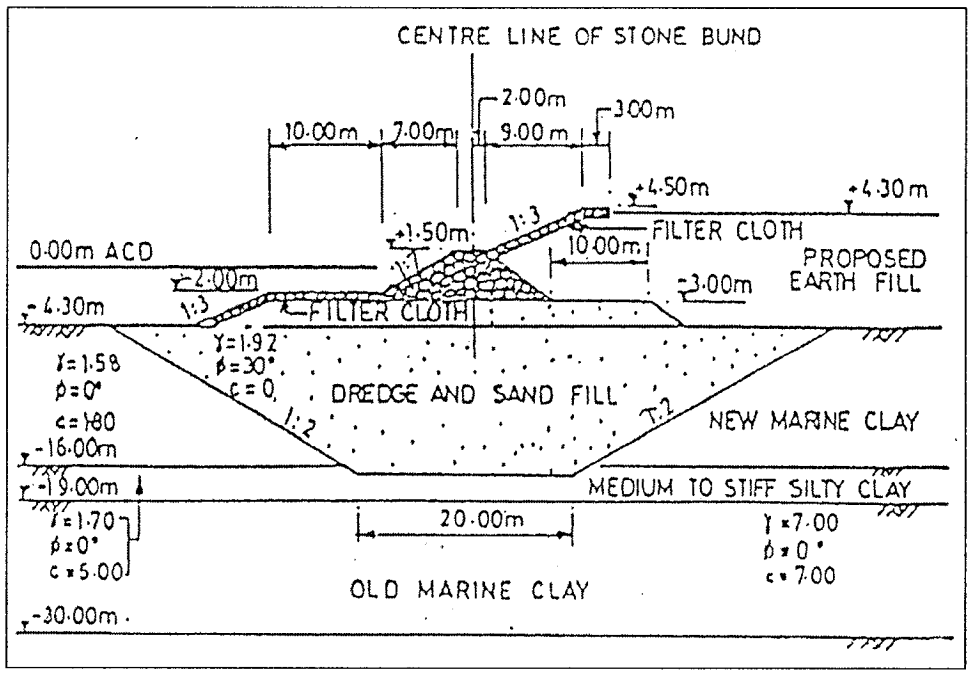

Figure 2.7 Removal and replacement method (Lee et al. (1999))

Transport and deposition of granular material were excavated either from adjacent sea bottom or land to build the underwater embankment. Quarry stones are dumped on each side of the embankment as counter weights. The loose pockets can be compacted either during or after replacement. However, the embankment could suffer large settlements due to long term consolidation of the underlying soft soils and even due to its self weight. The weakest zone extends usually from the sea or water level to few meters below. The limitations of this method are the variations in grain size, the placement unit weight and the ways of placement (Lee et al. (1999)).

Earthquakes could cause large settlements unless the reclaimed ground is improved or treated properly by one of the dynamic densification methods (Van Impe and Madhav (1995)). Mitchell (1988) presented a summary of various methods available for improvement of hydraulic fills. Improvement during placement is believed to be favorable to post reclamation. However, deep mixing methods necessitate the use of specialized construction equipments.

2.2.5 Near Surface Reinforcement or Geosynthetic Reinforcement

Near surface reinforcement with geosynthetics are by far the simplest, quickest and the most preferred method of reclaimed soft ground. One of these methods was proposed by Miki (1985) which is to enclose cement treated coal ash piles in geosynthetic stockings on which a granular bed was laid over for the construction of embankments over soft soils. Watari et al. (1986) and Broms and Shirlaw (1987) reported an earliest application of this method for reclaiming mining waste lagoons.

Martin et al. (1988) proposed using geotextile reinforced mat over soft soil dredging for assembly of offshore drilling rigs which is shown in Figure 2.8. The reinforced granular mat consists of multiple layers of reinforcement and high strength geosynthetic which act as separator and reinforcement.

Lawson (1999) described the sequence of reclamation with geosynthetic reinforcement. The construction procedure starts with laying a geosynthetic layer over the very soft soil and then with the use of soil berms, the edges of the geosynthetic are anchored. The construction of embankments fingers is then followed to stress the

reinforcement and finally the procedure ends with filling and spreading the fill in between the embankment fingers.

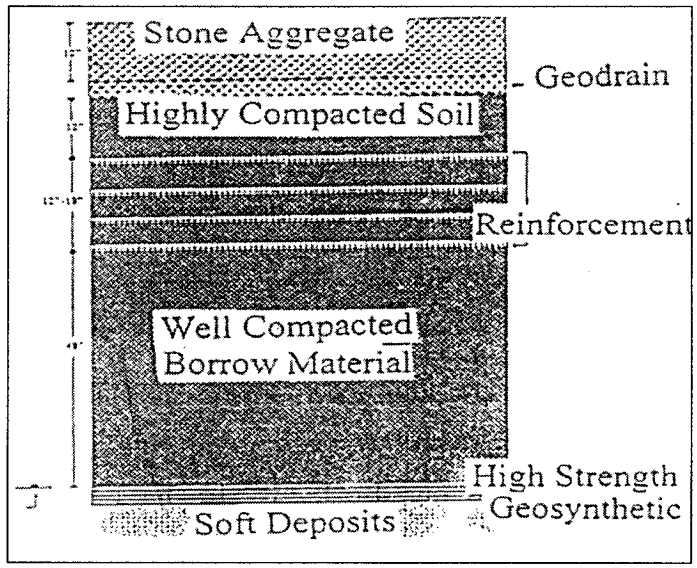

Figure 2.8 Multiple geosynthetic reinforcement for reclaiming lagoons (Martin et al. (1988))

The floating mat method by Yonezu et al. (1993) has also been used to construct a layer of sand on extremely soft soil. The ground had cone bearing values increasing from zero at the surface at a rate of 10*z kPa and a tensile strength of 5 kPa for the net. The floating mat method is described in Figure 2.9.

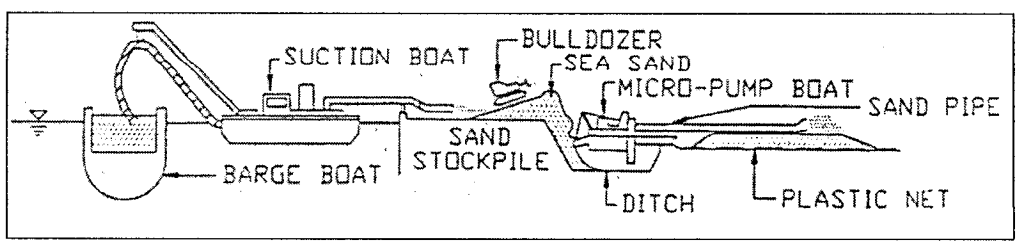

Figure 2.9 Floating mat method (Yonezu et al. (1993))

The application of geosynthetic reinforced granular mat has also been useful for the construction over waste and sludge ponds. The reinforced granular fill provides not only a strong platform but also a resistance to the large installation stresses. The geotextile reinforced sand mat along with 'Cakar Ayam System' has been used for the construction of a twenty kilometer highway embankment across a swampland in research conducted by Risseeuw and Voskamp (1993b). The geosynthetic reinforcement with 'Cakar Ayam System' is highlighted in Figure 2.10.

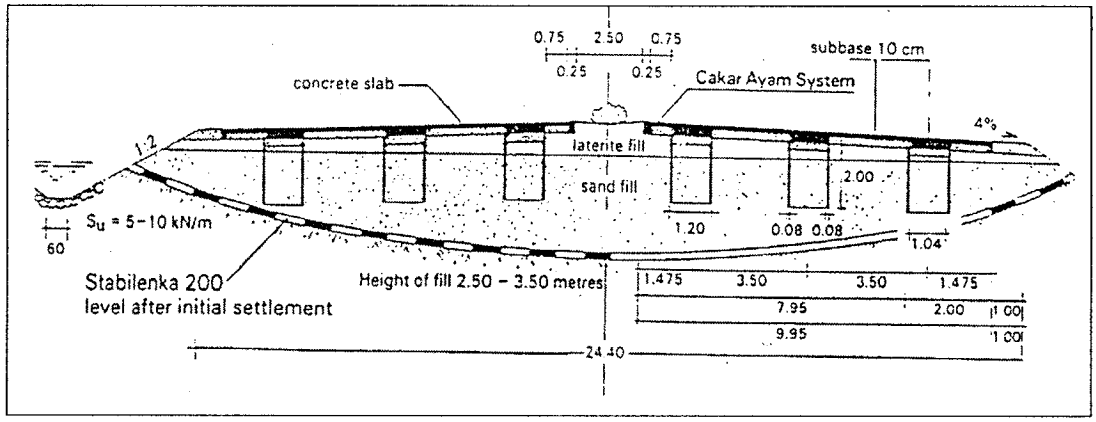

Figure 2.10 Geosynthetic with Cakar ayam system (Risseeuw and Voskamp (1993b))

Other reinforcement techniques such as extra light fill consisting of polystyrene blocks, of unit weight of the order of 20 kg/m^3, are in use in the Scandinavian countries and Japan. It is one of the quickest methods of construction but is relatively expensive. Lawson (1999) presented an excellent summary on different earth reinforcement techniques including reclamation of very soft soil.

Imanishi et al. (1998) described the method of reclaiming soft marine clay with geonet and sand replacement in Figure 2.11. The use of geonet reduces the amount of sand fill required and prevents its lateral spread.

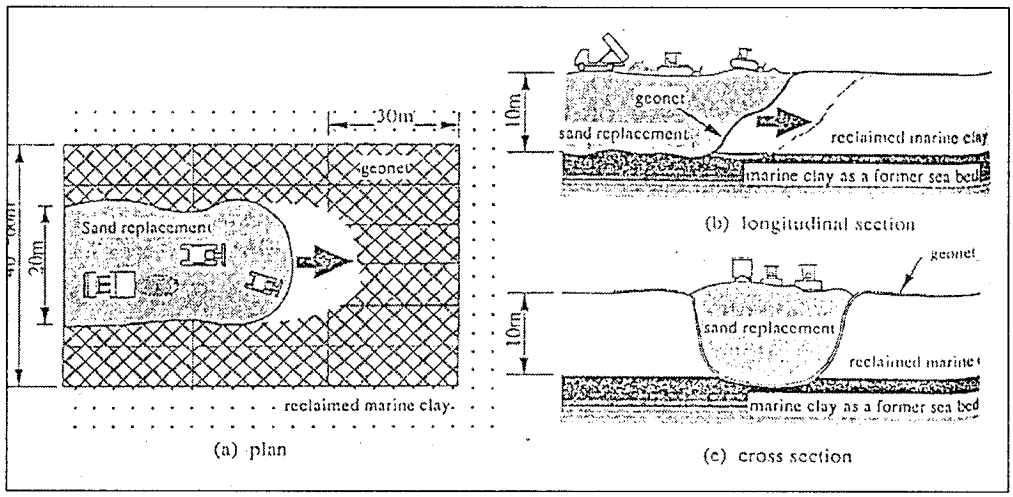

Figure 2.11 Sand replacement with geonet (Imanishi et al. (1998))

2.3 GEOTEXTILE DESCRIPTION AND PROPERTIES

Geotextiles are permeable, synthetic fiber fabrics used in the construction of civil engineering projects. There are many other names for geotextiles, some of these are: engineering fabrics, geofabrics, plastic filter clothe, filter fabric and synthetic fabric. The international term for these materials is geotextiles, which comes from the Latin "geo", meaning soil, and "textilis", meaning woven fabric. Geotextiles are manufactured from various synthetic materials. The most popular of these are polyethylene, polyester and nylon. Table 2.2 shows the conventional products used to reinforce soil along with the details of the rolling width, mesh width, and maximum strength mobilized due to axial

tensile strain in the machine denoted by MD and the cross section denoted by XD. The numbers of geosynthetics are also shown with the type and manufacturing process. These are biaxial products that are able to resist approximately the same force in both directions.

No.	Type of geosynthetic	Width (m)	Grid (mm)	Maximum tensile strength (kN/m)	
				MD	XD
02	PP slit tape woven	5.15	-	65	65
27	Biaxial extruded PP grid in 5 layers	4.50	60 x 60	55	35
28	PVC-coated knitted PET grid	5.10	20 x 20	55	55
32	PET flat rib grid	4.75	32 x 32	30	30
40	PP nonwoven (separation)	5.00	-	10	10
41	PP nonwoven (reinforcement)	5.00	-	20	20
42	PVC-coated knitted PVA grid	5.20	40 x 40	40	40
44	PET yarn reinforced PP nonwoven	5.20	8.5 x 8.5	50	50
45	PP slit tape woven	5.15	-	30	30
46	Biaxial extruded PP grid	3.80	65 x 65	30	30

Table 2.2 Conventional products used for reinforcing soil (Hufenus et al. 2006)

There are other types which are included under the term geosynthetic such as geogrids, geonets, geomembranes and geosynthetic clay liners (Koerner (1994)). Geogrids are made on weaving machinery and they function as reinforcement materials. Geonets are formed by a continuous extrusion of parallel sets of polymeric ribs at acute angles to one another. The primary function of geonets is drainage. Geomembranes are impervious thin sheets of rubber or plastic material used primarily as liquid or vapor barrier. Geosynthetic clay liners are rolls of factory fabricated thin layers made of bentonite clay and placed between two geotextiles or bonded to a geomembrane. They are used as hydraulic barriers or as secondary liners.

According to Koerner and Welch (1980), geotextiles fall into three broad categories based on the method of manufacture: nonwoven, woven and composite. Nonwoven geotextiles include spun-bonded and needle-punched. Spun-bonded geotextiles are constructed by randomly extruding a continuous filament over a belt and then bonding it by heat or resin. With needle-punched process, the fibers are mechanically entangled by punching needles through the geotextile. Woven geotextiles are generally constructed of monofilament, multifilament or slit film strands crossing each other at right angles. Because of the strength of the filaments used in the manufacturing process, woven geotextiles are generally stronger than nonwoven of the same weight. Very strong geotextiles are manufactured with steel strands woven into the synthetic filaments. Composite geotextiles are constructed of woven and nonwoven geotextiles sewn together.

The following is a general description of the physical properties of geotextiles shown in manufacturers' literature and used for construction project specifications. The Grab tensile strength is the strength of the geotextile of a specific width (usually 4 inches) gripped in one inch jaws. The elongation at failure is the percentage increase in length at failure expressed as the ratio of the length at failure to original length. The Mullen burst strength is carried out by an inflated rubber membrane where it is used to distort the geotextile out of its plane until it bursts. The permeability test is an adaptation of the normal soil permeability test. It measures the rate of diffusion of water under pressure through the geotextile. Since geotextiles are relatively thin a better measure of this ability is the water flow rate. The water flow rate is the volume of water that will pass through the geotextile at a given head for a given period of time. The equivalent opening size is

the size of the openings in a geotextile expressed as an equivalent U.S Standard Sieve No. The trapezoidal tear strength is the force required to continue a tear in the geotextile. The puncture strength is defined as the resistance to penetration by a blunt object. The ultraviolet stability is the ability of a geotextile to resist degradation due to exposure to ultraviolet light. The thermal shrinkage is the amount of shrinkage of a geotextile at a specified temperature expressed as a percentage of the original length.

Most of these tests for these properties were developed for the textile industry and were not meant to measure properties for engineering applications. They represent a marriage between the textile industry and civil engineering. For a complete description of all physical properties, laboratory tests, and their significance one can refer to the list of the references by Bell and Hicks (1980).

2.4 UNREINFORCED GRANULAR BED ON SOFT SOIL

In practice, the bearing capacity of foundations on soft clay can be improved by placing a layer of compacted sand or gravel. The lack of design information concerning the bearing capacity of non-homogeneous soil profiles is due primarily to the difficulty of obtaining exact solutions. In recent years, approximate solutions have been presented for a number of encountered non-homogeneous soil profiles in attempt to provide acceptable design data. A two parametric Pasternak subgrade model, in which the granular fill is represented by a shear layer and the soft soil by Winkler springs, has been found physically feasible and mathematically simple in representing a two layer soil.

2.4.1 Bearing Capacity of Sand Overlaying Soft Clay

Terzaghi and Peck (1948) were the first to calculate the bearing capacity of a strong layer over a weak soil by assuming that the upper layer spreads the footing load onto a larger area of the lower soil, therefore reducing its intensity as shown in Figure 2.12.

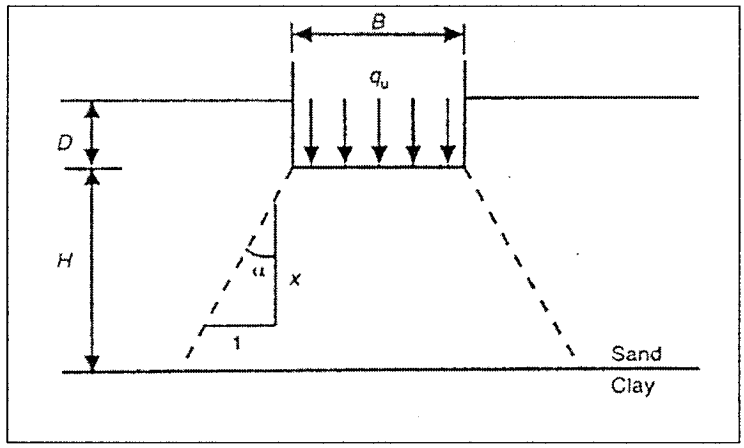

Figure 2.12 Load spread through sand overlaying clay (Terzaghi and Peck (1948))

It has been assumed that the load spreads through an angle corresponding to two vertical units to one horizontal unit of distance (a load spreading angle α where tan α = 0.5). The bearing capacity, q_u, of a surface footing is therefore given by the expression:

$$q_u = q_c \{1+2(H/B) \tan \alpha\} \leq q_s \quad (2.1)$$

where q_c and q_s are the bearing capacity of clay and sand respectively. H is the thickness of sand layer below the footing and B is the width of the footing.

Meyerhof (1974) presented a semi-empirical method with punching mode of failure to estimate the bearing capacity of a footing on or within sand layer overlaying

clay. The results were compared with those from model tests on circular and strip footings and some field observations were made for two cases of a dense layer on a soft deposit and of a loose stratum on firm bed.

Meyerhof and Adams (1968) developed an approximate theory for the bearing capacity of a footing punching through a thin sand layer into a thick clay bed by assuming that the ultimate bearing capacity, q_s, of a homogeneous thick bed of sand is much greater than the one of the underlying clay deposit, q_c. At ultimate load, a sand mass having an approximate friction angle, ϕ, of the sand and the undrained cohesion, 'c', of the clay are mobilized in the composite failure zones illustrated in Figure 2.13.

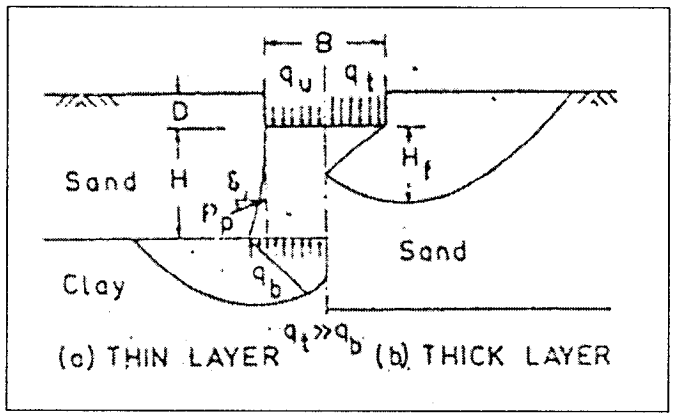

Figure 2.13 Soil failures below footing on dense sand (Meyerhof and Adams (1968))

The ultimate bearing capacity of a strip footing resting on dense sand overlaying clay bed is expressed by:

$$q_u = cN_c + \gamma H^2 (1 + 2D/H) K_s \tan \Phi / B + \gamma D \qquad (2.2)$$

with a maximum of q_u:

$$q_u = \gamma B N_\gamma / 2 + \gamma D N_q \qquad (2.3)$$

where N_γ and N_q are the bearing capacity factors. The punching shear coefficient, K_s, has been determined from the corresponding earth pressure coefficient K_P, and is shown in Figure 2.14.

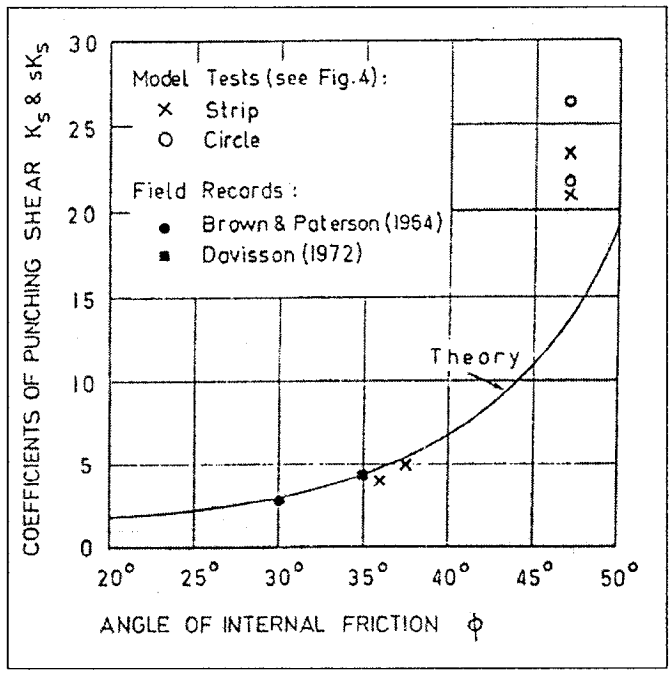

Figure 2.14 Coefficient of punching shearing resistance (Meyerhof and Adams (1968))

It is important to note that K_s increases rapidly with Φ from about one to two times the Rankine value of $\tan^2(45^0 + \Phi/2)$. The analysis for the strip footing can be extended to circular footings by considering the passive resistance, P_P, to be inclined at δ on a vertical cylindrical surface through the footing edge (Figure 2.13). Thus the ultimate bearing capacity becomes:

$$q_u = 1.2cN_c + 2\gamma H^2 (1 + 2D/H)sK_s \tan \Phi / B + \gamma D \quad (2.4)$$

with a maximum of q_u:

$$q_u = 0.3\gamma BN_\gamma / 2 + \gamma DN_q \quad (2.5)$$

where 's' is the shape factor governing the passive earth pressure on a cylindrical wall. The ultimate bearing capacity of rectangular footings of width B and length L can be obtained by interpolation between the bearing capacities of strip and circular footings. The corresponding values of q_u are computed from equation 2.2 after multiplying the first term of the right hand side by (1+0.2B/L) and the second term by (1+B/L), with the maximum q_u interpolated between equations 2.3 and 2.5.

2.4.2 Stress-Strain Behavior of Soil and Models

The stress-strain behavior of soil depends on a number of factors such as unit weight, water content, structure, drainage conditions, strain conditions (plane strain and triaxial), duration of loading, stress path, stress history, confining pressure and shear stress. In many cases, it may be possible to take into consideration these factors in selecting a soil specimen and testing conditions which stimulate the corresponding field situation. When this can be done accurately, the strains resulting from the given stress changes in the laboratory would be expected to be representative of the strains which occur in the field under the same stress changes. Lambe (1964, 1967) had described a procedure to predict strains and movements in soil masses without developing an analytical stress-strain relationship for the soil.

The concept of duplicating field conditions can greatly simplify the procedure required for determining stress-strain behavior of soil. However, the behavior over a wide range of stresses is nonlinear, inelastic and dependent upon the magnitude of the confining pressure used in the test.

In the past, only linear elastic soil behavior could be assumed to perform analyses of stresses in soil masses. Nowadays, with the availability of computing facilities and numerical techniques, it is possible to estimate the nonlinear stress response of soil. Duncan and Chang (1970) have presented nonlinear responses of soil mass and some of the models are described below.

Bilinear and Multi-linear Models

It is the simplest form of nonlinear model in which the material maintains linearity until the stress reaches a yield value beyond which the response is strain hardening or strain softening. The multi-linear model or also called piece wise linear model can be represented by the tangents to each of the segments of nonlinear stress-strain curve.

Hyperbolic Model

The stress-strain curve obtained from triaxial test can be represented by a hyperbolic relation in the form of:

$$\sigma_1 - \sigma_3 = \frac{\varepsilon}{(a + b\varepsilon)} \qquad (2.6)$$

where σ_1 and σ_3 are the major and minor principal stresses in the triaxial sample, 'ε', the axial strain, and 'a' and 'b' are the constants of hyperbola Kondner (1963).

The hyperbolic relation was extended to generate stress-strain curves in function of shear strength and initial tangent modulus by Duncan and Chang (1970) as:

$$E_t = E_i \left[1 - \frac{R_f(\sigma_1 - \sigma_3)(1 - \sin\phi)}{2\sigma_3 \sin\phi + 2c\cos\phi} \right]^2 \tag{2.7}$$

where E_t is the tangent modulus, K the modulus number, R_f the strength ratio and E_i the initial tangent modulus which is equal to

$$E_i = KP_a \left(\frac{\sigma_3}{P_a} \right)^n \tag{2.8}$$

where P_a is the atmospheric pressure and n is the exponent determining the rate increase of E_i with σ_3. The strength ratio is

$$R_f = \frac{(\sigma_1 - \sigma_3)_f}{(\sigma_1 - \sigma_3)_{ult}} \tag{2.9}$$

where $(\sigma_1 - \sigma_3)_f$ is the stress difference at failure and $(\sigma_1 - \sigma_3)_{ult}$ is the asymptotic value of stress difference.

2.4.3 Foundation Response

Idealized subgrade models prove to be particularly useful in the analysis of soil-foundation interaction problems. The choice of choosing an idealized behavior of the soil depends on a number of factors including the type of soil and soil conditions, the type of foundation and the nature of external loading. The response of each idealized model is characterized by the surface deflection it experiences under the application of external forces. These surface deflections represent the displacement of the upper soil layer which is in contact with the foundation or so called soil-foundation interface. These models are intended to model the response of the soil media and not the response of the elements within the soil.

Kerr (1964), Selvadurai (1979) and Chandra (1979) presented an excellent survey on the existing foundation models for soils as subgrades and are introduced below.

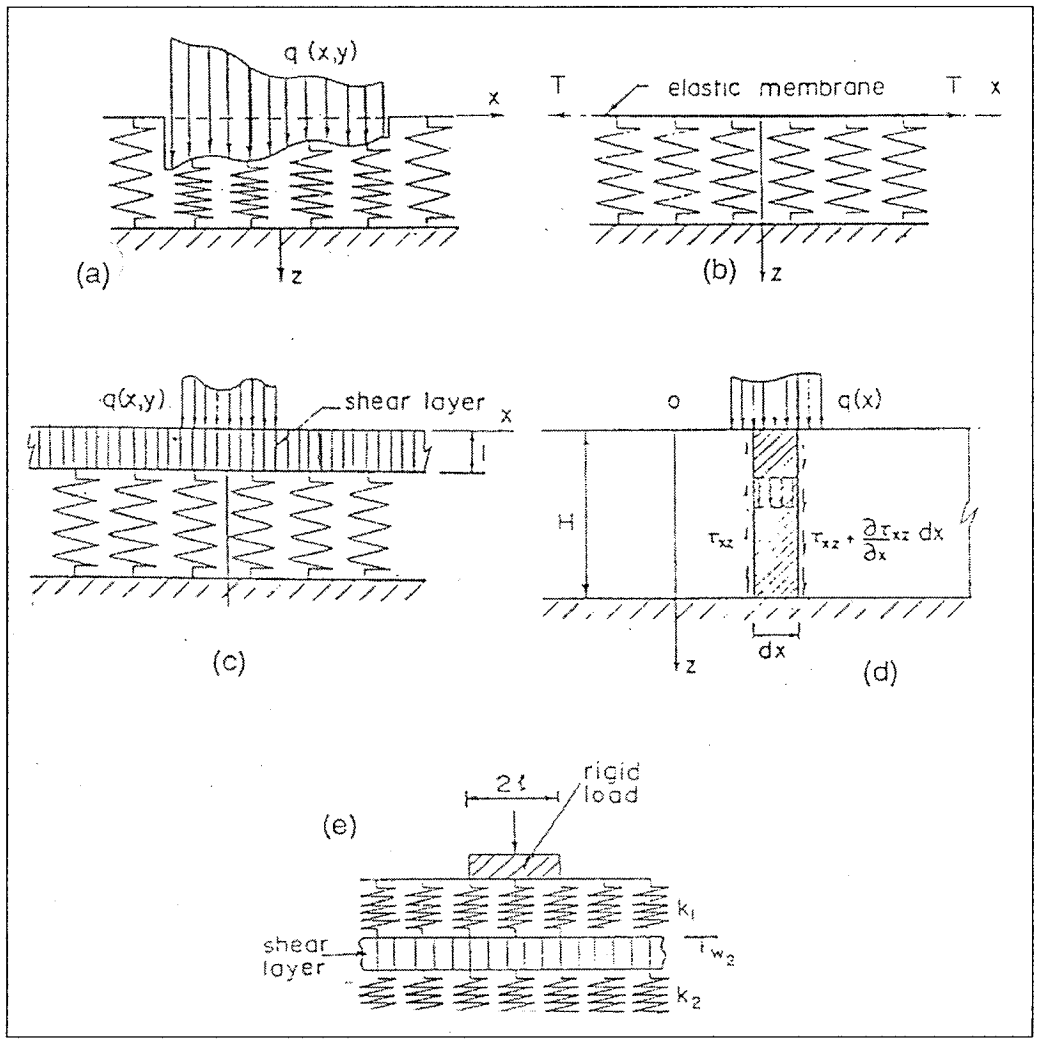

Figure 2.15 Models: a) Winkler b) Filenenko-Borodich c) Pasternak d) Vlasov e) Kerr (Chandra (1979)

The Winkler model shown in Figure 2.15a is the simplest and relates the stress on the soil, q, with the displacement, w, as:

$$w = \frac{q}{k} \tag{2.10}$$

where k is the spring constant or the modulus of subgrade reaction. The two parameter models are a significant improvement over the Winkler model and take into consideration the displacement of the soil outside the loaded region.

The Filonenko-Borodich model (Figure 2.15b) achieves continuity between individual springs through a thin smooth membrane stretched over them. The equation governing the response is:

$$kw - T\frac{d^2w}{dx^2} = q \tag{2.11}$$

where T is the constant tension in the membrane.

The Pasternak model (Figure 2.15c) considers the shear interaction between compressible soil elements (springs). Characterizing the shear layer by its shear modulus, G, and thickness, H, the response is

$$kw - GH\frac{d^2w}{dx^2} = q \tag{2.12}$$

The Vlasov model (Figure 2.15d) is very similar to Pasternak model but with the parameters K and G reduced from a simplified continuum as:

$$K = \int_0^H \frac{E}{(1-\nu^2)}\left[\frac{dh(z)}{dz}\right]^2 dz \tag{2.13}$$

and;

$$G_p = \frac{1}{2}\int_0^H \frac{E_0}{(1+\nu_0)}[h(z)]^2 dz \tag{2.14}$$

where the constant k is the measure of compressibility of the soil medium under applied compressive stresses, G_p is the measure of the transmissibility of an applied force to

neighboring elements or the load-spreading capability and h(z) is a function for variation of displacement with depth.

Kerr (1964) modified the Pasternak model with another spring layer on the top of the shear layer (Figure 2.15e). The derived differential equation is:

$$\left\{1+\frac{k}{c}\right\}q-\frac{GH}{c}\nabla^2 q = kw = GH\nabla^2 w \tag{2.15}$$

where 'c' is an additional spring constant of the upper spring layer and all the other parameters are previously defined.

Rhines (1969) developed Kerr's model by assuming that the shear layer interconnecting the spring elements is capable of sustaining finite shear stress. The shear stress-shear strain relationship for the elastic layer is of an elastic-rigid plastic type.

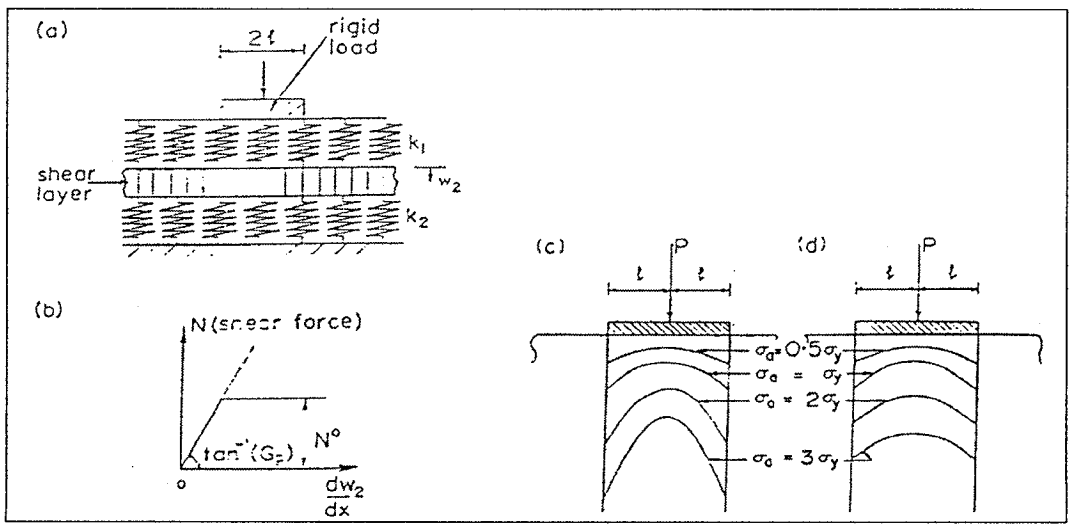

Figure 2.16 a) Kerr model b) Elastic-perfectly plastic response of shear layer
c) Contact stress distribution for the perfectly elastic model
d) Contact stress distribution for the elastic perfectly plastic model
(after Rhines (1969))

The results indicate that the inclusion of such yielding characteristics can alter both the magnitude and distribution of contact stresses that are developed at the soil-foundation interface. The effects become significant when the average stress beneath the foundation exceeds the critical shear strength of the shear layer (Figure 2.16).

Madhav and Poorooshasb (1989) have extended the Pasternak concept for reinforced granular fill, by filling the effect of confinement in the fill due to the reinforcing effect.

2.5 REINFORCED GRANULAR BED ON SOFT SOIL

Since the development of the reinforced earth concept (Vidal, 1966), various attempts have been made to study the soil-reinforcement interaction mechanisms of near surface reinforced foundation beds. The interaction mechanism resulting from the integration of various reinforcing elements, their position and orientation, the number of layers and the surface characteristics has not been fully examined yet. The basic purpose of providing an inclusion is to improve the foundation response to the unreinforced one. The reinforced foundation bed consists of a layer of granular fill over soft clay. The reinforcement (geogrid or geonet) is placed within the fill or at the interface of the soft clay and the fill. Properly used inclusions possess more stability and deform less than the soil alone. In most cases, the tensile forces are generated in the reinforcement as a result of mobilization of the interface frictional forces. The flat shape of the inclusion results in a longitudinal extension which causes the inclusion to act only in pure tension.

2.5.1 Review of Various Analytical Methods

Binquet and Lee (1975a, b) studied the problem of the bearing capacity of a strip footing on a granular soil containing horizontal layers of tensile reinforcement. Based on their model test results, a failure hypothesis is proposed which forms the basis for the bearing capacity analysis. The analytical results are then compared with experimental data. A design method for the bearing capacity of a footing on a reinforced earth foundation is proposed by specifying preliminary footing dimensions, location, the reinforcement size and then checking the adequacy.

Broms and Massarsch (1977) proposed an analytical method for grid mat foundation and verified the theory with model tests. Experiments have been conducted with triangular and rectangular steel cells on both cohesive and cohesionless soils of different densities. Punching and general shear failures have been assumed for relatively small and large cell height to circumference ratios.

Niewenhuis (1977) developed a simple model for describing the behavior of a road base membrane subsoil system. The load transferred through the road base is derived from the Boussineq equation. The membrane is smooth and anchored at its ends and the subsoil is represented by Winkler springs. The membrane and the subsoil were assumed to behave as linear elastic materials.

Andrawes et al. (1978) discussed the soil-inclusion interaction with respect to two kinds of internal strain mechanisms, one controlled by compressive strains and the other by tensile strain. Piles under compressive and tensile applied loads are shown in Figure 2.17 (a) and (b) and soil strain controlled inclusions are shown in Figure 2.17 (c) and (d).

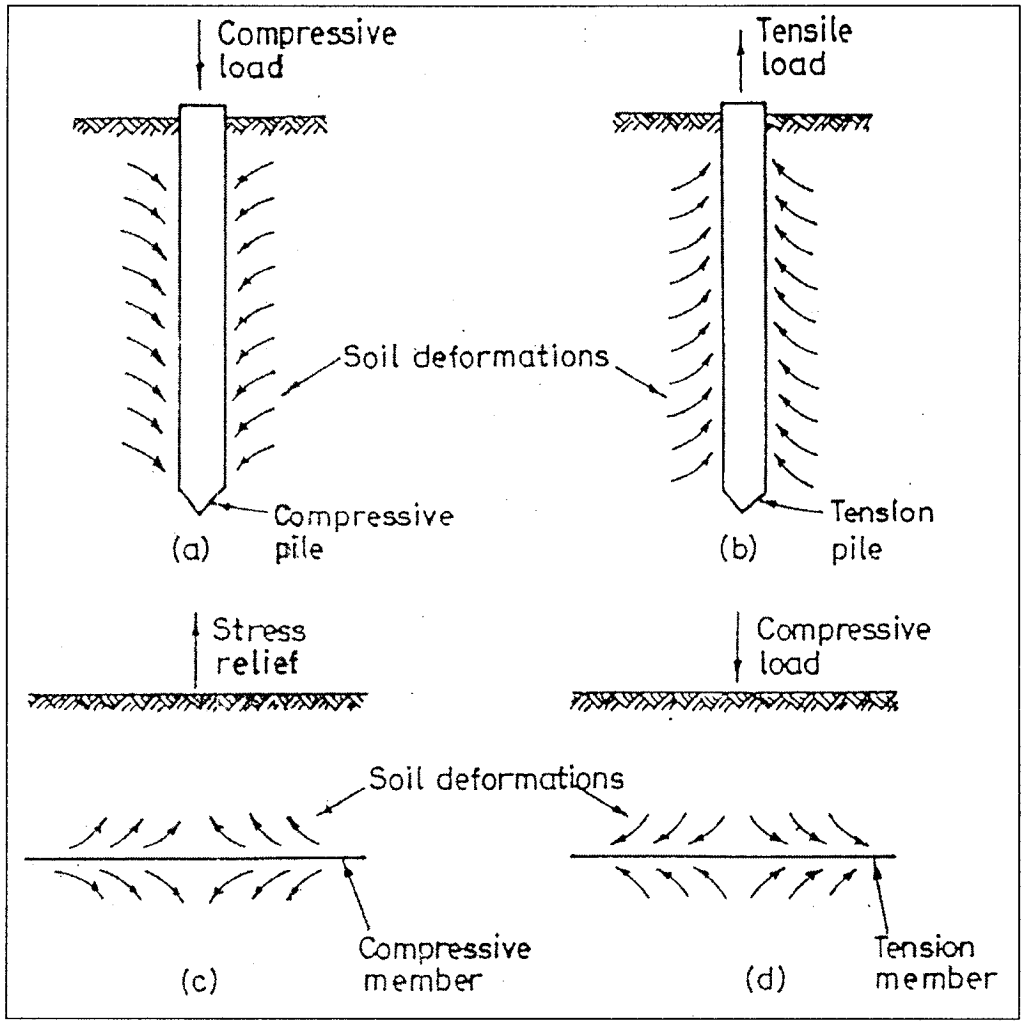

Figure 2.17 Loading characteristics of piles strain controlled inclusion

(Andrawes et al. (1978))

In piling system, both external compression and tension loads induce internal deformations in the soil in which they are installed. In reinforced earth systems, the inclusions are loaded by the soil itself.

Basset and Last (1978) have investigated the modification of natural strain field caused by the presence of reinforcement in the soil. The load transfer mechanism between soil and reinforcement is dependent on the limiting interface friction or

adhesion. Figure 2.18a shows the conventional Mohr's circle of strain rate. The pole of origin of planes determines the major (ε_1) and minor (ε_3) principal strain rate directions from which α and β characteristics can be found for the planes 'A' and 'B' (Figure 2.18b).

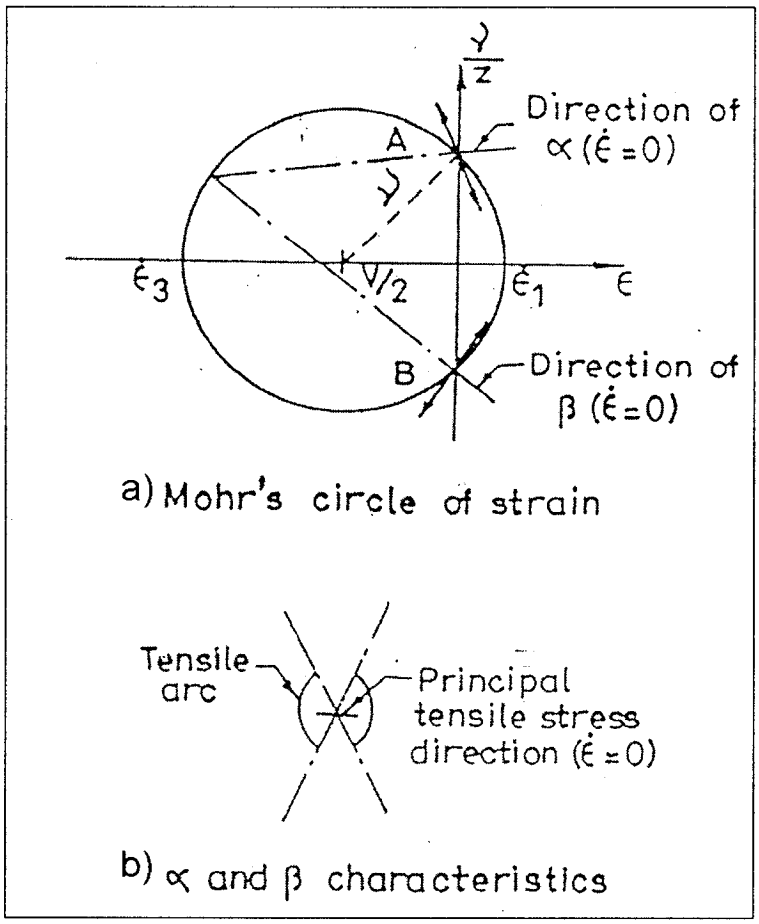

Figure 2.18 Internal strain field (Basset and Last (1978))

Normal strains within the arc segment containing minor principal strain direction (ε_3) are tensile and reinforcement laid along the tensile stress zone would be effective in improving the bearing capacity and settlement response of the soil. Figure 2.19 illustrates

the zero extension lines of the internal strain field, developed due to strip load applied at the surface.

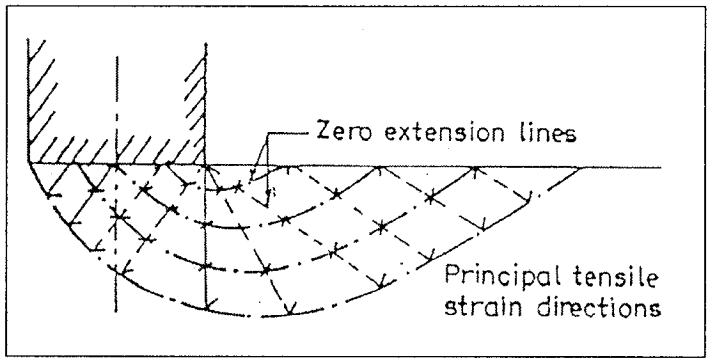

Figure 2.19 Zero extension lines characteristics (Basset and Last (1978))

Accordingly, the reinforcement below the footing is to be placed horizontally. Its direction becomes progressively vertical at some distance away from the footing edge. The ideal as well practical pattern of reinforcements under the footing is suggested to be along the direction of principal tensile strain (Figure 2.20).

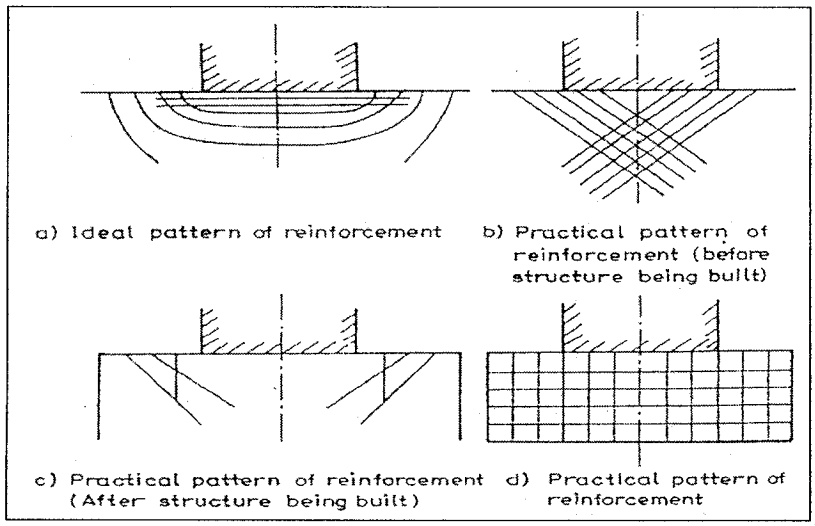

Figure 2.20 Pattern of reinforcement beneath footing (Basset and Last (1978))

Bourdeau et al. (1982) presented a theoretical model for soil-membrane interaction using a probabilistic concept for the vertical stress in a particulate media. The geotextile is introduced at the interface of the two layers. The Mohr-Coulomb friction criteria are satisfied at the soil-geotextile interfaces. The soil below the geotextile is represented by Winkler springs. The governing expression from the vertical force equilibrium of the membrane element is given by:

$$T_H(x)\frac{d^2w}{dx^2} + \tau(x)\frac{dw}{dx} + k_s w = S_{1z}(x, h_1) \tag{2.16}$$

where $S_{1z}(x,h_1) = \frac{p}{S_1\sqrt{2\pi}} \exp\left[-\frac{x^2}{2S_1^2}\right]$ and $S_1 = h_1\sqrt{2\upsilon}$, υ is the coefficient of lateral stress.

$T_H(x)$ is the horizontal component of the tensile force in the membrane along the x-axis. It is expressed as:

$$T_H(x) = T_0 - \int_0^x \{\tau_1(x) = \tau_2(x)\}dx$$

Where

$$\tau_1(x) = F_1[S_{1z}(x, h_1) + \gamma h_1] \tag{2.17}$$

and

$$\tau_2(x) = F_2[S_{1z}(x, h_1) + \gamma h_1] = F_2(k_s w + \gamma h_1)$$

γ and h_1 are the bulk unit weight and the thickness of the upper soil layer respectively, T_0 is the maximum tensile force occurred below the membrane, and P is the point load at the surface.

Nishigata and Yamaoka (1990) developed an equation to calculate the bearing capacity of reinforced unpaved road by considering the restraint of the soft subgrade soil

and the confinement effect of the aggregate layer. The stress condition assumed is highlighted in Figure 2.21.

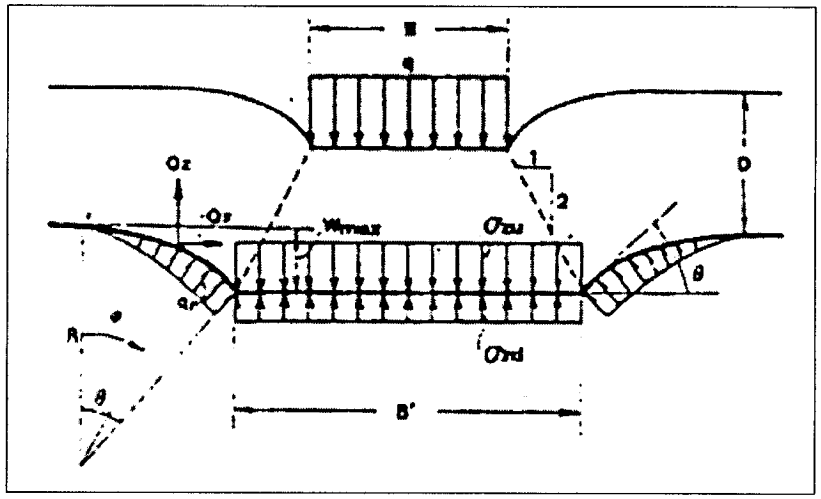

Figure 2.21 Stress condition in the reinforced region (Nishigata and Yamaoka (1990))

They extended the bearing capacity theory for the unpaved roads given by Yamanouchi and Gotoh (1979) by introducing an additional horizontal force caused by geotextile to the passive earth pressure term defined by Meyerhof (1974) for ultimate bearing capacity of sand overlaying clay. The following formula was obtained for the ultimate bearing capacity of the road system as:

$$q_{ult} = c_u N_c + 2Q_z / B' + q_r N_q + [2P_p + 2Q_x] Tan\delta / B + \gamma w_{max} N_q \qquad (2.18)$$

where q_{ult} is the ultimate bearing capacity, N_c and N_q are the bearing capacities factors, P_p is the passive earth resistance (Meyerhof (1974)), γ the unit weight of the subgrade and w_{max} the maximum settlement under the footing. The vertical component of the pressure

was found to be $Q_z = \int_0^{\partial} q_r \cos\phi * R * d * \phi$ and the horizontal component of pressure was

$Q_x = \int_0^{\partial} q_r \sin\phi * R * d * \phi$.

2.5.2 Review of Numerical Methods

Brown and Poulos (1981) used finite element method for the analysis of reinforced soil by incorporating elasto-plastic soil model satisfying Mohr-Coulomb failure criterion. Their results indicate that the reinforcement layers have negligible effect on the initial response of the footing. Collapse load and displacement increase at failure with the increase of number of layers and surface area rather than the stiffness of the reinforcing layers. Tensile forces increase in each of the reinforcement with depth. The analysis brings out that the provision of reinforcement helps in spreading the load over a wider area and within lesser depth.

Floss and Gold (1990) used finite element technique to stimulate tests conducted by Bauer and Preissner (1986) for a reinforced two layer system. The shear modulus was defined to be independent of the Young's modulus and the movement of soil elements relative to the elements of the reinforcement was possible by large shear distortion of the thin layer elements, which were additionally supplied with a joint parallel to the reinforcement, to limit the transfer of forces from the soil into the reinforcement by a yield criterion. The Young's modulus of the thin layer elements is equal to the one of the surrounding soil. The shear modulus and the friction parameters between the

reinforcement and the soil were determined from pull-out or direct shear tests. The following findings were observed with the reinforcement in the granular bed:

- The peak shear stresses were about 25% lower in the reinforced system.
- The horizontal strains were reduced due to the reinforcement and the horizontal stresses were concentrated in the areas where high vertical stresses were found.
- The vertical stress distribution indicated the load spreading effect of reinforcement.

2.5.3 Laboratory and Field Testing Results

A large number of results are available on reinforced foundation beds to analyze their behavior and study their mechanisms. However, few test results are mentioned below.

Binquet and Lee (1975) carried out model tests with strip footings on reinforced sand foundations for these three conditions: homogenous deep sand, sand above an extensive layer of very soft material stimulating soft clay or peat and sand above a finite size pocket of very soft material such as a pocket of organic soil or limestone. The tests resulted in an improvement of the load-displacement responses and the allowable bearing capacities by a factor of 2 to 4 times the values for an unreinforced soil for identical conditions. The improvement was obtained for a linear density ratio (LDR) equal to 42.5%, a relative spacing of reinforcement of S/B equal to 0.3 and for a number of layers (N) equal to 4 to 6 layers of the reinforcement strips.

Andrawes et al. (1983) conducted load tests on strip footings resting on deep layer of dense sand with and without a single layer of geotextile at different depths below the surface. The deformation fields for the sand and the geotextile up to and beyond the limited conditions have been directly measured. On the basis of the test results the following general points were made regarding the reinforcement of roads, airfields and railways:

- The inclusion must be placed in the zone and direction of the tensile strains to generate tensile resistance which will restrict the development of these tensile strains.
- The tests have shown that the soil-geotextile surface friction/adhesion is less than the soil-soil friction/adhesion.
- If the geotextile is placed close to the directions of zero extension lines with the soil, slip surface may form along the geotextile surface and this will limit the tensile resistance of the geotextile.

Bauer and Preissner (1986) investigated the effect of geotextile on the bearing capacity and the deformation of the two layered system that has been reinforced. A two-fold approach was proposed for the analytical treatment of the stability problem. Consideration of the membrane effect, and, the effect of transfer of shear stress to the reinforcement were jointly put forward. Due to failure in cases of elasto-plastic and plastic deformations, commencing from the flow action of the system, force redistribution from overloaded areas to the reinforcement areas with lesser load is produced. The load stages as yet did not bring on these plastic deformations. The stress

transducers demonstrate a distinct increase in stress under the loading beam upon use of reinforcements despite the envisaged relief of the subsoil due to the membrane. This demonstrates that stress redistributions are induced by the reinforcement.

Milligan et al. (1986) conducted and presented full-scale trails of the reinforcing effect of a geogrid for modifying the behavior of a granular layer over a weak clay subgrade subjected to monotonic loading. Large scale tests in combination with numerical analysis using a finite element program were used in the investigation. The tests conducted were plane strain and axi-symmetric conditions of two kinds of subgrades. First one is a weak subgrade with an undrained strength, c_u = 8kN/m^2 and the second was strong subgrade with undrained strength, c_u = 33 kN/m^2. The trials indicate that, under the conditions involved, reinforcements at the interface result in an increase of 50 mm in the layer thickness for a given deformation. These results do propose a number of situations where alternately, a grid could be more effective:

- A geogrid would be more effective in less stiff material as suggested by calculations from the finite element program.
- As may occur in temporary roads, the results of both the full scale and model tests propose that a geogrid is more effective at larger deformations.
- The mathematical modeling and the large scale tests jointly demonstrate that further improvement could be achieved by optimum location of the geogrid, as well as by ensuring interlock between geogrid and aggregate.
- These tests are not necessarily applicable in considering the effect of a geogrid under repeated loading as they had been primarily concerned with static loading.

Das (1989) performed tests with and without a geotextile at the sand clay interface to determine the ultimate bearing capacity of strip and square foundations supported by a compact sand layer with underlying soft clay. Based on these, the following is concluded:

- With the use of geotextile at the sand-clay interface, the maximum bearing capacity ratio of a foundation will increase. The increase was approximately 24% for square foundations and about 8% for strip footing.
- The critical values of the H/B ratio, where H is the height and B is the width of the foundation, at which the maximum bearing capacity ratio occurs is 0.75 for strip foundations and 0.5 for square footings upon use of geotextile.
- The most advantageous width of the geotextile layer for deriving the maximum bearing capacity ratio is about 4B for strip foundations and 3B for square foundations.
- The increase of the bearing capacity ratio obtained by using a geotextile at the sand-clay interface may also be a function of the tensile strength of the geotextile itself.

2.5.4 Modeling of Reinforced Foundation Beds

Pooroqshasb (1985) extended the concept of Pasternak by taking into consideration both the material non-linearity and body forces. Both the failure as well as the pre-failure stages of the loading are dealt with in the model. Main conclusions drawn from this work are:

- If the sand layer is normally consolidated, the existence of a sand layer between the footing and the supporting soft bed does not appear to be very effective in reducing settlements.
- The settlements can by reduced up to 50% with the inclusion of a compacted cohesionless layer.

A new model for the analysis of footing on a reinforced granular bed was developed by Madhav and Poorooshasb (1988). The subgrade soil, granular bed and reinforcement have been modeled by Winkler springs, Pasternak shear layer and rough membrane respectively. Results demonstrate that the role of shear layer is more significant in reducing the settlements of the reinforced soft soil at small displacements. Hence, it is shown that the effect of the reinforcement is significantly more effective at higher loads.

To solve a certain class of problems associated with the performance of heavily reinforced mats supported by weak subgrades, an analytical procedure was proposed by Poorooshasb (1991). The granular fill is considered as a rigid strain hardening plastic material having a yield function, 'f', a hardening function, 'h', and flowing in accordance with a plastic potential function, 'φ'. A specific hypothesis regarding the mode of deformation of the granular fill states that vertical planes in the unloaded system remain both vertical and planar after the loading has been imposed. Every element of the fill undergoes a state of simple shear in the vertical direction. All elements along an original vertical plane undergo identical flow patterns.

The basic governing equation is:

$$\eta^2(x)-\left[\frac{H}{2}+\int_x^{\infty}\eta(s)ds+\frac{p_0}{\gamma_S}\right]\frac{d\eta}{dx}=\alpha\left[\int_x^{\infty}\gamma(s)ds-\frac{p-p_0}{k_s}\right]+\beta\left[1+\upsilon(e_0,\eta)-\frac{1}{\{1+\gamma^2(\eta)\}^{1/2}}\right]\frac{d\gamma}{dx} \quad (2.19)$$

where $\alpha = k_s / k_0 \gamma_s H$ and $\beta = nE/k_0\gamma_s H$. The integral function $\gamma(s)$ is between the limits x to infinity to represent the magnitude of the u(x) which the displacement in the x direction. The yield function $\eta = \tau/\sigma$. The shear strain is γ, the subgrade modulus is k_s, ν the volumetric strain, p is the applied load, p_0 the surcharge and H the thickness of the fill.

Ghosh and Madhav (1994a) elaborated the Madhav and Poorooshasb (1988) model by including a non-linear stress-displacement relation for soft soil as well as a non-linear shear stress-shear strain response for the granular fill. The combined effects of the system on the response of the footing resting on the reinforced granular bed were quantified. Ghosh and Madhav (1994b) and (1994c) quantified the membrane effect on the load-settlement response of the footings resting on reinforced granular bed and also developed another model by taking into account the confinement effect of reinforcement on the granular fill. These models assume the granular fill as incompressible.

Alternatively, the compressibility of the granular fill was considered in the modified model of Shukla and Chandra (1994a). In order to study the effect of the compressibility of the granular fill on the load-settlement response of the footing resting on the reinforced granular bed, a mechanical model was presented. This model considered simultaneously all of the compressibility of the granular fill, the compaction

of the granular fill, the time-dependent behavior of soil and pre-stress in the geosynthetic reinforcement and soil-geosynthetic interface characteristics. The Madhav and Poorooshasb (1988) model was further modified and extended by Shukla and Chandra (1995) by considering the vertical and horizontal component of shear stresses on the reinforcing element. Then, Yin (1997a) presented a different model by analyzing the compatibility of displacements at the interface of the fill and the reinforcing layer. Similarly to the Madhav and Poorooshasb (1988) model, he also modeled the soil, the granular fill and the reinforcement layer. Yin (1997b) further modified the original Yin (1997a) model by considering the non-linear response of the soil and the fill.

3. MODELING THE NON-LINEAR BEHAVIOUR OF COHESIONLESS GRANULAR MEDIA

3.1 INTRODUCTION

Any soil material undergoes both elastic and plastic deformation when subjected to loading. The deformation is called elastic if it is recoverable and independent of time as soon as unloading takes place. On the other hand, the deformation is called plastic if it is irrecoverable and enduring. Many definitions were given out in textbooks to describe the theory of plasticity. However, elastic-plastic constitutive models help distinguish between the recoverable and irrecoverable deformations for understanding the stress-strain behavior of soil during loading and unloading.

Theory of plasticity was first based and observed on the behavior of metals. The theory applies very well on these materials that it led to satisfying analytical results. Despite the use of the theory in different areas, there is no need to start from the definitions of elastic and plastic deformation used in other fields than soil mechanics. Elastic deformations are described as reversible in a closed cycle of loading and unloading and during which energy is preserved. The strain increments occur in the direction of the increments of applied stresses. Alternatively, plastic deformations are permanent as the cycle carries on and energy is dissolved. During plastic deformations, the strain increments occur in the direction of the current stress and during a small increment they are slightly affected by the direction of the stress probe.

When Tresca published his yield principle in 1864, the door was opened to many researchers in plasticity theory. Based on his experimental results on punching and extrusion, he stated that metal yielded plastically when the shear stress reached a critical value. Since then over 140 years of remarkable progress has been made in theory of plasticity which is nowadays an active field in soil mechanics.

In plasticity, the failure surface is assumed to be the yield surface when the state of stress reaches that surface. A state of stress acting below the yield surface is to behave elastically. Therefore, one failure surface defines the yielding of the material. De Saint-Venant (1870) was one of the first who attempted to develop a stress-strain relationship for plastic deformation. His main work was on plane strain problems using Tresca's principles. He assumed that the work hardening is zero and that the principal axes of strain increment coincided with the axes of principal stress. De Saint-Venant's idea for the three dimensional case between stress and strain was worked on by Levy (1871) and then by Von Mises (1913). Based on normality concept, Von Mises developed a constitutive relation that relates the plastic strain rate to the yield surface. He also stated that a material behaves plastically when the distortional energy reaches a critical value. This theory was named afterward the Levy-Mises theory of plasticity and stated that the elastic strain is so small as to be ignored and that the direction of principal plastic strain increment tensor coincides with the ones of the stress tensor (this is known as coaxial). The relationship is the following:

$$\dot{\varepsilon}_{ij} = \dot{\lambda} s_{ij} \tag{3.1}$$

where $\dot{\lambda}$ is called the proportional parameter and determined from the yield criterion,

$\dot{\varepsilon}_{ij}$ is the strain rate and s_{ij} is the deviatoric stress. This equation is called the flow rate and the strain rate has been generalized for the constitutive equation of plastic strain rate, $\dot{\varepsilon}^{p}$ and therefore the plastic deformation is called plastic flow. Prandtl (1924) and Reuss (1930) developed constitutive equations for linear elastic perfectly plastic soils of the assumption of $\frac{\partial f}{\partial \sigma_{ij}} = s_{ij}$ (3.2a)

$$e_{ij} = d\lambda s_{ij} + \frac{s_{ij}}{2G} \tag{3.2b}$$

$$\varepsilon_{kk} = \frac{\sigma_{kk}}{3K} \tag{3.3}$$

where e_{ij} is the deviatoric strain, s_{ij} is the deviatoric stress, G is the shearing modulus, ε_{kk} is the bulk strain, K , the bulk modulus, $d\lambda$, the loading parameter and σ_{kk} is the bulk stress.

Another historical criterion was found by the Coulomb (1773), where he proposed the failure mode in soil mechanics. His research was based on hydrostatic pressure affecting the strength parameters of granular materials. The Coulomb failure law is defined by:

$$\tau = \sigma_n \tan\phi + c \tag{3.4}$$

τ is the shearing stress, σ_n is the normal stress, ϕ the angle of friction and c the cohesion. The graphical solution for the above equation is represented by Mohr's stress circle. Later on, Meyerhof (1951) proposed a conservative method to measure the bearing capacity of foundations using the perfectly plastic theory. However, this theory was not mathematically accurate enough for solving soil problems (Drucker and Prager (1952)).

Drucker and Prager (1952) proposed a new failure criterion, by depending on and modifying the hydrostatic stress, which is close to Coulomb's approximation. They assumed the following:

$$f(J_1,J_2) = 0 \tag{3.5}$$

The Drucker-Prager yield equation is:

$$\alpha_{DP} J_1 + \sqrt{J_{2DP}} = K_{DP} \tag{3.6}$$

α_{DP} , K_{DP} are the Drucker-Prager material constants. The graphical representation of this surface in (σ_1, σ_2, σ_3) space is a circular cone shown in Figure 3.1. The Drucker-Prager parameters could be extracted from Mohr-Coulomb parameters values.

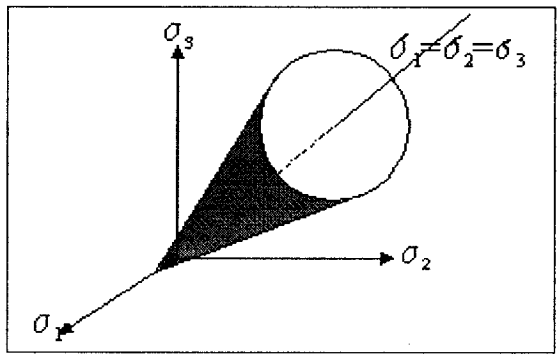

Figure 3.1 Drucker-Prager yield surface

During the 1950's and 1960's, major advancements were made in the theory of plasticity. One of them was the work hardening behavior which triggered so many investigations in soil mechanics. In addition to that, the vital part of all these developments was the critical state concept developed by Poorooshasb (1961) at Cambridge University. This concept was earlier referred to as the critical void ratio by Roscoe et al. (1958). The critical state is the end of all state or failure paths for all shear

tests under drained and undrained conditions and where large shear distortions (change in shape) occur without any change in state parameters.

Associated flow rule, which means that the plastic potential curve would take the same form as the yield function, was used in plasticity to find the deformation of frictional materials. However, it was proven experimentally that it predicts large volumetric expansions. Poorooshasb et al. (1966, 1967) studied the deformation of a sand sample under a triaxial test and proved that it is necessary to employ a non-associated flow rule i.e. the plastic potential surface and the yield surfaces are not coincidental. His research which examined the flow and yielding of cohesionless granular medium led to the existence of a potential function, known as the plastic potential of the form Ψ (σ, e) where σ is the stress and e the void ratio. The plastic potential curves draw a family of similar curves when plotted in the stress space. The yield loci, lines of constant stress ratio, were found to be independent of void ratios and are used to describe the yielding of sand as followed:

$$\eta = q / p \tag{3.7}$$

Shortly after, Poorooshasb (1971) confirmed that the yield function for the same sand tested under a triaxial test was computed regardless of the density and the stress path by the following relation:

$$f = \eta + m \ln p \tag{3.8}$$

where m is a constant assumed to be 0.6 for that specific sand.

A two surface model was developed by Poorooshasb and Pietruszczak (1986) to describe the mode of deformation of sand undergoing complicated loading paths of the generalized stress space. The proposed model assumes the existence of a yield surface

and a bounding surface (Dafalias and Popov, 1975; Pietruszczak and Mroz, 1983). The bounding surface is created by any active loading upon a virgin material and separates this loading from the other types of loadings such as stress reversals and unloading. On the other hand, the yield surface encloses all the stress points for which the material behaves elastic i.e. reversible and all stress reversals involved. The two-surface model assumes an isotropic-kinematic hardening law including the Lode angle (θ) in the calculation of the surfaces and its formulation is based on incorporating a non-associated flow rule and the concept of reflected plastic potential. The applicability of the model has been proven to be very efficient for loose and dense sand. An alternative model has been proposed by Pietruszczak and Stolle (1987) to simplify the kinematics of the model by considering a circular section independent of the Lode angle for the yield surface. Poorooshasb (1989) proposed another scheme following mainly the same line of thought presented previously by Poorooshasb and Pietruszczak (1986). During virgin loading the yield surface is tangential to the bounding surface along a meridian as it moves with the bounding surface and the simplified scheme is highlighted in Figure 3.2.

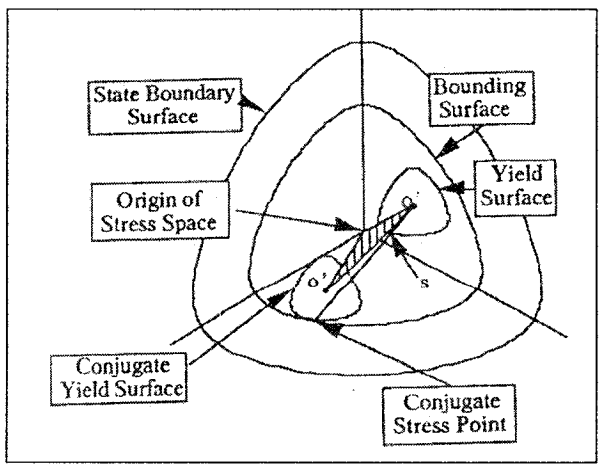

Figure 3.2 Bounding surface and yield surface (Poorooshasb (1989))

During stress reversals or unloading, the yield surface is no longer in contact with the bounding surface and must follow special kinematical constraints.

Recently, a lot of developments have been made in elastic-plastic models for the solution of complex geotechnical problems. Constitutive models based on experimental and theoretical research have been developed as well for reliable solutions in this area. However, the most efficient ones are being measured by their simplicity and their representation.

3.2 BACKGROUND ON IMPORTANT CONCEPTS AND LAWS

3.2.1 The Concept of Critical Void Ratio

In the mid 1930s, Rendulic and Hvorslev carried out their research by working on the direct shear test which is nowadays the foundation of soil mechanics mainly in plasticity and strength theories. From the direct shear test, the only components measured are the shear stress (τ) and the normal effective stress (σ). If several tests are carried out at different vertical stress value, each of which are kept constant during each test, and the peak shear stress values are plotted against the vertical stress, the angle of friction can be computed. The angle of friction obtained from a loose sample is called the critical angle of friction and is represented by ($\phi_{critical}$). However, these plots are not actually straight lines if the void ratios are the same for each line but are slightly curved because of the inclination of the so called Casagrande Critical Void Ratio line. The volume change that takes places during loading is mainly due to the contraction or expansion of the voids into

the soil mass and it was first pointed out by Reynolds (1885). Reynolds showed that dense sands tend to expand increasing their total volume when they are subjected to shear stresses. This phenomenon was called by "The Reynolds dilatancy".

From the observation of the volumetric strains on dense and loose sands, Casagrande (1936) realized the actual importance of the volumetric strain in the soil response developing the concept of "critical density or critical void ratio". Using direct shear tests, Casagrande observed that during shearing dense sand expands and therefore increases its void ratio, while very loose sand reduces its volume and accordingly its void ratio. In dense sand, the grain are pretty well interlocked, thus any deformation causes a loosening up of the initial compact structure. On the other hand, very loose sand tends to contract in order to achieve a more stable structure. Based on this observation Casagrande developed the concept of the critical void ratio: when dense and loose sands are sheared in a drained condition, they change their void ratio until a common constant value is eventually reached. This ultimate common void ratio was termed the critical void ratio (C.V.R.) and today the line representing the critical state is often referred to as the Casagrande CVR line. At this state, the soil continues to deform under constant strength and constant volume, hence the soil behaves as a frictional fluid. The so-called critical void ratio line traces a straight line if the p axis is plotted in a logarithmic scale and is shown in Figure 3.3. The symbol e represents the void ratio of the sample and p the mean effective stress.

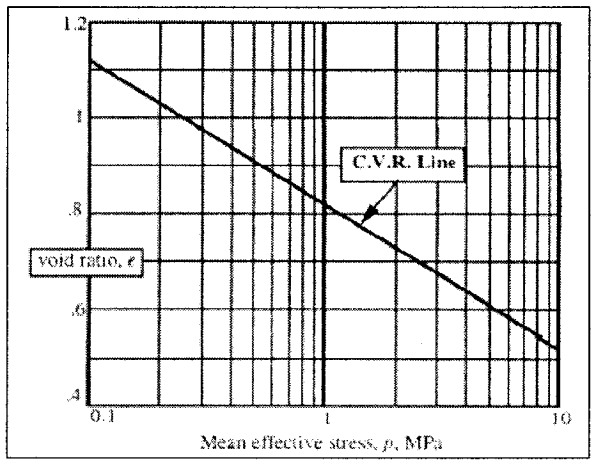

Figure 3.3 Casagrande C.V.R Line for Sacramento River Sand (after Lee (1965))

Critical void ratio is that void ratio at which a cohesionless soil can undergo deformation or actual flow without volume change. In general, it is a function of confining pressure, i.e., an increase in confining pressure yields a lower value of critical void ratio. Theoretically, a soil with a void ratio above the critical void ratio line for the confining pressure is subject to flow failure or liquefaction if it undergoes sufficient undrained stress, whether that stress is cyclic or monotonic (steadily increasing). However, if the void ratio is lower than the critical void ratio line for the given confining pressure, the soil will not liquefy under monotonic stress increase. Liquefaction resulting from monotonic stress increase and "initial liquefaction" occurring under cyclic stresses are not the same phenomenon. Liquefaction refers to the behavior of a mass of cohesionless soil during flow slides. For monotonic loading conditions, failure is caused by a substantial reduction in shear strength due to large increases in pore pressure and the consequent great reduction of effective stress.

Poorooshasb and Noorzad (1996) worked on simulating the cyclic simple shear behavior of loose and dense sand under constant cell pressure. The study showed that the

liquefaction of a sand sample falling below the Casagrande critical void ratio line depends on how far the state point is from the line representing the compact state line, the magnitude and duration of the earthquake it must resist. The compact state line traces a line parallel to the Casagrande critical void ratio line in the space of e vs. p. During the compact state the response of the granular sample to stress change is reversible. i.e. it behaves as an elastic material and as a result, plastic deformation does not take place due to the strong interlocked particles.

Roscoe et al. (1958) extended the Casagrande concept and presented a conclusive study proving the concept of critical void ratio using the simple shear test. The test results were in function of the void ratio and horizontal displacement for a constant normal stress. It was observed that the volumetric strain can be either positive or negative depending upon the initial void ratio and the level of deformation, but when the ultimate state is achieved, the volume change stops and the soil deforms under constant-volume condition reaching the critical void ratio associated with the normal stress under which the test is performed. For the same tests, results were also developed for the void ratio versus the shear stress. It was readily apparent that for a constant normal stress an ultimate unique critical void ratio can be reached. Furthermore, at this state a condition where the granular material deforms under constant volume, constant normal stress and constant shear stress was achieved.

Taking advantage of the above particular situation, Poorooshasb (1961) realized that when an element is undergoing constant shear deformation, it will reach a critical state condition under which it will continue to deform without any change in void ratio and effective stresses. He called this special case "the critical state".

3.2.2 The Concept of the Critical State Line

A soil is said to be in critical state when it undergoes large shear deformations at constant volume, constant shear and normal effective stress (Schofield and Wroth, 1968). The locus of all critical state points from all shear tests (drained and undrained) on a soil is called the Critical State Line (C.S.L.). The critical state line is plotted in a three-dimensional state space. The state space consists of the two stress components, the shear stress (τ) and the normal effective stress (σ'), and the void ratio (e) of the sample. The use of this space is permissible only if the soil material is isotropic. The line representing the critical state which is also known as the Casagrande Critical Void Ratio Line traces a straight line in the e-σ subspace if the σ axis is in a logarithmic scale. Figure 3.4 shows what is referred to as a state space.

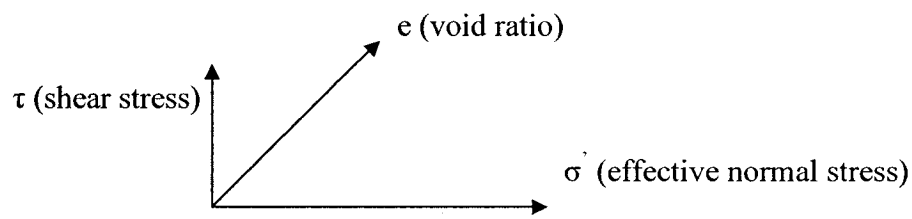

Figure 3.4 The state space

If the critical state line, whose projection onto the e-σ' plane is the Casagrande CVR line, is plotted in the state space, a curve is obtained in the state space and shown in Figure 3.5.

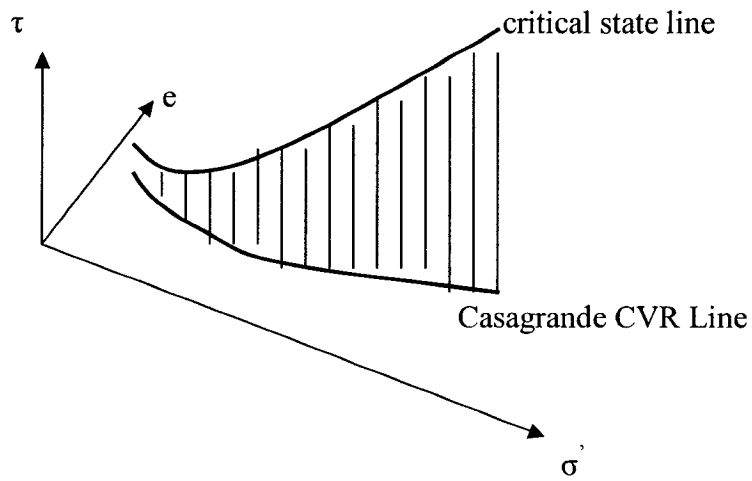

Figure 3.5 The Critical State Line

Officially the critical state line is defined as the set of states at which states the condition;

$$\frac{\partial \tau}{\partial \varepsilon} = \frac{\partial \sigma}{\partial \varepsilon} = \frac{\partial e}{\partial \varepsilon} = 0 \tag{3.9}$$

holds true at every point on the line. The projection of the critical state line in e-σ' and τ-σ' subspaces are highlighted in Figure 3.6.

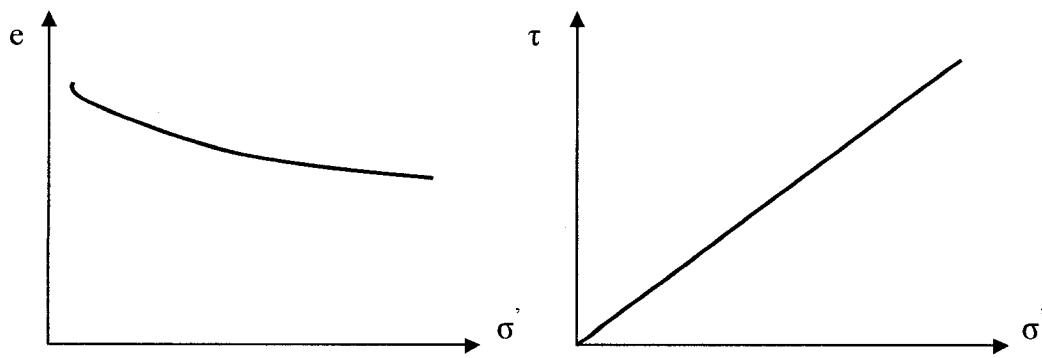

Figure 3.6 Projection of the Critical State Line

Figure 3.7 shows typical undrained shear responses of sand with different densities but the same initial confining pressure. Specimen A, which has a low relative density, is in a loose state. The sand tends to contract when sheared, resulting in a reduction of the effective confining pressure and a significant drop in shear strength, yielding flow liquefaction. Specimen B with a higher relative density is in a dense state. The sand tends to dilate after a phase transformation state (Ishihara et al. 1975), at which the reversal from contractive to dilative response takes place. Both the loose and the dense specimens finally reach a state called the critical or steady state, where q is the deviatoric stress, ε_v and ε_q are the volumetric strain and deviatoric strain, respectively.

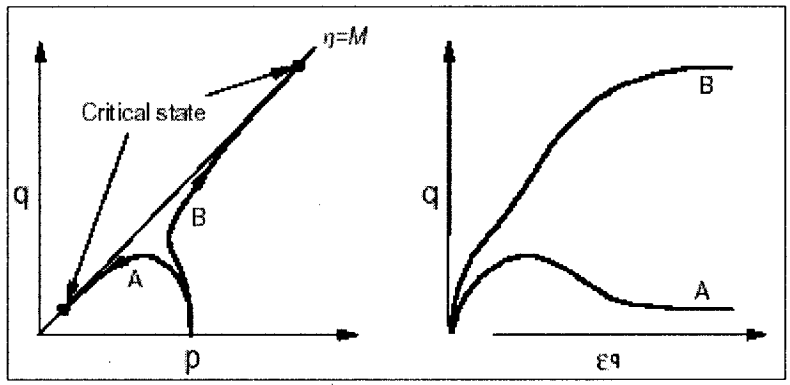

Figure 3.7 Influence of density on undrained shear (after Been and Jefferies (1985))

Figure 3.8 shows the typical undrained responses of two specimens of same density but with different initial p. The specimen A with the higher p is in a loose state, which tends to contract towards flow liquefaction. The specimen B with the lower p is in a dense state, tending to dilate. The two specimens finally reach an identical critical state because they have the same void ratio e.

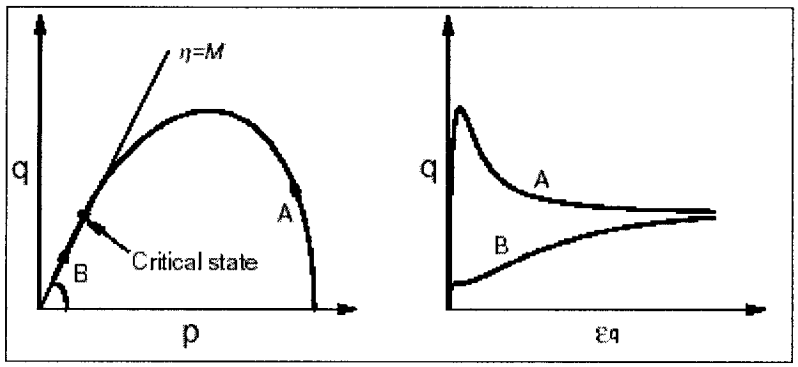

Figure 3.8 Influence of initial confining pressure

(after Been and Jefferies (1985))

In conclusion, a unique critical state line exists for a given sand sample and is the locus of all critical state points from drained and undrained tests. In addition to that, the critical state line is independent of sample preparations, drainage conditions and stress path, while on the other hand before reaching the critical state, the soil sample is strongly dependent on these factors.

3.2.3 Steady State of Deformation

Castro (1969) studied the behavior of cohesionless soils with different densities under undrained conditions. As demonstrated in Figure 3.9, three different behaviors were displayed when undergoing shearing and termed as follows: liquefaction (steady state curve), limited liquefaction (quasi-steady state curve) and dilative (strain hardening). At high strain values, these curves reach a state at which they continuously shear under constant effective stress and constant shearing resistance. This state has been defined as the steady state by Castro and Poulos (1977). The effective stress and the

shearing resistance are a function of the density, and both the loose and dense samples are able of reaching the steady state.

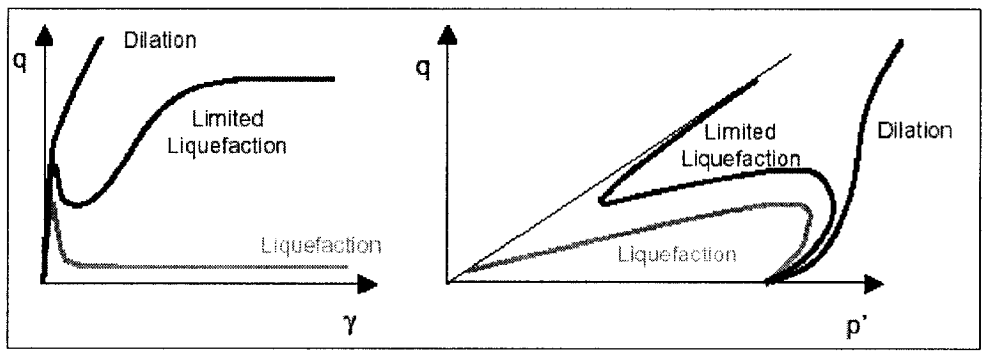

Figure 3.9 Undrained stress-strain curves and stress path behavior (after Castro (1969))

Figure 3.9 shows that very loose samples developed a peak shearing resistance at first and collapsed at a low strain level, and then a reduction in shearing resistance occurred as pore pressures increased and the specimen failed rapidly at large strains toward the steady state. Dense specimens initially dilated when shearing, with high effective stress and high shearing resistance and finally reached the steady state. Medium dense soils exhibited contractive behavior with a peak shearing resistance at relatively low strains, followed by a period of strain-softening behavior. Unlike the loose samples, medium dense soils did not strain at constant effective stress, but began to dilate at intermediate strains and eventually reached the steady state at large strain levels. On further shearing, strain hardening behavior will take place. The point of minimum effective stress, which coincided very nearly with the point of minimum shearing resistance, marked a boundary between contractive and dilative behavior that Ishihara et

al. (1975) later termed the "phase transformation boundary". At the phase transformation point, the soil strains with very nearly constant effective stress and constant shearing resistance under constant volume conditions; the conditions at this point are so close to those of the steady state that the soil is often described as being in a quasi-steady state. The range of strain is variable when the soil is in the quasi-steady state and the phase transformation points can exist for conditions in which the quasi-steady state does not develop i.e. conditions in which phase transformation occurs without a post-peak reduction in shearing resistance.

Following the concept of Casagrande Critical Void Ratio, Poulos (1981) developed the concept of steady state and stated: "the steady state of deformation for a soil mass is that state in which the mass is continuously deforming at constant volume, constant normal effective stress, constant shear stress, and constant velocity. The steady state of deformation is achieved after all particle orientation has reached a statistically steady-state condition and after all particle breakage, if any, is complete, so that the shear stress needed to continue deformations and the velocity of deformation remains constant". He also added that if the velocity of deformation is zero or changing, the sample is not in steady state. Roscoe et al. (1958) had earlier suggested the term "critical state" to describe the same phenomenon described by Poulos (1981), and indicated that there is a unique steady-state line in the void ratio versus stress space for a given sand.

Poorooshasb (1989) stated that zero velocity is a constant velocity and a very stable steady state, and therefore Poulos condition regarding zero velocity can not be met. In addition to that, he argued that the steady state of deformation and the critical state are both identical and represent a state of sample, which it will reach eventually. The term

"state" was used by Poulos in association with the steady state flow in liquids. As for Poorooshasb (1961), it was used to refer to the state of a sample. The state of a sample of sand is described by the complete set of the pertinent state parameters. A state parameter is any quantity related to the sample that can directly be measured at the moment of examination without any previous references or situations. If homogeneity and isotropy of a sample is assumed, the void ratio 'e' is considered to be a pertinent state parameter. So are the pore water pressure 'u' and the effective stress tensor represented by the stress tensor 'σ_{ij}' which is related to the total stress tensor '$*\sigma_{ij}$'. The pore water pressure and the total stress tensor are directly measurable at the moment of examination of a sample which qualifies the effective stress tensor to be a pertinent state parameter. To avoid all confusions, Poorooshasb (1989) decided to use the term ultimate state for the simple reason that if all samples went under large distortions they would end up at this ultimate state.

Desrues et al. (1996) have provided direct evidence, using a computed tomography technique to measure the local void ratios of drained triaxial sand samples, to verify the concept of the critical void ratio. They found that under the same effective confining stress, the global and local void ratios of a loose sample were the same, and equal to the local void ratio within the shear zone of a dense sample, even though the local void ratio was much higher than the global void ratio in the dense sample. Furthermore their test results showed that a "steady state" could be reached at an axial strain of 8% in drained triaxial tests on loose samples.

Based on the above arguments, the term "critical state" is preferred throughout this study to avoid possible confusion between the critical and steady state.

3.2.4 Similarity Laws

Some problems in geotechnical engineering such as stability and deformations of media can not be solved by numerical techniques due to their complexity and lack of understanding of the material response. Carrying out full scale tests on these types of problems was not cost effective. The alternative solution was to construct economical model testing which can give reliable results.

Centrifuge model testing is a major physical modeling tool available in geotechnical engineering. By artificially constructing a gravitational field, one can replicate the behavior of the in situ soil structures under various loading conditions. The model is a reduced scale version of the prototype where the soil behavior is reproduced in terms of strength and stiffness. Soil models are placed at the end of a centrifuge arm and are accelerated so that they are subjected to inertial radial acceleration field, where as far as the model is concerned, it feels like a gravitational acceleration field that can be stronger than earth's gravity. In addition to that, some models include a shaking base to ensure dynamic loading. The model container, in which the soil is held, has a stress free surface and the magnitude of stress within the soil body increases with depth at a rate related to the soil density or void ratio and the strength of the acceleration field.

In order to have valuable results in centrifuge model testing, certain laws of similarity, other than geometric similarity, must be taken into consideration. Roscoe and Poorooshasb (1963) proposed a principle using the linear theory of soil deformation. Even though more sophisticated descriptions of soil behavior were proposed using the theory of plasticity, their theory appears to be very solid and stands true so far. Using the

critical state concept, they showed that at the initial mean stresses the effective void ratio to the critical state line must be the same for both the model and the prototype. Poorooshasb (1989, 1995) extended the version by incorporating the third invariant of stress deviation tensor J_3 through the parameter θ. The principle of similarity stated that two elements are in similar states if;

$$\left[\frac{q}{p},\theta,e'\right]_{element1} = \left[\frac{q}{p},\theta,e'\right]_{element2} \tag{3.10}$$

and that if these elements are loaded in a similar fashion, then they would deform similarly and the resulting state paths would be the same. (q/p) is the stress ratio, θ is analogous to Lode's angle and e' is the effective void ratio. In other words, the mentioned above means that any two samples of a given soil will have similar strains when undergoing similar stress paths, if the difference between the initial void ratio and the void ratio at the critical state at the same normal stress is the same for both samples.

Scott (1989) used the same principle as Roscoe and Poorooshasb (1963) to examine the scaling relations between centrifuge modeling and their prototype. He also considered the behavior of the prototype and replaced the effective void ratio by the density index.

Altae and Fellenius (1994) emphasized the role of the effective void ratio by running tests on sand samples undergoing similar stress paths and examining the results. They indicated that, in order to be able to compare behaviors between the model and the prototype at various stress levels, the original soil states must be very close until it reaches the critical state line or steady state.

The usefulness of the similarity laws will become evident in the section where the constitutive formulation of sand is described under the modeling of the elastic-plastic response of non-linear soil.

3.3 THE CANAsand CONSTITUTIVE MODEL

The CANAsand model is a constitutive model which describes the soil behavior of a cohesionless granular media. The granular medium is composed mainly of sand, gravel and certain chemicals. The original CANAsand model suffered from major problems and lacked generality. Reasonable predictions of the soil behavior were impractical during a complicated loading program. Over the years it has been modified and now it can simulate and handle very complex problems such as stress reversal and static liquefaction. In the latest version of CANAsand model, two concepts, which are the critical state and the compact state, play an important role in the model since all the coefficients needed to describe the soil behavior are related to these states. It has become an integrated model which includes the critical state, the compact state concept and the state boundary surface.

3.3.1 General Features

The fundamental issue of CANAsand model is that the state of a sand element can be completely described by the state parameters: the void ratio and the parameters related to the effective stress acting on that element. The state of sand sample is defined by the

complete set of the pertinent state parameters. Any quantity that is associated with the sample and that can be directly measured at the moment of examination (during a triaxial test), is a state parameter (Poorooshasb, 1989). The effective stress, represented by the stress tensor σ_{ij}, is related to the total stress tensor, σ_{ij}^{Total}, by the following equation:

$$\sigma_{ij} = \sigma_{ij}^{Total} - u\delta_{ij} \tag{3.11}$$

where u is the pore water pressure and δ_{ij} is the Kronecker delta. Since the pore water pressure and the total stress tensor are directly measurable during the test, it would qualify the effective stress tensor to be a pertinent state parameter.

The effective stress tensor has three invariants, I_1, the first invariant of stress tensor, J_2, the second invariant of stress deviation tensor, and J_3, the third invariant of the stress deviation tensor, from which the parameters, p (the mean stress component or hydrostatic pressure) is derived, and q (the deviator component) and θ are defined respectively:

$$p = \frac{I_1}{\sqrt{3}} \text{ where } I_1 = \sigma_{ii} \tag{3.12}$$

$$q = \frac{J_2}{\sqrt{2}} \text{ where } J_2 = (s_{ij}\, s_{ij})^{1/2} \tag{3.13}$$

$$\theta = \frac{1}{3}\sin^{-1}\left(-\frac{3\sqrt{3}J_3}{2q^3}\right) \text{ where } J_3 = (s_{ij}\, s_{jk}\, s_{ki})^{1/3} \tag{3.14}$$

and the stress deviation tensor $s_{ij} = \sigma_{ij} - \sigma_{kk}\,\delta_{ij} / 3$ and θ is analogous to Lode's angle ranging from $-\pi/6$ to $\pi/6$.

Hence, the state of a sand element is represented by the three quantities (p, q, θ) and the void ratio e of the element and the state space is four dimensional of (e, p, q, θ).

3.3.2 Critical State Surface

In a four dimensional state space of (e, p, q, θ), the critical void ratio line, which is referred to as the critical state line in a state space, is transformed into a surface. The concept of the critical state surface states that there exists a surface for which the following relation holds true at every point on this surface:

$$\frac{\partial p}{\partial \varepsilon} = \frac{\partial q}{\partial \varepsilon} = \frac{\partial \theta}{\partial \varepsilon} = \frac{\partial e}{\partial \varepsilon} = 0 \qquad (3.15)$$

where the parameter ε, which is not a state parameter, is the distortion of the sample and is derived from the second invariant of the strain deviation tensor. At the critical state, unlimited distortions can take place in the sample without any change in the state parameters. If all samples are sheared far enough, they would eventually reach this critical state.

A two dimensional graphical representation of the critical state surface is practically impossible on a sheet of paper. However, there exists a relationship between the void ratio e and the mean stress component p which reduces the number of dimensions by one. The Casagrande equation for the critical void ratio line that has been shown graphically in Figure 3.3 is in the form of:

$$e = e_h - \lambda \ln (p) \qquad (3.16)$$

where e_h and λ are fundamental constants for a given sand. e_h is the value of e corresponding to a p of one kpa and λ is the slope of the Casagrande line. As a result, the number of independent variables has been reduced to three and the state space to (q, θ, e). Figure 3.10 shows the critical state surface in the (q, θ, e) space determined by Poorooshasb (1989).

One has to emphasize here that at the critical state the element flows freely and experiences unlimited deformation. Hence, the plastic shearing strain tends to infinity:

$$\dot{\varepsilon}(e,p,q,\theta) \Rightarrow \infty \tag{3.17}$$

where all the quantities within the brackets are at their critical values.

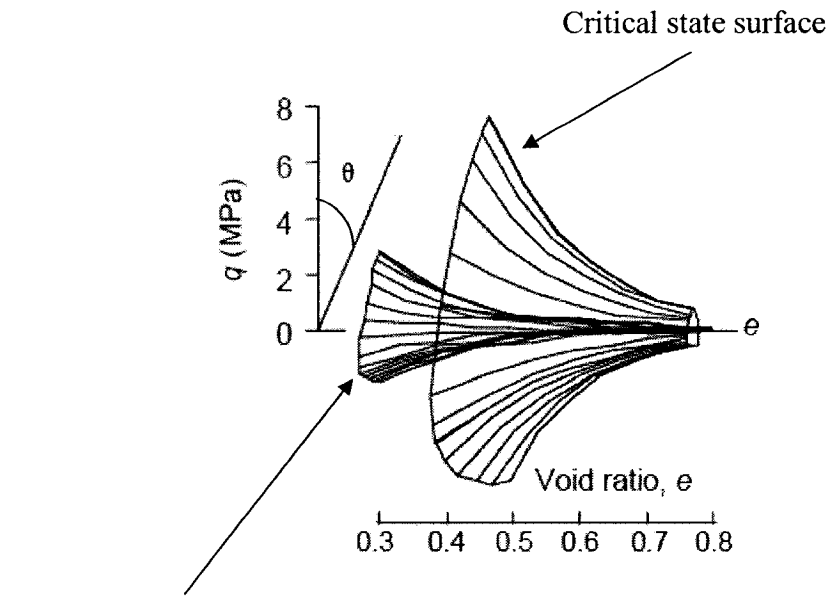

Figure 3.10 Critical and compact states for gravel (Poorooshasb (1989))

3.3.3 Compact State Surface

Poorooshasb and Noorzad (1996) postulated that the compact state lie on a surface in the state space (q, θ, e) that is parallel and similar in shape to the critical state surface. The isometric view of the compact state surface is shown in Figure 3.10. and it conforms to the laws of similarity of a cohesionless granular media when subjected to loading.

Another important hypothesis to be taken into account is that the compact state traces a line parallel to the critical void ratio line in the (e, $\ln p$) space. This is an essential consideration if the laws of similarity proposed by Roscoe and Poorooshasb (1963) and Scott (1989) are to be followed. The relationship between the void ratio e and the state parameter p at the compact state is as follows:

$$e = e_c - \lambda \ln (p) \tag{3.18}$$

where $e_c = e_h - c$, and c is the vertical distance between the Casagrande critical void ratio line and the compact void ratio line. The compact void ratio line is highlighted in Figure 3.11.

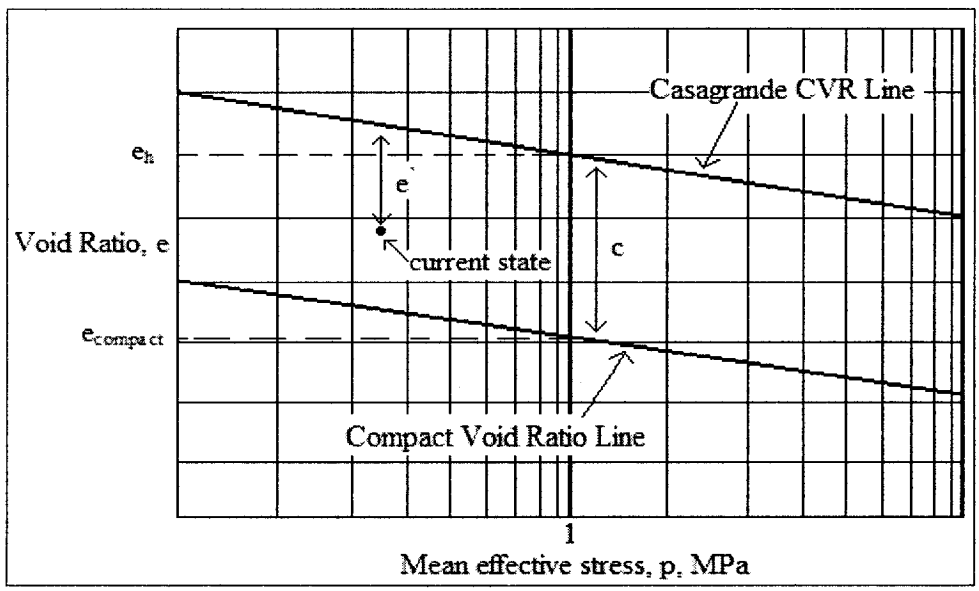

Figure 3.11 The compact void ratio line

In contrast to the critical state, the granular sample does not experience any plastic deformation at the compact state and behaves as a purely elastic material (the response to a stress change is reversible). This behavior is due to the strong interlocking between

the particles which avoids particle slippage that causes plastic deformation. At the compact state one has:

$$\dot{\varepsilon}(e, p, q, \theta) = 0 \tag{3.19}$$

where all the parameters between the brackets are at values related to the compact state.

3.3.4 The State Boundary Surface

When the various stages of the stress state (τ and σ') that a sample goes through are plotted in the stress space, the resulting curve is called a stress path. Figure 3.12 shows a possible stress path.

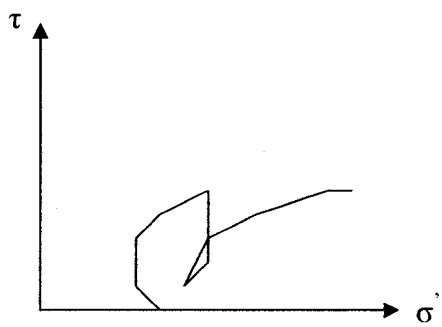

Figure 3.12 A possible stress path

In a constant (σ') drained test or what is usually referred to as a fully drained test, the state paths are parallel to the (τ, e) plane. In Figure 3.13, a state path is shown in the three dimensional space of (τ, σ', e).

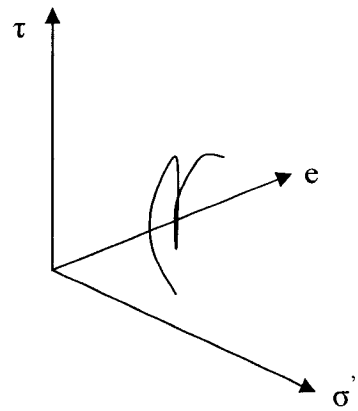

Figure 3.13 A state path in (τ, σ', e) space

Typical results of a sample tested at different void ratios under a constant normal stress (σ) or drained test are illustrated in Figure 3.14. All state paths end at the critical state where the loose samples contracting and the dense samples expanding. The boundary of all paths is called the state boundary surface and on which a sample fails at a point on that surface.

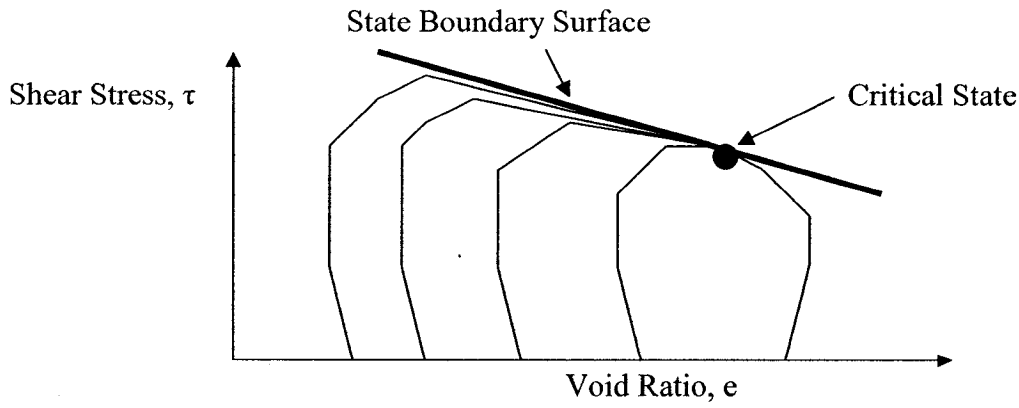

Figure 3.14 State path followed and the state boundary surface

Figure 3.15 shows the state boundary surface (SBS) plotted in the (p, q, e) domain and the position of both the critical and the compact state surfaces for a constant void ratio e. This Figure deserves some attention and certain features need to be explained as follows. In this Figure, the critical and the compact state have been reduced to bands and they trace two distinct curves on the state boundary surface. Also shown, are the yield surface and the bounding surface (Dafalias and Popov (1975)) where the former encloses the set of all stress points for which the material behaves elastic and becomes involved in all stress reversals and the latter is used when stress reversals are encountered. Such loadings are experienced by earthquakes or vibrations caused by traffic.

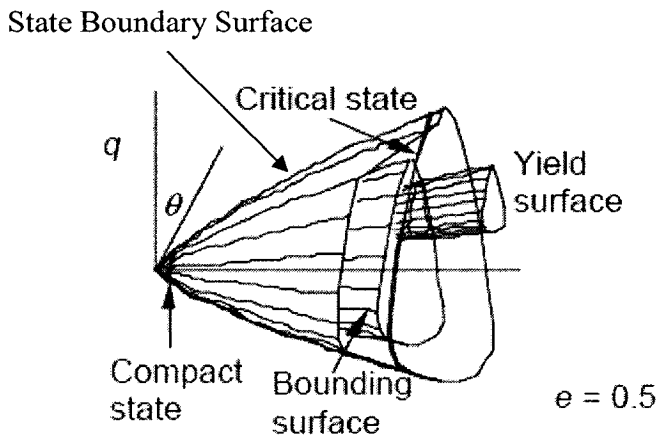

Figure 3.15 Critical, compact and state boundary surface (Poorooshasb, (1998))

Note that a sand element may experience all states within the state boundary surface (Poorooshasb, 1961). However, if the state point of a sand element lies to the left of the vertical plane holding the compact state curve and the origin then its behavior would be purely elastic, otherwise it may experience both elastic and plastic deformations. In a

drained test, when a very dense soil is subjected to loading, its stress path fails on the state boundary surface and if the loading proceeds, it follows a path on or ride on it until the critical state is reached. The state boundary surface in conjunction with the critical state surface is essential for describing the strain softening of the sample.

Reverting to Figure 3.14, a simplified version of it is shown below to analyze the maximum shear stress at the state boundary surface under a σ' constant condition.

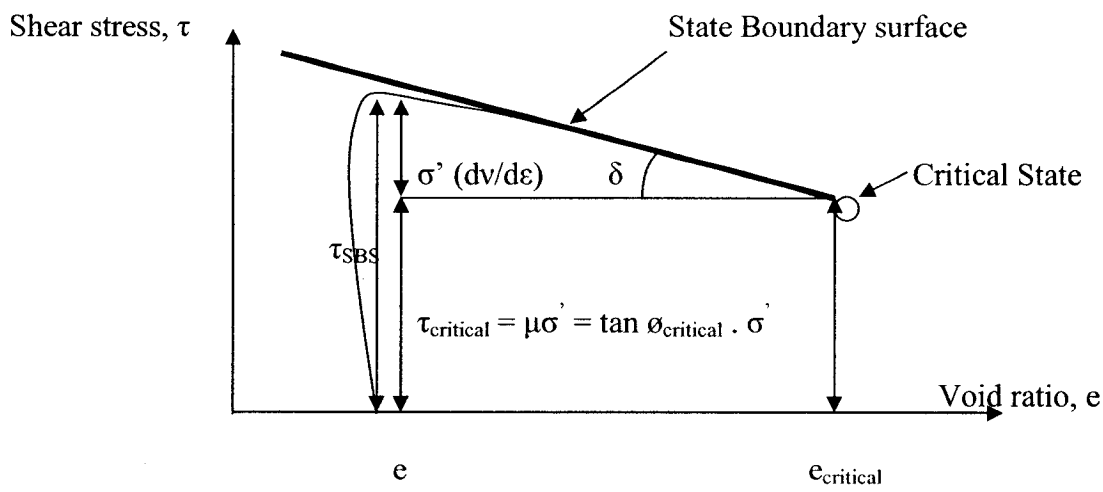

Figure 3.16 Shear stress at the state boundary surface

It may be noticed that the peak value of the state path is in the proximity of the state boundary surface. Hence, at peak stress, for a given value of σ' one can write the following equation:

$$\tau_{max} = \tau_{SBS} = \tau_{crittical} + \sigma' (dv/d\varepsilon) = \sigma' \tan \varnothing_{critical} + \sigma' (dv/d\varepsilon) \quad (3.20)$$

where $(dv/d\varepsilon)$ represents the rate of dilation, which in other words is the rate of change of volume with respect to the shearing strain. The component $\sigma' (dv/d\varepsilon)$ is known as the energy correction factor. This factor is related to the behavior of dense sand and would be

explained by considering two rough blocks sliding at an angle relative to the direction of the imposed movement, which is the direction of shearing in this case. The total energy spent in this system would be equal to the energy spent in friction plus the work done in moving the block and therefore the work done would be:

$$\tau\delta\varepsilon = \mu\sigma'\delta\varepsilon + \sigma'\delta v \qquad (3.21)$$

and which upon dividing the equation by $\delta\varepsilon$, it would result in equation 3.20. Noting that: $\tau\delta\varepsilon = \mu\sigma'\delta\varepsilon$ is the situation at the critical state and $\mu = \tan \varnothing_{critical}$.

Considering the situation relating to the peak stress point in Figure 3.16, one may write:

$$\text{Tan } \delta = \sigma' \, (dv/d\varepsilon) / (e_{critical} - e) \qquad (3.22)$$

and

$$\sigma' \, (dv/d\varepsilon) = \tan \delta \, (e_{critical} - e) \qquad (3.23)$$

where δ is the angle of interlocking between the particles. If the void ratio e of a sample is greater than the critical void ratio, $e_{critical}$, ($e > e_{critical}$) then the expression within the brackets is negative and indicates a tendency of the sand to contract, and if the void ratio, e is smaller than the critical void ratio, $e_{critical}$, ($e < e_{critical}$) then the expression is positive indicating the material has a tendency to dilate.

Equation 3.20 is rewritten as follows:

$$\tau_{max} \text{ or } \tau_{SBS} = \tau_{crittical} + \tan \delta \, (e_{critical} - e) = \sigma' \tan \varnothing_{critical} + \tan \delta \, (e_{critical} - e) \qquad (3.24)$$

which upon dividing by σ', equating the critical void ratio to the Casagrande equation and rearranging the terms, the angle of friction at maximum shear is:

$$\phi_{max} = \tan^{-1}\left(\frac{\tau_{max}}{\sigma'}\right) = \tan^{-1}\left[\frac{\tau_{critical}}{\sigma'} + \frac{\tan\delta}{\sigma'}\left(e_h - \lambda \ln \sigma' - e\right)\right] =$$

$$\tan^{-1}\left[\tan\phi_{critical} + \frac{\tan\delta}{\sigma'}\left(e_h - \lambda \ln \sigma' - e\right)\right] \qquad (3.25)$$

A sample with a void ratio e at high initial normal stress reaches the critical state point and the expression $\frac{\tan\delta}{\sigma'}\left(e_h - \lambda \ln\sigma' - e\right)$ approaches zero and $\phi_{\max} \Rightarrow \phi_{critical}$. However, the same sample at the same void ratio with low stress level results in high values of ϕ and the expression $\frac{\tan\delta}{\sigma'}\left(e_h - \lambda \ln\sigma' - e\right)$ can be quite significant. This fact explains the curvature of the $\phi_{\max}$ versus σ' of samples at same void ratio but different initial normal stress.

The rate of dilatation (dv/dε), which is associated with the energy correction factor σ' (dv/dε), plays a central role and very important one in the theory of plasticity. It was shown that during a loading process the dilatation factor is independent of the stress path a sample is following. Unless, the stress path undergoes an unloading process then the value of this dilatation factor associated with every stress point is unique.

3.4 MODELING THE ELASTIC-PLASTIC RESPONSE OF SOIL

3.4.1 Stress-Strain Response of Granular Soil

The shear strength of granular material is affected largely by the initial void ratio of the soil and can be determined from the results of a constant drained test. Typical stress-strain response of a granular soil under a drained test is shown schematically in Figure 3.17 for a loose and dense state. Here, it is seen that the stress versus shear strain relation is non-linear and depends on the material's void ratio. In dense sand there is a considerable degree of interlocking between particles, and before shear failure can take

place this interlocking must be overcome in addition to the frictional resistance at the points of contacts.

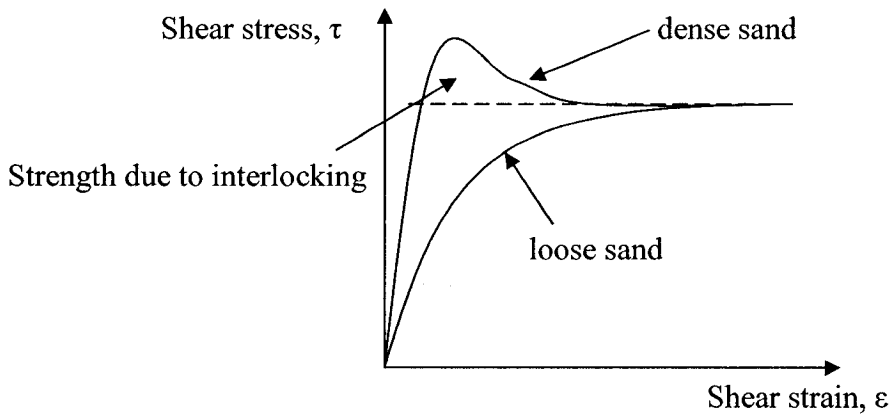

Figure 3.17 Schematic shear behaviour of sand

The stress-strain curve shows a peak stress at a relatively low strain and as interlocking is progressively overcome the stress necessary for additional strain decreases until it levels out to a residual value. The reduction in the degree of interlocking produces an increase in the volume of the specimen during shearing as characterized by the relationship between the volumetric strain ε_v and the shearing strain ε, shown schematically in Figure 3.18a. A similar relationship can be obtained in a direct shear test between the change in specimen thickness and shear displacement.

The change in volume is also shown in terms of void ratio e in Figure 3.18b. Eventually the specimen would become loose enough to allow particles to move over and around their neighbors without any further net volume change and the principal stress difference would reach an ultimate value.

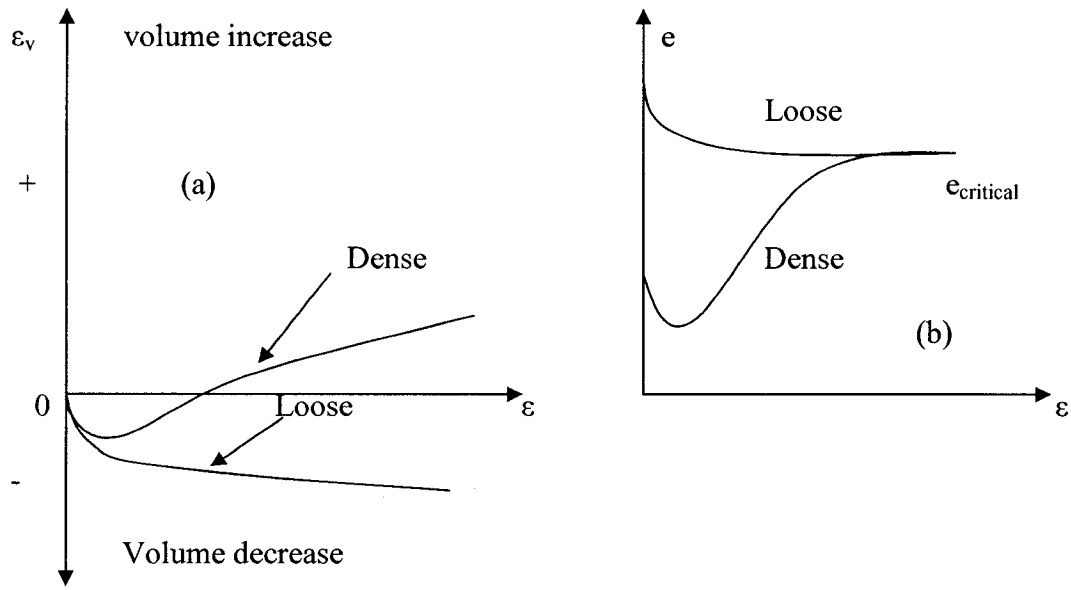

Figure 3.18 a) Volumetric behaviour, b) Change in volume in (e, ε) space

The loose sand decreases in volume as the shear is increased. The dense sample shows a slight decrease in volume during the earliest stages of loading, but with increased strain the sample increases in volume until the volume of the sample is larger than the initial volume, even though it has decreased in length. This increase in volume is referred to as dilatancy in dense sand and the rate of dilatation is represented by the gradient ($dv/d\varepsilon$) as seen earlier. At some stage between the loose and dense states, the sample changes very little in volume as shearing continues because it has reached the critical state and the void ratio at this state is referred to as the critical void ratio.

The differences in the volume change described above for loose and dense sand is a result of the different particle arrangements at the time of application of a disturbing shearing stress. The particles in loose sand tend to seek a more compact shape on

application of the shearing stress, whereas the volume of the dense sample tends to increase, because the particles must either fracture or raise out of their positions to pass by one another, thus leading to an increase in volume. In other words, the increase in volume of dense sand is due to the strong interlocking between the particles at the compact state. Considering the situation in Figure 3.19, one can obtain the angle of interlocking of a dense sand in a (τ, e) space, where the angle of friction is denoted by $\phi_{compact}$ at the compact state and $\phi_{critical}$ at the critical state.

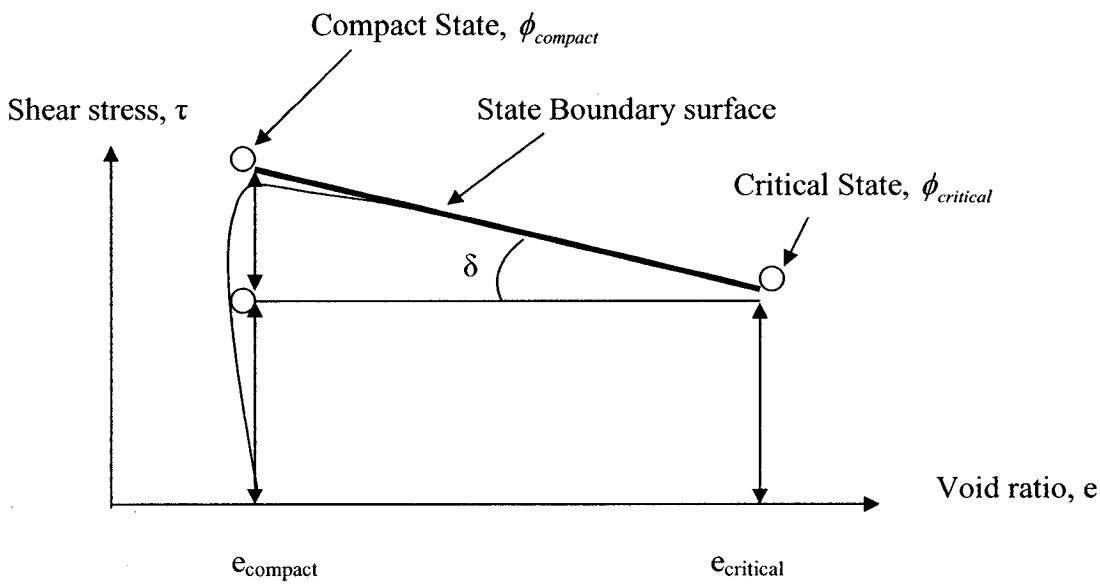

Figure 3.19 Angle of interlocking, δ

From Figure 3.19, $\text{Tan } \delta = (\phi_{compact} - \phi_{critical}) / (e_{critical} - e_{compact})$ (3.26)

and therefore, the angle of interlocking is obtained:

$\delta = \tan^{-1} [(\phi_{compact} - \phi_{critical}) / (e_{critical} - e_{compact})]$ (3.27)

Having determined the value of δ, the angle of friction of a given sand can be evaluated from Figure 3.20 using equation 3.24 which is the following:

τ_{max} or $\tau_{SBS} = \tau_{crittical} + \tan\delta\,(e_{critical} - e) = \sigma' \tan \phi_{critical} + \tan\delta\,(e_{critical} - e)$ (3.24)

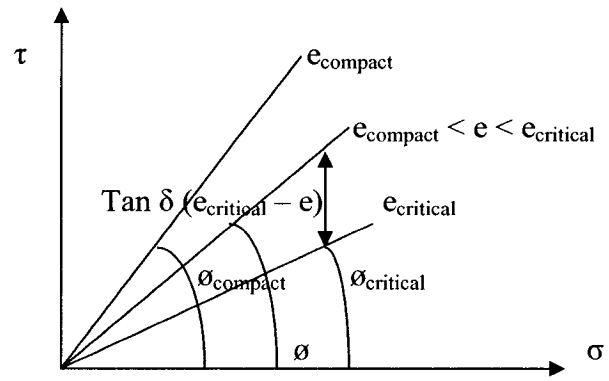

Figure 3.20 Angle of friction, ø

Similarly to equation 3.24, the angle of friction of sand at a given void ratio e can be estimated as follows:

$$\phi = \phi_{critical} + \tan\delta(e_{critical} - e) \tag{3.28}$$

Replacing tan δ by equation 3.26;

$$\phi = \phi_{critical} + (e_{critical} - e)\frac{(\phi_{compact} - \phi_{critical})}{(e_{critical} - e_{compact})} \tag{3.29}$$

where $e_{critical} = e_h - \lambda \ln(p)$ from equation 3.16 and $e_{compact} = e_c - \lambda \ln(p)$ from equation 3.18 and $e_c = e_h - c$. Substituting these two last equations in the above relationship, the angle of friction would be:

$$\phi = \phi_{critical} + (\phi_{compact} - \phi_{critical})\frac{(e_{critical} - e)}{c} \tag{3.30}$$

The stress-strain model is used to simulate the sand behavior under shearing and its response depends mainly on its density or void ratio, the applied stresses and the stress ratio.

3.4.2 Constitutive Formulation of Sand

The CANAsand constitutive model is very simple and fairly robust in solving complex elastic-plastic problems in geotechnical engineering. The aim of this section is to present a simple but realistic mathematical formulation for sands. It is an incremental elastic-plastic model, with the plastic shear strain as the hardener, which uses a non-associated flow rule.

During shear loading, the stress-strain relationship is non-linear, elastic and plastic strains occur simultaneously and are additive, whereas only elastic strains takes place during unloading and reloading (Figure 3.21).

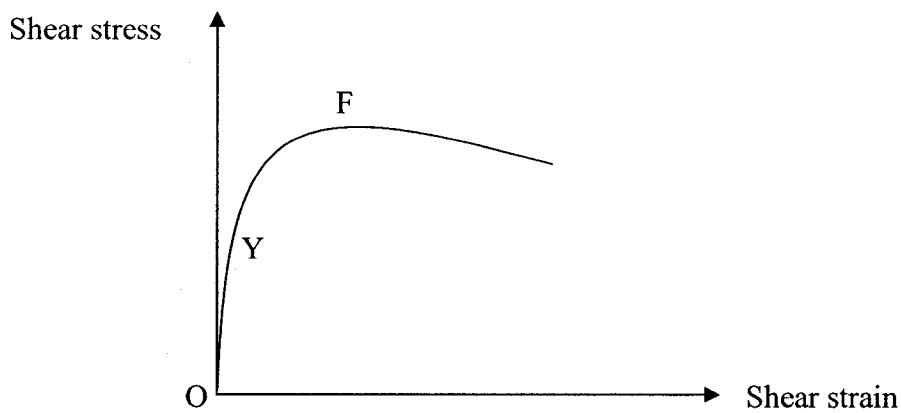

3.21 Stress-strain relationship

Initially, between point O and Y the relationship is approximately linear for most soils then beyond point Y significant plastic strain becomes apparent, i.e. Y is the point at which yielding takes place. The peak shear strength is reached at point F. Between the points of yielding and failure (Y and F) further plastic strain will occur only if the stress

is increased, but a progressively smaller stress increment is required to produce a given plastic strain increment: this characteristic is known as strain hardening. Hardening occurs only if plastic work is done. In certain cases the resistance to shear shows a decrease after the peak strength has been reached, this characteristic being referred to as strain softening.

In CANAsand model, as most elastic-plastic formulations it is not possible to correlate the magnitude of the total strain to the stress level directly, one should relate the strain increment (or rate) to the stress increment (or rate). In a two dimensional deformation, the invariants of stress are τ and σ and those of strain ε, ν with their associated rates, $\dot{\tau}$, $\dot{\sigma}$, $\dot{\varepsilon}$ and $\dot{\nu}$. It is emphasized that the upper dot denotes the rate and does not indicate any derivative with respect to time. The strain increment experienced by an element has an elastic and a plastic component. Therefore, the shear strain $\dot{\varepsilon}$ (associated with the change of shape) as well as the volumetric strain $\dot{\nu}$ (associated with the change of volume) each have two components composed of an elastic and a plastic part:

$$\dot{\varepsilon} = \dot{\varepsilon}^{e} + \dot{\varepsilon}^{p} \text{ or } d\varepsilon = d\varepsilon^{e} + d\varepsilon^{p} \tag{3.31}$$

$$\dot{\nu} = \dot{\nu}^{e} + \dot{\nu}^{p} \text{ or } dv = dv^{e} + dv^{p} \tag{3.32}$$

The elastic strain component is related to the stress increment (or its rate) by the elastic constitutive laws (Hooke's law where isotropy is almost always assumed) through the shear modulus G and the bulk modulus K, which in turn are related to the Young's modulus E, the magnitude of which is dependent on the state of the element (mostly on σ and e), and to the Poisson's ratio ν which is a constant:

$$\dot{\varepsilon}^e = \frac{\dot{\tau}}{G} \tag{3.33}$$

$$\dot{\nu}^e = \frac{\dot{\sigma}}{K} \tag{3.34}$$

where the shear modulus G = E / 2(1+ ν) and the bulk modulus K = E / 3(1-2ν) (3.35)

The direction of the plastic strain increment (or its rate) is independent of the direction of the stress increment. Therefore, the plastic strain rates are given by the following equations:

$$\dot{\varepsilon}^p = \dot{\beta}\frac{\partial \varphi}{\partial \tau} \text{ or } d\varepsilon^p = d\beta\frac{\partial \varphi}{\partial \tau} \tag{3.36}$$

$$\dot{\nu}^p = \dot{\beta}\frac{\partial \varphi}{\partial \sigma} \text{ or } d\nu^p = d\beta\frac{\partial \varphi}{\partial \sigma} \tag{3.37}$$

where φ is the so called plastic potential, ε^p the plastic shear strain and ν^p the plastic volumetric strain. Superimposing the two spaces stress (τ, σ) and strain (ε^p, ν^p) on each other, the result is similar to Figure 3.22 where shown is the unit vector along the plastic strain rate. This space will be referred to as the combined space.

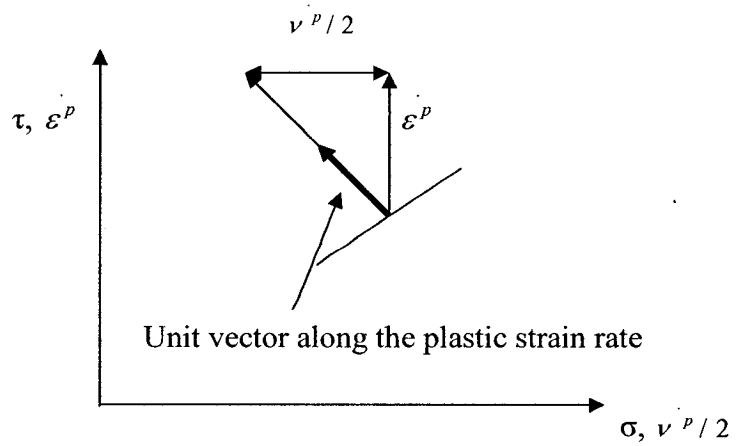

Figure 3.22 Plastic strain rate

Based on equations 3.36 and 3.37, the combined space is now covered with a set of constant φ curves. The normal to each of these curves at each stress point would indicate the direction of the unit vector showing the rate of plastic flow (normality condition). Figure 3.23 demonstrates two such curves. The function φ is the plastic potential.

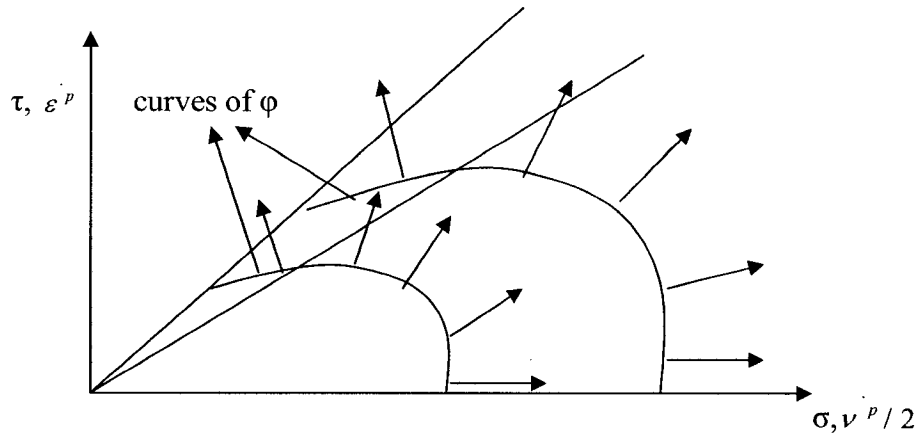

Figure 3.23 Curves of constant φ

Adding the elastic strain rates to the plastic strain rates, will result in the following relation between the strain rate and the stress rate:

$$\dot{\varepsilon} = \frac{\dot{\tau}}{G} + \dot{\beta}\frac{\partial \varphi}{\partial \tau} \tag{3.38}$$

$$\dot{\nu} = \frac{\dot{\sigma}}{K} + \dot{\beta}\frac{\partial \varphi}{\partial \sigma} \tag{3.39}$$

where:

$$\dot{\beta} = h(\frac{\partial f}{\partial \sigma}\dot{\sigma} + \frac{\partial f}{\partial \tau}\dot{\tau}) \text{ or } d\beta = h_l df = h_l(\frac{\partial f}{\partial \sigma}d\sigma + \frac{\partial f}{\partial \tau}d\tau) \tag{3.40}$$

where h_l is the loading index, $d\beta$ is an incremental quantity or constant relating strain components to the gradient of plastic potential and f is the yield function. Within the yield

surface the material behaves as an elastic material, however once the stress point approaches the surface and tends to move outside, the material behaves as an elastic-plastic material. In other words, a material is said to undergo plastic deformation if the state of stress rate is such that it increases the magnitude of the yield function *f*. In its simplest form, the yield function is assumed to be a function of state of stress and lately it has been assumed to be a function of state of the sample i.e. τ, σ and e. Thus, since the yield function f = f (τ, σ), yielding takes place if $[\frac{\partial f}{\partial \sigma}\dot{\sigma}+\frac{\partial f}{\partial \tau}\dot{\tau}] > 0$ leading the plastic flow (deformation) and no yielding takes place if $[\frac{\partial f}{\partial \sigma}\dot{\sigma}+\frac{\partial f}{\partial \tau}\dot{\tau}] \leq 0$ with no associated plastic flow. Hence the set of equations 3.38 and 3.39 can be rewritten as:

$$\dot{\varepsilon} = \frac{\dot{\tau}}{G} + h\frac{\partial \varphi}{\partial \tau} < \frac{\partial f}{\partial \sigma}\dot{\sigma} + \frac{\partial f}{\partial \tau}\dot{\tau} > \tag{3.41}$$

$$\dot{v} = \frac{\dot{\sigma}}{K} + h\frac{\partial \varphi}{\partial \sigma} < \frac{\partial f}{\partial \sigma}\dot{\sigma} + \frac{\partial f}{\partial \tau}\dot{\tau} > \tag{3.42}$$

where the symbol < > stands for singularity brackets or as Macauley bracket, i.e. $<\dot{\beta}> =$ $\dot{\beta}$ if $\dot{\beta} > 0$ and $<\dot{\beta}> = 0$ if $\dot{\beta} \leq 0$.

The form of function φ is derived from the equation of balance 3.20 which is as follows:

$$\tau = \tau_{critical} + \sigma\frac{dv^p}{d\gamma^p} = \tau_{critical} + \sigma\frac{dv^p/2}{d\gamma^p/2} = \tau_{critical} + \sigma(\frac{dv^p/2}{d\varepsilon^p}) = \tau_{critical} + \sigma(m) \tag{3.43}$$

where m is the tangent of the angle between the direction of strain rate vector and the τ axis (Figure 3.22). If an element is traced along a plastic potential curve (φ constant curves) passing through a typical stress point, equation 3.43 can be transferred to:

$$\tau = \tau_{critical} + \sigma \frac{d\tau}{d\sigma} \tag{3.44}$$

dividing by σ on both sides and rearranging the terms:

$$\frac{\tau}{\sigma} = \mu + \frac{d\tau}{d\sigma}; \text{ or}$$

$$\frac{d\tau}{d\sigma} - \frac{\tau}{\sigma} = -\mu \tag{3.45}$$

where μ is the slope of the normal projection of the critical state line into the stress space. The last equation can be written in a different form using the quotient rule:

$$\frac{d}{dx}\left(\frac{f}{g}\right) = \frac{\frac{df}{dx} g - \frac{dg}{dx} f}{g^2} \text{ and hence;}$$

$$\frac{d}{d\sigma}\left(\frac{\tau}{\sigma}\right) = \frac{d\tau}{\sigma d\sigma} - \frac{\tau}{\sigma^2} \tag{3.46}$$

dividing equation 3.45 by σ and equating it to the previous equation will result in the following:

$$\frac{d}{d\sigma}\left(\frac{\tau}{\sigma}\right) = -\frac{\mu}{\sigma} \tag{3.47}$$

integrating the last equation with respect to σ;

$$\frac{\tau}{\sigma} = \eta = -\mu \ln\left(\frac{\sigma}{\sigma_0}\right) = \mu \ln\left(\frac{\sigma_0}{\sigma}\right) \text{ or}$$

$$\sigma \exp(\eta / \mu) = \sigma_0 = \text{constant} \tag{3.48}$$

where σ_0 is the constant of integration and represents the abscissa of the point of intersection of a φ (constant contour) with the σ axis. Therefore, the plastic strain increment, φ, is derived from the plastic potential in the form of the following relationship:

$$\varphi = \sigma \bar{\varphi}(\eta) \tag{3.49}$$

where η is the stress ratio (τ / σ) and a particular form of the function $\bar{\varphi}(\eta)$ adopted by many and referred to as the critical state formulation is:

$$\bar{\varphi}(\eta) = \exp(\eta / \mu) \tag{3.50}$$

In its simplest form, the yield function is a straight ray passing through the origin of the stress space (τ, σ). The yield function is given by the simple expression:

$$f = \frac{\tau}{\sigma} = \eta \tag{3.51}$$

where η is the stress ratio. This form is only valid if the Casagrande line is parallel to the σ axis (Figure 3.11) i.e. the slope λ of the Casagrande line is equal to zero. Since this is not generally true, a slight curvature of the yield function is always present as shown in Figure 3.15 and as reported by Poorooshasb (1971). In this study the value of λ is taken to be very small and the choice regarding this assumption is a matter of convenience. Otherwise, the formulation of the stress-strain behavior would be incredibly complicated causing it to be rather impractical. In addition to that, this assumption simplifies the numerical evaluations and it provides a simple rule of similarity where two systems with similar geometry are to behave similarly for a given void ratio. If, for a granular material, the value of λ is small then both the critical and the compact void ratio are pressure insensitive and the soil is said to have a unique critical void ratio and a unique compact void ratio. Since this is a non-associated flow rule, then the direction of the plastic strain increment vector is not perpendicular to the yield loci, which are line of constant stress ratio. In other words, the plastic potential differs from the yield function and the latter does not serve as the plastic potential and it is illustrated in Figure 3.24.

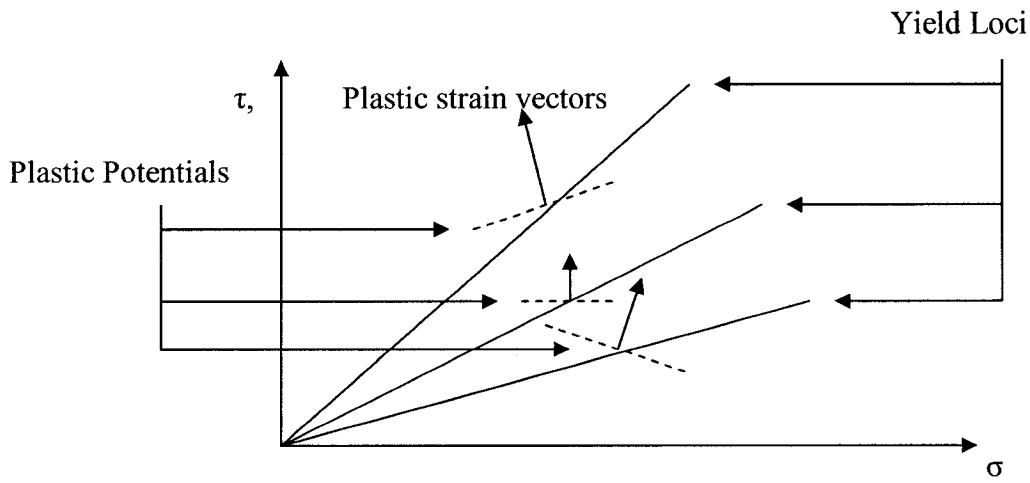

Figure 3.24 Yield loci, plastic potentials and plastic strain vectors

The value of the parameter h in equations 3.38, 3.39 and 3.39 depends on whether the element is loading, unloading or reloading. In a loading process, its value is determined using the "plastic strain curve", which is usually expressed by a hyperbolic stress-strain relation in the form:

$$\varepsilon^{p} = a\left(\frac{\eta}{\eta_{SBS} - \eta}\right) \tag{3.52}$$

where a is function of state, η the stress ratio and η_{SBS} is the value of the stress ratio at the state boundary surface (SBS) corresponding to the present value of σ and e. It may be noted that when $\eta \rightarrow \eta_{SBS}$, $\varepsilon \rightarrow \infty$ and that η_{SBS} indicates the failure of the element at the state boundary surface. When using equation 3.52, the strain hardening and strain softening of the medium can be modeled, and in the case of the strain softening, the loaded element may have to ride on the state boundary surface till it reaches the critical state (as shown in Figure 3.16). In a constant normal stress test (or constant σ drained test), the following is derived from the plastic strain curve:

$$\frac{d\varepsilon^p}{d\eta} = a\frac{(\eta_{SBS}-\eta)+\eta}{(\eta_{SBS}-\eta)^2} = \frac{a\eta_{SBS}}{(\eta_{SBS}-\eta)^2} \text{ and}$$

$$d\varepsilon^p = \frac{a\eta_{SBS}}{(\eta_{SBS}-\eta)^2}d\eta \tag{3.53}$$

On the other hand, from equation 3.36 for a constant σ test, using the critical state formulation of the plastic potential:

$$d\varepsilon^p = h\frac{\partial\varphi}{\partial\tau}d\eta$$

where dη = df, η = f = τ / σ and φ = σ exp (η / μ)

$$\text{or } d\varepsilon^p = h\frac{\partial\varphi}{\partial\tau}d\eta = h\frac{\partial\varphi}{\partial\eta}\frac{\partial\eta}{\partial\tau}d\eta = h\frac{\sigma}{\mu}\exp(\eta/\mu)\frac{1}{\sigma}d\eta = \frac{h}{\mu}\exp(\eta/\mu)d\eta \tag{3.54}$$

Equating the right hand side of equations 3.53 and 3.54:

$$\frac{a\eta_{SBS}}{(\eta_{SBS}-\eta)^2}d\eta = \frac{h}{\mu}\exp(\eta/\mu)d\eta$$

$$\text{or the parameter } h = \frac{a\mu\eta_{SBS}}{(\eta_{SBS}-\eta)^2\exp(\eta/\mu)} \tag{3.55}$$

This concludes the description of the constitutive formulation used in this study and the behavior of cohesionless granular media when subjected to shearing and CANAsand model is a non-associated one for as stated earlier where f = η, $\varphi = \sigma\bar{\varphi}(\eta)$ and where $\bar{\varphi}(\eta)$ may take the form of ($\exp(\eta/\mu)$).

4. MODELING OF THE REINFORCED EARTH PROBLEM OVERLAYING VERY SOFT SOIL

4.1 INTRODUCTION

Reclamation of grounds consists of raising the ground to the level required to make it safe for construction facilities. The ground is raised by filling and compacting the granular fill over the subgrade. If the subgrade is very soft, the fill will sink into the ground under its own weight and more fill will be required. By placing a geosynthetic reinforcement over the subgrade, the mixing of the fill and the soft soil will be avoided. The reinforcement improves the reclaimed area in such a way that it prevents the spreading of the fill over a wide area causing more uniform settlements resulting in a reduction of fill volume. In addition to that, the developed tension in the reinforcement spreads the loads away from the reclaimed area leading to a decrease in the fill settlement.

This chapter presents a brief description of the reclamation technique used for reinforcing a very soft soil. It is followed by modeling and analyzing the system under study prior to the filling. Finally, results and some discussions are presented.

4.2 THE CONSTRUCTION PROCESS OF REINFORCING A SOFT SOIL

The general construction procedure for reclaiming a very soft soil using a geosynthetic reinforcement is followed according to Lawson (1999) shown in Figure 4.1. The process of reclamation consists of laying a geosynthetic reinforcement, often a geotextile, over the very soft soil where the edges of the geosynthetic are anchored with

the soil berms. Embankment fingers are subsequently constructed to stress the reinforcement and to avoid slippage of the geosynthetic. The final step involves the spreading and the compaction of the granular fill over the reinforcement and between the embankment fingers. Therefore, the immediate settlement of the fill is due to its own weight and to the surface loading. Since the ground is very soft, very large settlements are expected to occur after the filling. Moreover the embankment fingers will undergo some settlements depending on how loose or compact the void ratio of the fill is.

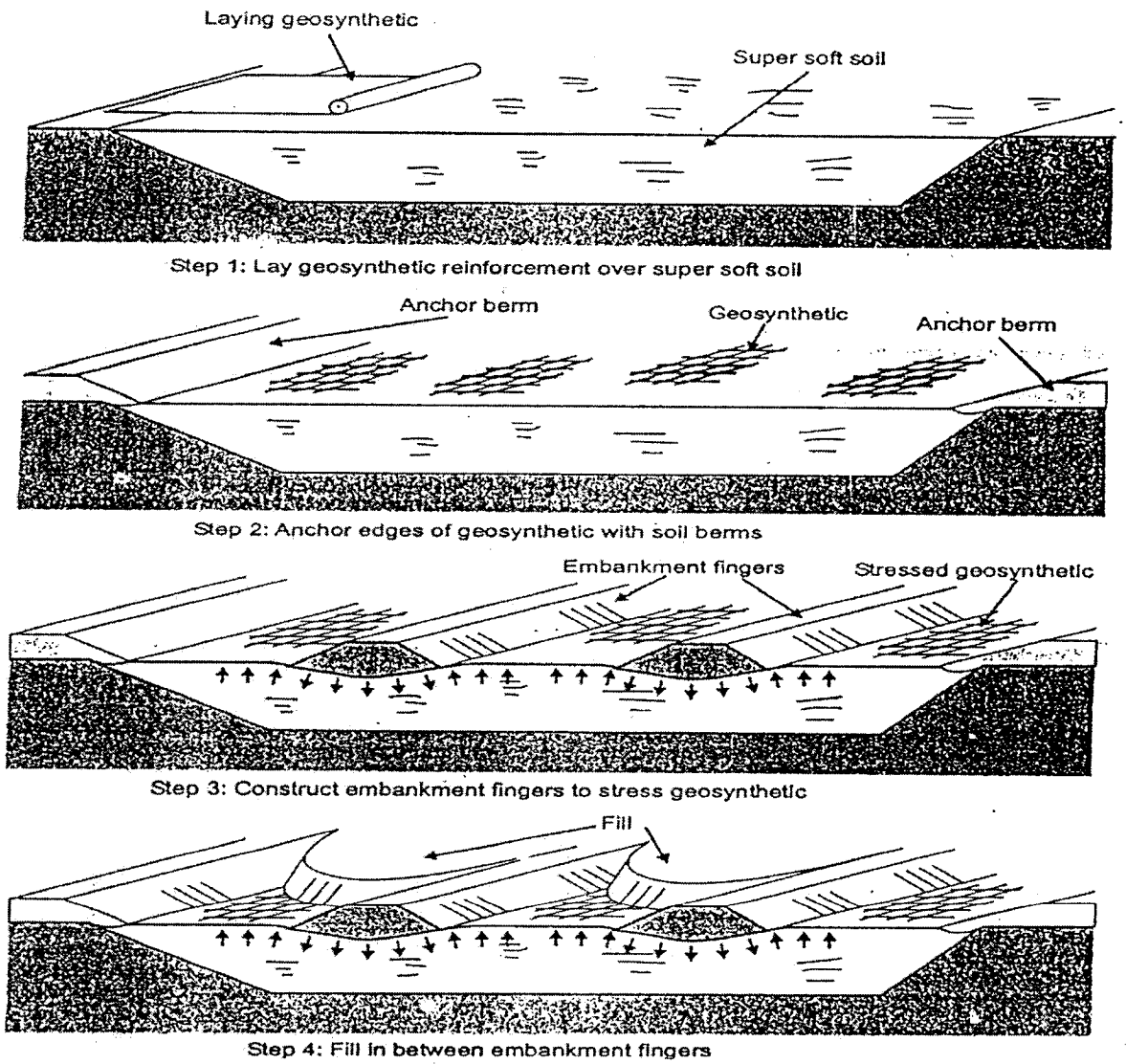

Figure 4.1 Sequence of reclamation using geosynthetic reinforcement (Lawson 1999)

4.3 MODELING OF THE REINFORCED EARTH PROBLEM

The real and idealized model under study are illustrated in Figure 4.2a and 4.2b respectively where geotextile reinforcement is placed at the base between the soft soil and the granular fill. Two embankments fingers are constructed on each side of the reinforcement to provide supports and to avoid slippage. The inclusion plays two important roles in this model. First, it acts as a reinforcement tool and second as a separator between the fill and the soft soil where the fill can sink into the ground in the case of a very soft ground.

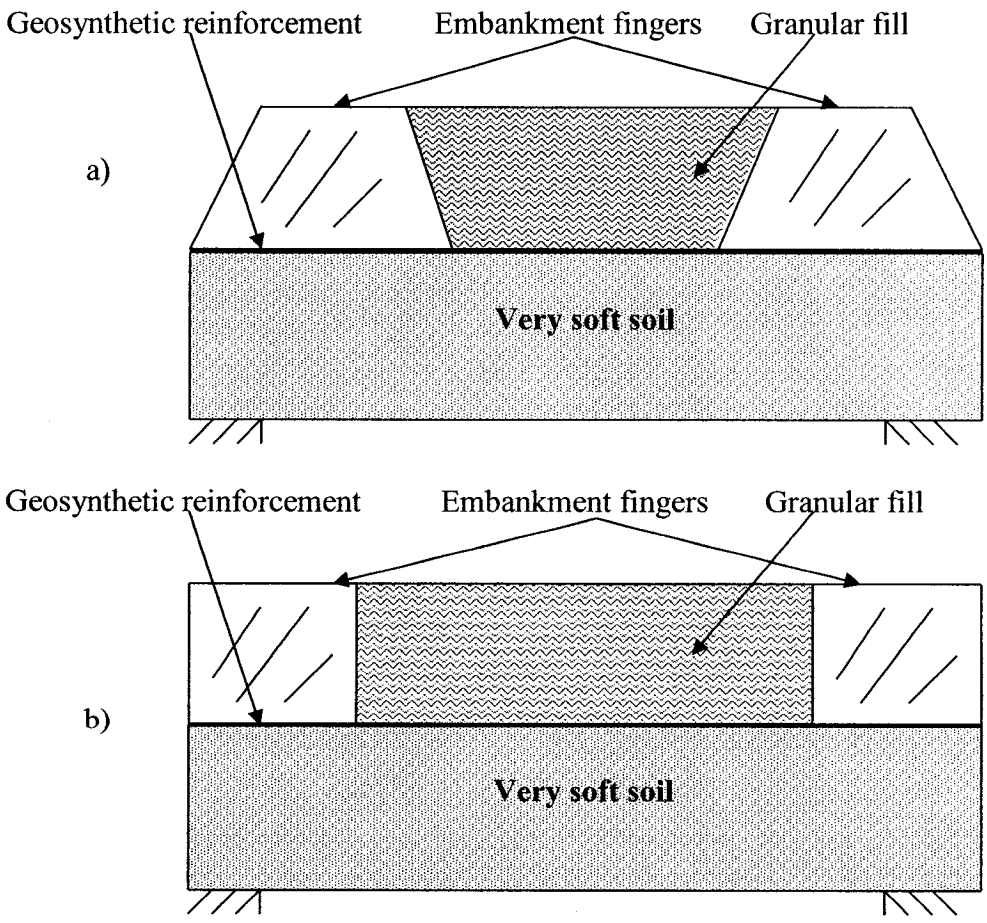

Figure 4.2 Sketch of a) Real model b) Idealized model

In order to determine the settlement profile of the system prior to the spreading of the granular fill, the system has to be converted into a system with forces. The embankment fingers are transformed into uniform load and the tension force created in the membrane is a function of its stiffness. Figure 4.3 shows the acting forces on the system.

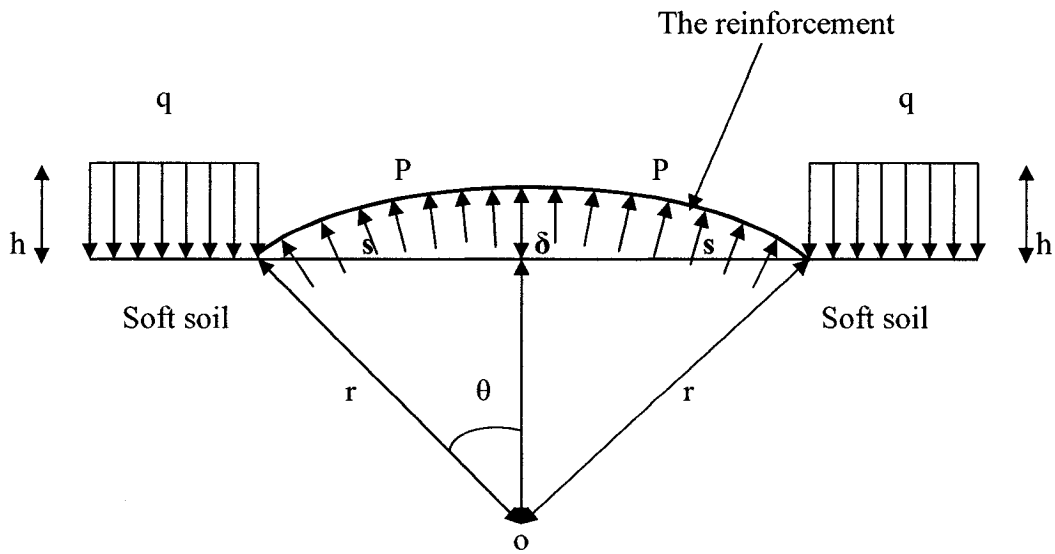

Figure 4.3 Forces acting on the system

q is the uniform load from the embankment loading and is equal to the following:

$$q = \gamma h \tag{4.1}$$

where γ (kN / m^3) is the unit weight of soil used in building the embankment fingers and h (m) is the height of the embankment fingers. P are the forces acting on the membrane from the pressure of the very soft soil and which are normal to the reinforcement. 2s is the spacing between the embankment fingers. r is the distance taken from a point o in the soft soil. θ is the angle created between the distance r and the vertical line dividing the

system into two symmetric parts. The angle θ is a function of r and s and therefore it is equal to:

$\text{Sin}\,\theta = s / r$;or; (4.2)

$\theta = \sin^{-1}(s / r)$ (4.3)

Since the system under study is symmetric and all the variables needed are incorporated in this system, one part of it is examined and can lead to an agreeable solution. Figure 4.4 shows this symmetric system.

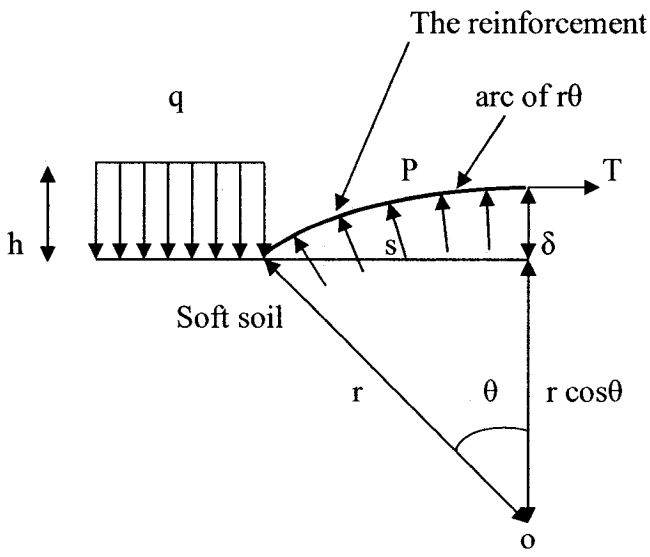

Figure 4.4 Symmetric components of the system

The arc formed by the reinforcement is equal to (rθ) and the geosynthetic strain or the stretch of the membrane is in the form of the following equation:

$$\text{Strain of membrane} = \left(\frac{r\theta - s}{s}\right) \quad (4.4)$$

δ is the settlement or deformation profile of the model when subjected to the embankment loading. The vertical projection of the distance r is r (cosθ) and it is along

the vertical center line. The tension T produced in the inclusion is in function of the stretch and the stiffness modulus of the latter. Therefore the tension T is:

$$T = \left(\frac{r\theta - s}{s} \right) E_r \tag{4.5}$$

where E_r is the stiffness modulus of the reinforcement and is taken per its unit width (kN/m). Furthermore, the tension formed in the membrane depends on the spacing between the embankment fingers and on the pressure acting on the membrane. Taking into consideration the free body diagram containing the reinforcement and the forces acting on it, the tension is determined from the Figure 4.5 and as follows:

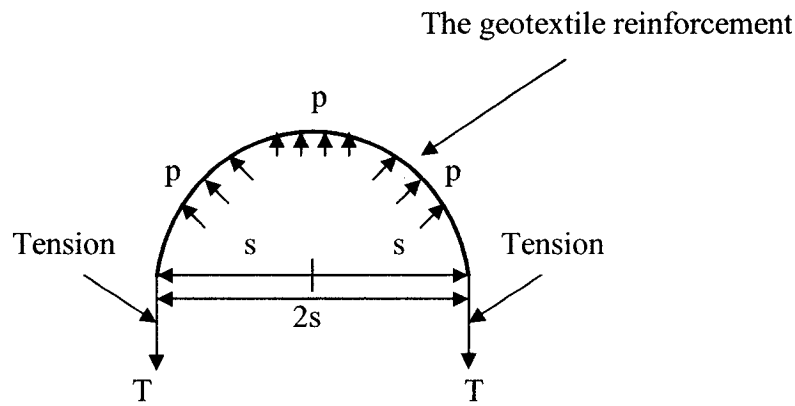

Figure 4.5 Free body diagram of the reinforcement

By taking a moment at one of the sides of the reinforcement and since the pressure is very small the uniform load p is assumed to be vertical and is transferred into a force acting in the middle of the free body diagram:

$$\sum M = 0 \Rightarrow -(T * 2s) + (p(2s) * (\frac{2s}{2})) = 0 \text{ or;}$$

$$T(2s) = P(2s) * (\frac{2s}{2}) \text{ and the tension T is:}$$

$$T = ps \tag{4.6}$$

The tension is considered to be vertical here when the distance r is equal to s and δ. The pressure or the forces p exerted on the reinforcement coming from the soft soil is almost negligible. Therefore, it is assumed to act uniformly on the surface adjacent to the embankment loading q. The loading scheme is highlighted in Figure 4.6.

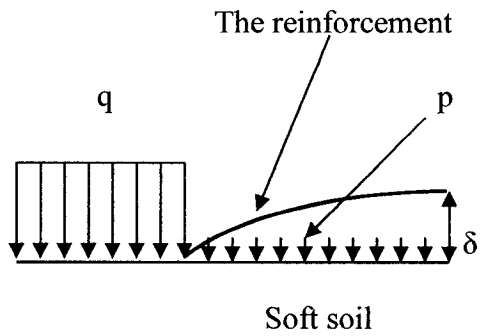

Figure 4.6 The loading of pressure p

In order to determine the loading q, it is assumed here to be the bearing capacity of a footing on a very soft soil where it is going to fail along a circular plane. The chosen solution to this particular problem is both kinematical and statically admissible and thus the solution obtains from it an upper bound and a lower bound at the same time. This can only occur if the solution is the exact answer to the problem. Figure 4.7a shows the characteristics of the stress field due to the loading q. Along these lines the value of the shear stress is at its maximum and is equal to the cohesion c of the soft soil. In Figure 4.7b, the velocity field is shown indicating the possible movements along these lines. The stress field in Figure 4.7a is divided into three zones as shown below where each zone has to be analyzed separately.

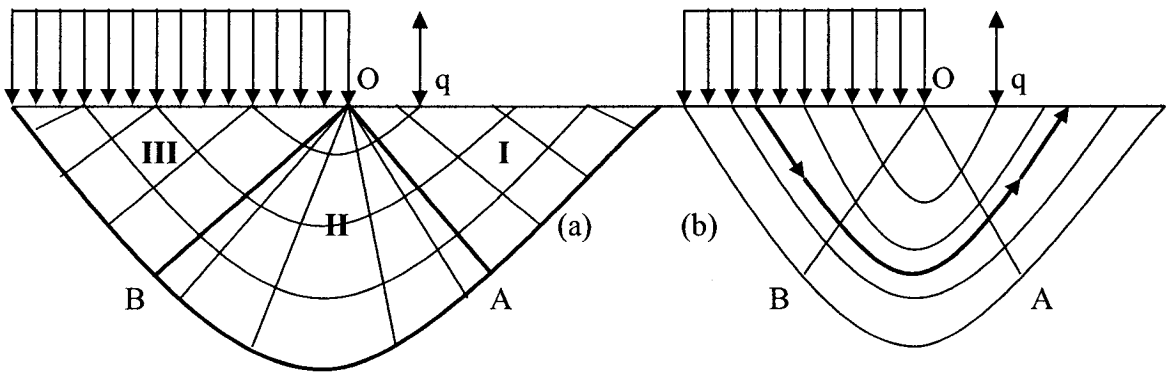

Figure 4.7 a) Characteristics of the stress field, b) Velocity field

The aim of this analysis is to determine the stress components acting on sides OA and OB; however the vertical and the horizontal stresses are to be resolved first for an element in soil in each zone. Since there is no friction involved and hence $\sigma_{xz} = 0$, the incremental equation of equilibrium can be integrated to yield to the vertical stress component, σ_{zz}. The incremental equations of equilibrium for an element in soil are:

$$\frac{\partial \sigma_{xx}}{\partial x} + \frac{\partial \sigma_{xz}}{\partial z} = 0 \tag{4.7}$$

$$\frac{\partial \sigma_{xz}}{\partial x} + \frac{\partial \sigma_{zz}}{\partial z} = \gamma \tag{4.8}$$

The second equation can be integrated and leads to the subsequent:

$$\sigma_{zz} = \gamma z \tag{4.9}$$

The horizontal stress components are based on the active and passive earth pressures exerted on sides OA and OB. In zone I, the vertical stress component, σ_{zz}, is zero in view of the fact that there is no pressure on the outside loaded area. The horizontal stress component, σ_{xx}, is based on the passive earth pressure equation where the side OA is being moved towards the soil in this zone:

$$\sigma_{xx} = \gamma z \tan^2(45 + \frac{\phi}{2}) + 2c\tan(45 + \frac{\phi}{2}) \text{ or}$$

$$\sigma_{xx} = \sigma_{passive} = K_p \gamma z + 2c\sqrt{K_p} \tag{4.10}$$

where K_p is known as the passive earth pressure coefficient, γ is the unit weight of soil, z is the depth of soil, c the cohesion, and ϕ is the angle of friction of sand. In Figure 4.7 the soil underneath the loading is very soft that it can be similar to clayey soil and thus the angle of friction ϕ is assumed to be zero. The stress component σ_{xx} is therefore equal to:

$$\sigma_{xx} = 2c \tag{4.11}$$

To satisfy the boundary condition, the Mohr's circle is shown in Figure 4.8 where the pole is located at the extreme right of the circle and denoted by PI.

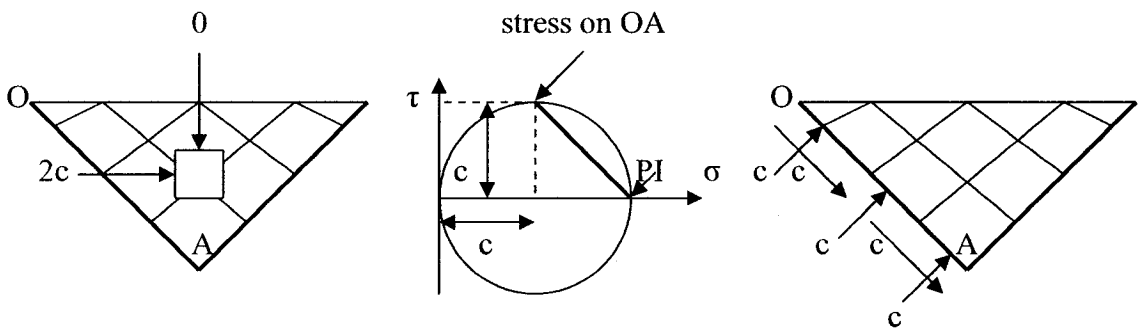

Figure 4.8 Zone I

From the Mohr's circle in Figure 4.8, the stress components acting on side OA are determined and shown on the last Figure. The shear stress τ is equal to the radius of the Mohr's circle:

$\tau = c$; and the normal stress σ is (4.12)

$$\sigma = \frac{\sigma_{zz} + \sigma_{xx}}{2} = \frac{0 + 2c}{2} = c \tag{4.13}$$

In zone III, the vertical stress component σ_{zz} is estimated using equation 4.9 as follows:

$$\sigma_{zz} = \gamma z = q \tag{4.14}$$

due to the loading q on top shown in Figure 4.7a. The horizontal stress component σ_{xx} is derived from the active earth pressure equation where in this case the side OB is being moved away from the soil in this zone:

$$\sigma_{xx} = \gamma z \tan^2(45 - \frac{\phi}{2}) - 2c\tan(45 - \frac{\phi}{2}) \text{ or}$$

$$\sigma_{xx} = \sigma_{active} = K_a \gamma z - 2c\sqrt{K_a} \tag{4.15}$$

where K_a is known as the active earth pressure coefficient and ϕ is the angle of friction of the soft soil which is still assumed zero in this case. Hence, σ_{xx} is estimated and is equal to:

$$\sigma_{xx} = \gamma z - 2c = q - 2c \tag{4.16}$$

Having determined the stress components on an element within the soil in zone III, the Mohr's circle can be complete and its representation is illustrated in Figure 4.9 with its pole denoted by PIII.

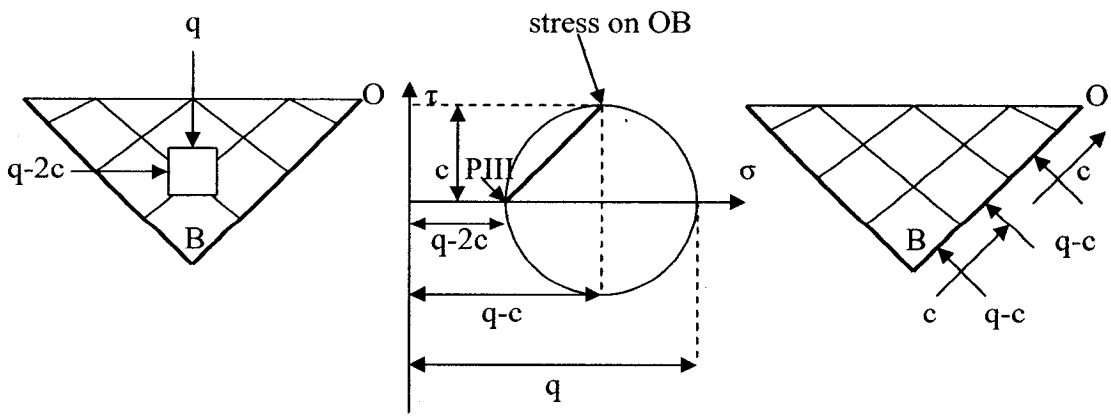

Figure 4.9 Zone III

From the Mohr's circle in Figure 4.9 the stress components acting on side OB are evaluated and shown on the last diagram. The shear stress is equal to the radius of the Mohr's circle and therefore:

$\tau = c$; and the normal stress is (4.17)

$$\sigma = \frac{\sigma_{zz} + \sigma_{xx}}{2} = \frac{q + (q - 2c)}{2} = q - c \tag{4.18}$$

Finally, the equilibrium of the radial fan zone, zone II in Figure 4.7a, is considered with the stress components applied on sides OA and OB found previously. The two sides are assumed to have the same length L and the arc formed by these two sides is equal to $\pi L/2$. Zone II is illustrated in Figure 4.10.

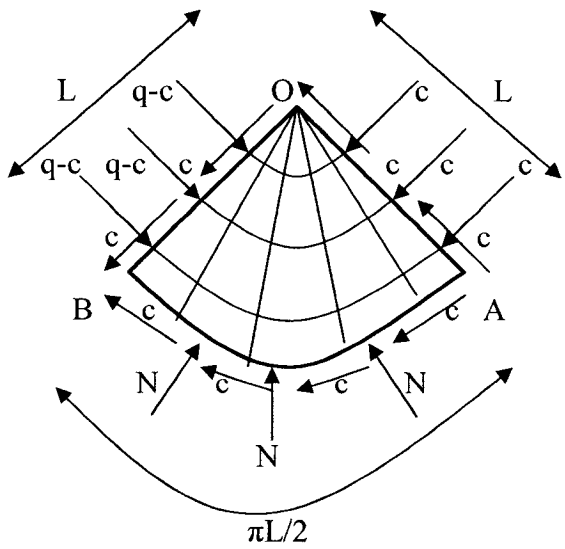

Figure 4.10 Radial fan zone: Zone II

Having determined the shear stress and the normal stress acting on sides OA and OB from zone I and zone III, a moment can be taken about point O in zone II to determine the loading q as follows:

$$cL\frac{L}{2}+c\frac{\pi L}{2}L=(q-c)L\frac{L}{2} \text{ or;}$$

$$c+\pi c=q-c \text{ or;}$$

$$q=(\pi+2)c=5.14c \tag{4.19}$$

where c is the cohesion of the soft soil.

Reverting to Figure 4.6, the pressure p is assumed to be very small as mentioned earlier and therefore it can be added to the loading q by modifying equation 4.19 to:

$$q=(2+\pi)c+p \tag{4.20}$$

By using equation 4.6 the pressure p can be determined in function of the tension created in the reinforcement and the spacing s:

$$T=ps \text{ and;}$$

$$p=\frac{T}{s} \tag{4.21}$$

and upon substituting equation 4.5 into equation 4.21 results in:

$$p=\left(\frac{r\theta-s}{s}\right)E_r\frac{1}{s} \text{ or;}$$

$$p=\left(\frac{r}{s}\theta-1\right)\frac{E_r}{s} \tag{4.22}$$

The angle θ was evaluated earlier by equation 4.3 where $\theta = \sin^{-1}(s / r)$ and replacing it in the previous equation will lead to the following relationship:

$$p=\left(\frac{r}{s}\sin^{-1}\left(\frac{s}{r}\right)-1\right)\frac{E_r}{s} \tag{4.23}$$

Swapping the value of p in equation 4.20 with equation 4.23, the outcome will be:

$$q=(2+\pi)c+\left(\frac{r}{s}\sin^{-1}\left(\frac{s}{r}\right)-1\right)\frac{E_r}{s} \text{ or;} \tag{4.24}$$

$$q-(2+\pi)c=\left(\frac{r}{s}\sin^{-1}\left(\frac{s}{r}\right)-1\right)\frac{E_r}{s} \text{ or;}$$

$$[q-(2+\pi)c]\frac{s}{E_r}=\left(\frac{r}{s}\sin^{-1}\left(\frac{s}{r}\right)-1\right) \text{ or;}$$

$$1+[q-(2+\pi)c]\frac{s}{E_r}=\left(\frac{r}{s}\sin^{-1}\left(\frac{s}{r}\right)\right) \tag{4.25}$$

In order to have a simpler relationship and to reduce the number of variables in the last equation, the value (r / s) is taken equal to ξ:

$$\xi=\left(\frac{r}{s}\right) \text{ and where;} \tag{4.26}$$

$$\frac{1}{\xi}=\left(\frac{s}{r}\right) \tag{4.27}$$

Equation 4.25 is rewritten using equation 4.26 and 4.27 as shown below:

$$1+[q-(2+\pi)c]\frac{s}{E_r}=\left(\xi\sin^{-1}\left(\frac{1}{\xi}\right)\right) \text{ or;}$$

$$\xi\sin^{-1}\left(\frac{1}{\xi}\right)=1+[q-(2+\pi)c]\frac{s}{E_r} \tag{4.28}$$

The very last equation is a highly nonlinear one and it is solved by using Maple, a comprehensive computer software for advanced mathematics. Hence solving equation 4.28 will result in finding the variable ξ which will result in determining the variable r as well. The vertical projection of r is r ($\cos\theta$) on Figure 4.11. Since θ is also found due to the fact that is related to r and s by equation 4.3, therefore it will lead to estimate the deformation δ of the system under study. As stated earlier, the deformation here is caused by the embankment loading and its profile is shown in Figure 4.11.

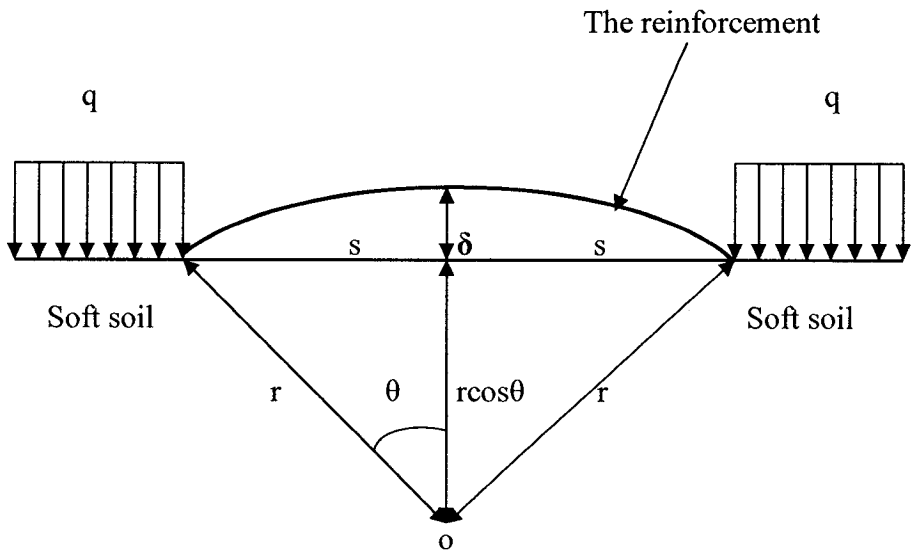

Figure 4.11 Settlement profile

The settlement profile δ is determined from Figure 4.11 in function of r and θ as follows:

$\delta = r - r\cos\theta$ or;

$$\delta = r(1-\cos\theta) \tag{4.29}$$

4.4 RESULTS AND DISCUSSION

In this section the results of some settlement profiles of the system under study are presented. The parametric study is carried out through the parameters q, c, s and E_r which are respectively the loading from the embankment fingers, the cohesion of the very soft soil, the spacing between the embankment fingers and the stiffness modulus of the reinforcement. In order to determine the settlement, equation 4.28 has to be solved with the four given parameters described above. In addition, the height h of the embankment

fingers is considered to be another important parameter by its relation to the loading q by equation 4.1 stated earlier as follows:

$q = \gamma h$

where the unit weight of soil γ, used to construct the embankment fingers, is taken to be 20 kN/m^3 in this present study. For the first settlement profile the height h of the embankments fingers is assumed to be 3 meters, the cohesion of the soft soil is 10 kPa, the spacing is 10 meters and the stiffness of the reinforcement is 800 kN/m. The result of these stated assumptions is presented in Figure 4.12.

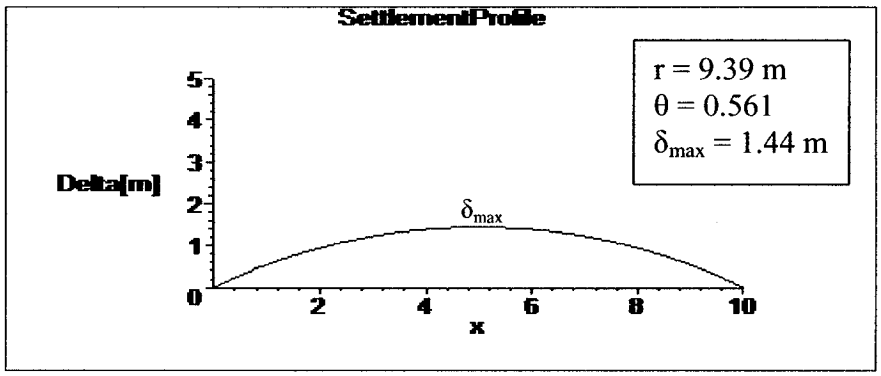

Figure 4.12 Settlement profile for a 10 meter spacing

The settlement δ is determined to be 1.44 meters with the corresponding values of r being equal to 9.39 meters and the angle θ equal to 0.56 radians. The parameters r and θ are clearly described in Figure 4.11. In this parametric study the height h of the embankment fingers is varied from 3 to 5 meters, the spacing between the fingers is varied from 8 to 12 meters and the stiffness modulus of the reinforcement is varied between 800 and 4000 kN/m. The soil cohesion or the undrained strength c of the soft ground is restricted to 10 kPa where at this value the soil is considered to be very soft behaving like a fluid.

In the second settlement profile the stiffness of the reinforcement is increased to 4000 kN/m, the cohesion is still 10 kPa, the spacing is 10 meters and the loading q is 60 kN/m^2 with a height h of 3 meters. The profile is illustrated in Figure 4.13.

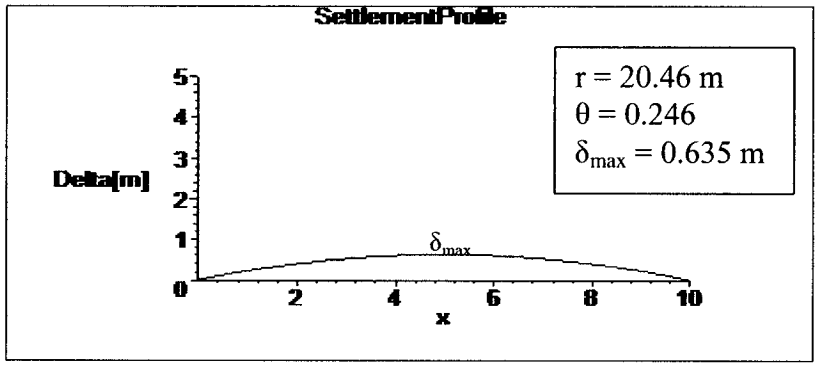

Figure 4.13 Settlement profile for a stiffness modulus of 4000 kN/m

The settlement here has decreased to 0.63 meters with an increased value of r equal to 20.46 meters and smaller angle θ of 0.24 radians. The reinforcement and its stiffness play a central role in reducing the ground settlement. The higher the stiffness modulus of the reinforcement the less settlement is expected. Moreover, the reinforcement avoids the sinking and the mixture of the fill of the embankment fingers with the soft ground and reduces the fill volume by not adding some to replace the sunken one.

In the next settlement profile the spacing is taken equal to 8 meters instead of 10 meters with a stiffness modulus of 4000 kN/m, a soil cohesion of 10 kPa, a height of 3 meters and a loading of 60 kN/m^2. The spacing has been reduced and therefore the settlement has decreased by comparing it to the previous profile where the deformation was equal to 0.63 meters. Figure 4.14 shows the ground profile for an 8 meter spacing between the embankment fingers.

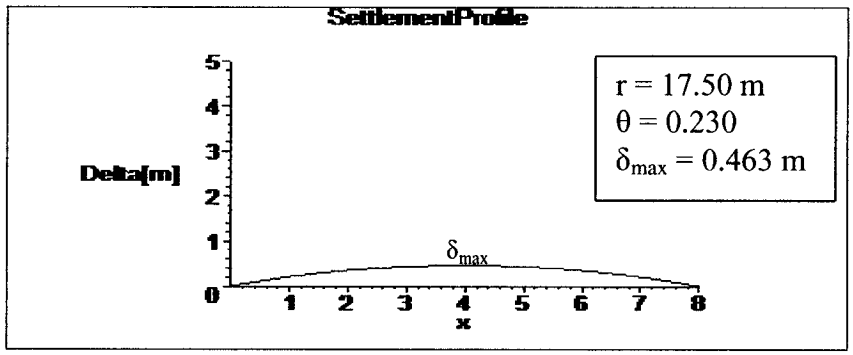

Figure 4.14 Settlement profile for an 8 meter spacing

The settlement has been reduced to 0.46 meters with decreasing values of r of and θ equal to 17.5 meters and 0.23 radians respectively. A decrease in the embankment spacing leads to a diminution in the ground settlement and on the other hand an increase in the spacing would lead to an increase in the settlement as discovered in the next outcome.

In Figure 4.15 the distance between the embankment fingers has been increased to 12 meters while previously it was assumed to be 8 and 10 meters. The other parameters remain unchanged with 4000 kN/m stiffness of the reinforcement, 10 kPa of soil strength for the soft ground and 60 kN/m^2 of loading on both sides of the inclusion. The outcome is highlighted in the Figure below.

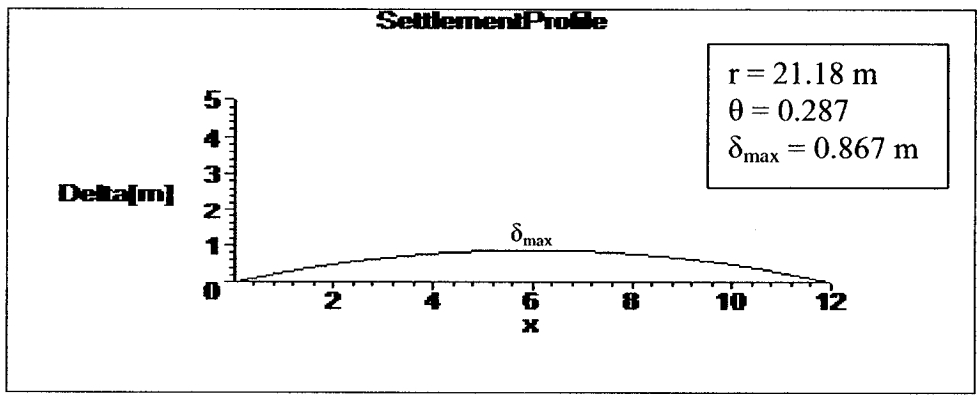

Figure 4.15 Settlement profile for a 12 meter spacing

The settlement increases to 0.86 meters as for an 8 meter spacing it was 0.46 meters and 0.63 meters for 10 m spacing. Hence, the settlement increases as the spacing enlarges between the embankment fingers. The adequate spacing in this present research would be 10 meters between two embankment fingers as it will be seen in the next chapter.

The height was assumed to be 3 meters in the previous results and in the following profile it has been increased to 4 meters with the same stiffness of 4000 kN/m, 10 kPa of soil strength and 10 meters of spacing. Therefore, the loading q is 80 kN/m^2 rather than 60 kN/m^2 acting on both sides of the system. Figure 4.16 shows the settlement profile for the above declared values.

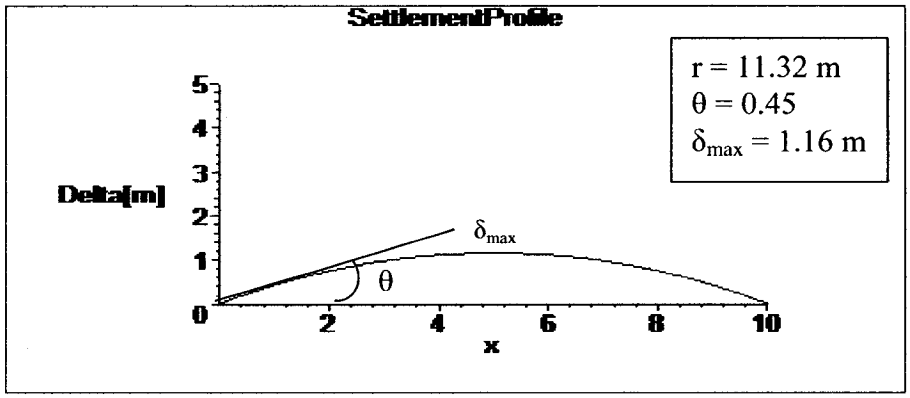

Figure 4.16 Settlement profile for a height of 4 meters and loading of 80 kN/m^2

It is observed here that the settlement, δ, has increased to 1.16 meters as compared to earlier outcomes with an r of 11.32 meters and an angle θ of 0.45 radians formed in the ground. The higher the embankment fingers are constructed, the higher the pressure will be on the reinforcement and the more the system is expected to settle. Hence, the loading q, which in terms is in function of the height, plays a fundamental role in designing a reinforced earth problem.

The angle, θ, is formed by the horizontal line and the reinforcement when subjected to ground deformation and is shown in Figure 4.16. Limitations have to be assigned to contain this angle in an acceptable degree. In this study the angle varied between 13 degrees and 32 degrees. This angle should not exceed a very high degree for the reason that it could cause damages to the reinforcement. On the other hand, some reinforcements are made of very high quality of synthetic material and may sustain larger angles.

4.5 CONCLUSION

In this chapter, a primary settlement profile has been evaluated for the system under study. The parameters involved were respectively, the loading acting on the system derived from the height of the embankment fingers, the stiffness modulus of the reinforcement, the cohesion or the undrained strength of the very soft soil and the spacing between the embankment fingers. These variables helped in estimating the settlement of such a model prior to the spreading of the granular fill between the embankment fingers.

The simulated results deduced that the parameters described above affect the system under study in many direct ways. A higher stiffness modulus of the reinforcement can decrease the settlement by creating a higher tension in the inclusion which will eventually spreads the loads away from the system. The higher the spacing between two embankment fingers is, the more the model has a tendency to settle. Finally, the height of the embankment fingers, which generates a uniform loading acting on the two ends of the

system, has an effect on increasing or decreasing the settlement depending on the design criterion.

The reinforcement plays the role of a construction expedient that prevents the local loss and the intermixing of the fill and the soft soil, allows a uniform settlement of the fingers and enhances the bearing capacity for construction equipment. Moreover, the reinforcement allows rapid construction of embankments fingers and the economies saved exceed the cost of the reinforcement. The use of reinforcement is attractive in this case because greater embankment heights can be built in any one stage which leads the reduction of construction time and to the improvement in the foundation strength during consolidation.

The final settlement of the reinforced earth system is based on the primary settlement approximated in this section. Moreover, the final settlement of the system is determined from the level at which the main settlement has attained. Therefore, it has to be taken into account that a first ground deformation has been validated in this section. The final and immediate settlement is determined after the dispersal of the granular fill between the embankment fingers and is discussed in depth in the next chapter.

5. NONLINEAR ANALYSIS OF THE REINFORCED GRANULAR LAYER

5.1 INTRODUCTION

In the previous chapter, the settlement profile was determined prior to the spreading of the granular fill. In this section, the dispersal of the granular fill between the embankments fingers will be taken into consideration to evaluate the surface profile due to the immediate settlement. The granular fill has been examined so far to be behaving in an elastic media to find the deformation. In this study, it is going to be treated as an elastic-plastic material since it is.

The stress-strain relationship or the response of the granular fill is non-linear when subjected to shear loading and depends on the materials' void ratio. During shear loading, elastic and plastic strains occur simultaneously and are additive. Therefore, it is an incremental elastic-plastic model using a non-associated flow rule, i.e. the direction of the plastic strain increment vector is not perpendicular to the yield loci which are line of constant stress ratio, used to analyze the behavior of the reinforced granular layer overlaying very soft soil.

This chapter presents the description of the constitutive equations used for analyzing and modeling the behavior of the granular fill of the system under study. Then, the integro-differential (ID) technique and the mathematical formulations used to analyze the problem are presented. It is followed by the numerical method used and the derivation of the governing equation of the problem and its characteristics. Finally, the results of the proposed model and the finite element model are illustrated.

5.2 FORMULATION OF THE CONSTITUTIVE EQUATIONS

As in most elastic-plastic formulations it is not possible to associate the magnitude of the total strain to the stress level directly, the strain is related to the stress by its rate or increment. In a two dimensional deformation, the invariants of stress are τ and σ and those of strain ε, v with their associated increments, $d\tau$, $d\sigma$, $d\varepsilon$ and dv. The strain increment experienced by an element has an elastic and a plastic component. Moreover, the strain increment is composed of two strain increments which are the shear strain $d\varepsilon$ (associated with the change of shape) and the volumetric strain dv (associated with the change of volume) and each have two components composed of an elastic and a plastic part:

$$d\varepsilon = d\varepsilon^e + d\varepsilon^p \tag{5.1}$$

$$dv = dv^e + dv^p \tag{5.2}$$

The plastic strain increment, φ, is derived from the plastic potential in the form of the following relationship:

$$\varphi = \sigma \bar{\varphi}(\eta) \tag{5.3}$$

where η is the stress ratio (τ / σ) and a particular form of the function $\bar{\varphi}(\eta)$ adopted by many and referred to as the critical state formulation is:

$$\bar{\varphi}(\eta) = \exp(\eta / \mu) \tag{5.4}$$

where μ is the slope of the projection of the critical state line into the (τ, σ) plane. In its simplest form, the yield function is a straight ray passing through the origin of the stress space (τ, σ) and is given by the simple expression:

$$f = \frac{\tau}{\sigma} = \eta \tag{5.5}$$

where η stated earlier as the stress ratio.

The shearing and the volumetric strain increments are derived from the plastic potential using the following equations:

$$d\varepsilon^p = d\beta \frac{\partial \varphi}{\partial \tau} \tag{5.6}$$

$$dv^p = d\beta \frac{\partial \varphi}{\partial \sigma} \tag{5.7}$$

where φ is the so called plastic potential, $d\varepsilon^p$ the plastic shear strain, dv^p the plastic volumetric strain and where $d\beta$ is:

$$d\beta = h_l df = h_l \left(\frac{\partial f}{\partial \sigma} d\sigma + \frac{\partial f}{\partial \tau} d\tau\right) \tag{5.8}$$

where h_l is the loading index, $d\beta$ is an incremental quantity or constant relating strain components to the gradient of plastic potential and f is the yield function. The parameter h was derived in the previous chapters when modeling the elastic-plastic behavior of non-linear soil and was determined from the plastic strain curve:

$$\varepsilon^p = a\left(\frac{\eta}{\eta_{SBS} - \eta}\right) \tag{5.9}$$

where the value of the scalar h:

$$h = \frac{a\mu\eta_{SBS}}{(\eta_{SBS} - \eta)^2 \exp(\eta/\mu)} \tag{5.10}$$

where a is function of state, η the stress ratio and η_{SBS} is the value of the stress ratio at the state boundary surface (SBS) corresponding to the current value of σ and e.

The constitutive equations described above must be expanded in order to be useful in the following analysis. Figure 5.1 shows the reinforced gravel layer overlaying very soft soil and the coordinate axis taken along and normal to the reinforced granular fill.

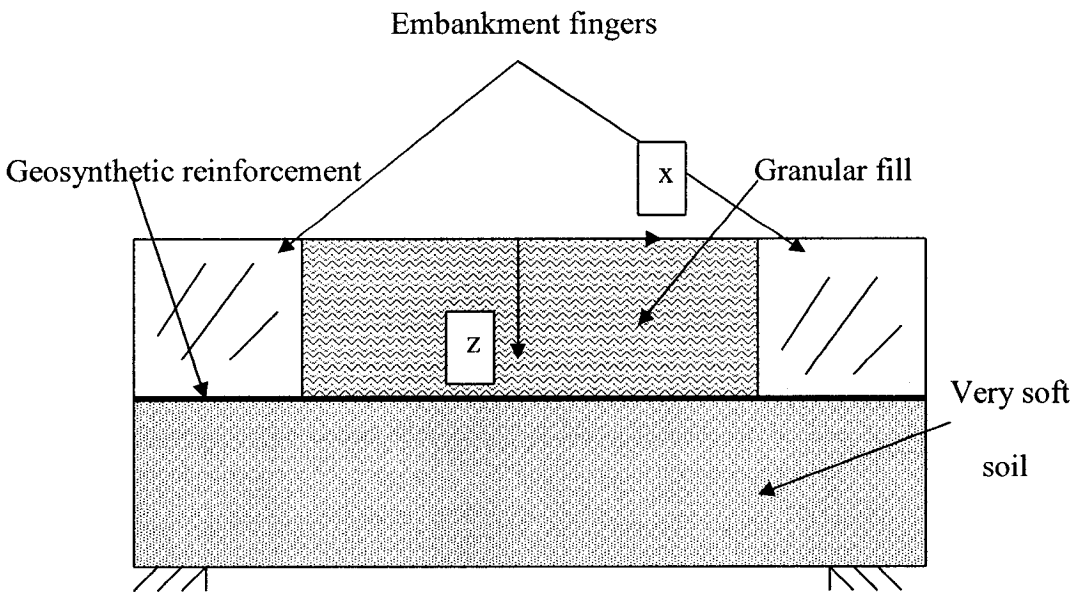

Figure 5.1 System under study and the coordinates system used in the analysis

In an incremental loading process, the plastic strain increments are derived from the plastic shear strain equation 5.6:

$$d\varepsilon^{p} = d\beta \frac{\partial \varphi}{\partial \tau}$$

where $d\beta = h_l df = h_l(\frac{\partial f}{\partial \sigma} d\sigma + \frac{\partial f}{\partial \tau} d\tau) = h_l d\eta$

based on equations 5.5 and 5.8. η is equal to the stress ratio and therefore it is in function of the stress and more precisely in function of σ_x, σ_z, τ_{xz} and τ_{zx} which are the stress

components acting on an element within the reinforced granular layer. Hence, dη can be written in the following:

$$d\eta = \frac{\partial \eta}{\partial \sigma_x} d\sigma_x + \frac{\partial \eta}{\partial \sigma_z} d\sigma_z + \frac{\partial \eta}{\partial \tau_{xz}} d\tau_{xz} + \frac{\partial \eta}{\partial \tau_{zx}} d\tau_{zx} \tag{5.11}$$

Since $\tau_{xz} = \tau_{zx}$, equation 5.11 can be rewritten as:

$$d\eta = \frac{\partial \eta}{\partial \sigma_x} d\sigma_x + \frac{\partial \eta}{\partial \sigma_z} d\sigma_z + 2\frac{\partial \eta}{\partial \tau_{xz}} d\tau_{xz} \tag{5.12}$$

From equation 5.6, $\frac{\partial \varphi}{\partial \tau}$ is derived from the plastic potential which is in the form of $\varphi = \sigma \exp(\eta / \mu)$ and where $\eta = \tau / \sigma$ as follows:

$$\frac{\partial \varphi}{\partial \tau} = \sigma \frac{1}{\mu \sigma} \exp(\tau / \mu\sigma) = \frac{1}{\mu} \exp(\tau / \mu\sigma) = \frac{\varphi}{\mu\sigma} \tag{5.13}$$

As a result, the plastic strain increment is determined in the form of:

$$d\varepsilon^p = h \frac{\varphi}{\mu\sigma} \left(\frac{\partial \eta}{\partial \sigma_x} d\sigma_x + \frac{\partial \eta}{\partial \sigma_z} d\sigma_z + 2\frac{\partial \eta}{\partial \tau_{xz}} d\tau_{xz} \right) \tag{5.14}$$

Following the coordinate system described in Figure 5.1 and differentiating with respect to each stress component, the plastic strain increments are given by the following set of equations:

$$d\varepsilon_x^p = \frac{h}{\mu} (\varphi_x \eta_x d\sigma_x + \varphi_x \eta_z d\sigma_z + \varphi_x 2\eta_{xz} d\tau_{xz}) \tag{5.15}$$

$$d\varepsilon_z^p = \frac{h}{\mu} (\varphi_z \eta_x d\sigma_x + \varphi_z \eta_z d\sigma_z + \varphi_z 2\eta_{xz} d\tau_{xz}) \tag{5.16}$$

$$d\varepsilon_{xz}^p = \frac{h}{\mu} (\varphi_{xz} \eta_x d\sigma_x + \varphi_{xz} \eta_z d\sigma_z + \varphi_{xz} 2\eta_{xz} d\tau_{xz}) \tag{5.17}$$

where: $\eta_x = \frac{\partial \eta}{\partial \sigma_x}$, $\eta_z = \frac{\partial \eta}{\partial \sigma_z}$, $\eta_{xz} = \frac{\partial \eta}{\partial \tau_{xz}}$, $\varphi_x = \frac{\partial \varphi}{\partial \sigma_x}$, $\varphi_z = \frac{\partial \varphi}{\partial \sigma_z}$ and $\varphi_{xz} = \frac{\partial \varphi}{\partial \tau_{xz}}$ (5.18)

In order to determine the equations in 5.18, the following Mohr's circle of stress is first considered with the stress components taken as the invariants of the stress tensor in two dimensions. They are defined as the radius of the Mohr's circle of stress and the distance between the center of the circle and the shear axis of the stress space, Figure 5.2.

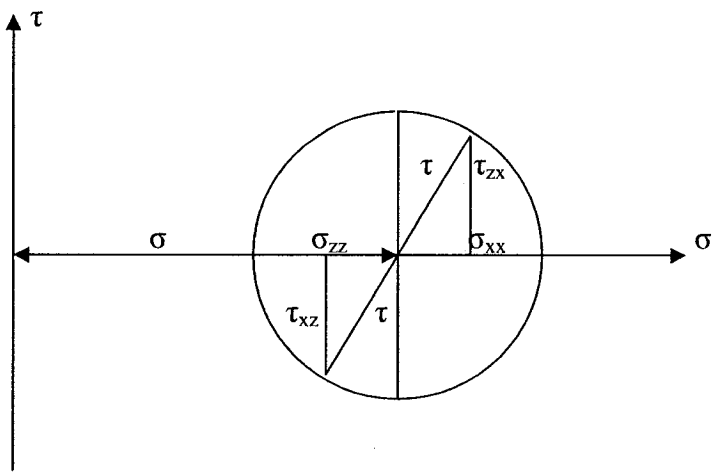

Figure 5.2 Stress invariants used in the present study

The shear stress, being the radius of the Mohr's circle, is determined as follows:

$$\tau = \left[(\frac{\sigma_x - \sigma_z}{2})^2 + \tau_{xz}{}^2 \right]^{1/2} = \frac{1}{2}\left[(\sigma_x - \sigma_z)^2 + 4(\tau_{xz})^2\right]^{1/2} = \frac{1}{2}\left[(\sigma_x - \sigma_z)^2 + (2\tau_{xz})^2\right]^{1/2} \quad \text{or;}$$

$$\tau = \frac{1}{2}\left[(\sigma_x - \sigma_z)^2 + (\tau_{xz} + \tau_{zx})^2\right]^{1/2} \tag{5.19}$$

The normal stress, being the distance between the center of the circle and the shear axis, is as follows:

$$\sigma = \left(\frac{\sigma_x + \sigma_z}{2}\right) = \frac{1}{2}(\sigma_x + \sigma_z) \tag{5.20}$$

As a result, the yield function, which was stated earlier as the stress ratio, will take the following form:

$$\eta = \frac{\tau}{\sigma} = \frac{\left\{(\sigma_x - \sigma_z)^2 + (\tau_{xz} + \tau_{zx})^2\right\}^{1/2}}{(\sigma_x + \sigma_z)} \tag{5.21}$$

The equations in 5.18 can now be derived with respect to each stress component with the plastic potential taking the form of $\varphi = \sigma\bar{\varphi}(\eta) = \sigma\exp(\eta/\mu)$ and where μ is the slope of the normal projection of the critical state line in the (τ, σ) plane, i.e. $\mu = \tan(\phi_{critical})$, as follows:

$$\eta_x = \frac{\partial\eta}{\partial\sigma_x} = \frac{1}{\sigma}\left[\frac{\sigma_x - \sigma_z}{\tau} - \eta\right] \tag{5.22}$$

$$\eta_z = \frac{\partial\eta}{\partial\sigma_z} = \frac{1}{\sigma}\left[\frac{-(\sigma_x - \sigma_z)}{\tau} - \eta\right] \tag{5.23}$$

$$\eta_{xz} = \frac{\partial\eta}{\partial\tau_{xz}} = \frac{1}{\sigma}\left[\frac{(\tau_{xz} + \tau_{zx})}{\tau}\right] = \frac{1}{\sigma}\left[\frac{2\tau_{xz}}{\tau}\right] \tag{5.24}$$

$$\varphi_x = \frac{\partial\varphi}{\partial\sigma_x} = \exp\left(\frac{\eta}{\mu}\right)\left[1 + \frac{1}{\mu}\left(\frac{\sigma_x - \sigma_z}{\tau} - \eta\right)\right] = \exp\left(\frac{\eta}{\mu}\right)\left[1 + \frac{1}{\mu}(\eta_x\sigma)\right] \tag{5.25}$$

$$\varphi_z = \frac{\partial\varphi}{\partial\sigma_z} = \exp\left(\frac{\eta}{\mu}\right)\left[1 + \frac{1}{\mu}\left(\frac{-(\sigma_x - \sigma_z)}{\tau} - \eta\right)\right] = \exp\left(\frac{\eta}{\mu}\right)\left[1 + \frac{1}{\mu}(\eta_z\sigma)\right] \tag{5.26}$$

$$\varphi_{xz} = \frac{\partial\varphi}{\partial\tau_{xz}} = \exp\left(\frac{\eta}{\mu}\right)\left[\frac{1}{\mu}\left(\frac{\tau_{xz} + \tau_{zx}}{\tau}\right)\right] = \exp\left(\frac{\eta}{\mu}\right)\left[\frac{1}{\mu}(\eta_{xz}\sigma)\right] \tag{5.27}$$

From the theory of elasticity, the stress is related to strain by the elastic constitutive law. For a homogeneous isotropic elastic material there exist only two materials constants which are E, the Young's modulus, and ν, the Poisson's ratio. All other quantities such as

the shear modulus, G, and the bulk modulus, K, are related to these two constants. The shear modulus is related to E and ν by the following relationship:

$$G = \frac{E}{2(1+\nu)} \tag{5.28}$$

Since the model is a two dimensional plain strain case, therefore the relation between stress and strain is:

$$d\varepsilon_x = \frac{1}{E}(d\sigma_x - \nu d\sigma_z) \tag{5.29}$$

$$d\varepsilon_z = \frac{1}{E}(d\sigma_z - \nu d\sigma_x) \tag{5.30}$$

$$d\varepsilon_{xz} = \frac{d\tau_{xz}}{2G} \tag{5.31}$$

The above elastic strains increments are added to the plastic strains increments, equations 5.15 to 5.17, to determine the total strain increments of the system and are given by the following set of equations:

$$d\varepsilon_x = \frac{h\varphi_x}{\mu}(\eta_x d\sigma_x + \eta_z d\sigma_z + 2\eta_{xz} d\tau_{xz}) + \frac{d\sigma_x}{E} - \frac{\nu}{E} d\sigma_z \tag{5.32}$$

$$d\varepsilon_z = \frac{h\varphi_z}{\mu}(\eta_x d\sigma_x + \eta_z d\sigma_z + 2\eta_{xz} d\tau_{xz}) - \frac{\nu}{E} d\sigma_x + \frac{d\sigma_z}{E} \tag{5.33}$$

$$d\varepsilon_{xz} = \frac{h\varphi_{xz}}{\mu}(\eta_x d\sigma_x + \eta_z d\sigma_z + 2\eta_{xz} d\tau_{xz}) + \frac{d\tau_{xz}}{2G} \tag{5.34}$$

In an isotropic elastic material the matrix of the coefficients relating stress to strain is symmetric and contains only two constants E and ν. In the elastic-plastic model, not only the matrix is non-symmetric but it is also full containing nine coefficients. The elastic strains have to be incorporated in the matrix; otherwise the matrix will become a singular

one where its determinant is zero. The relation between the strain and stress increments, equation 5.32 to 5.34, can be represented in a matrix form as:

$$\begin{bmatrix} d\varepsilon_x \\ d\varepsilon_z \\ d\varepsilon_{xz} \end{bmatrix} = \begin{bmatrix} \frac{1}{E}+\frac{h}{\mu}\varphi_x\eta_x & -\frac{\nu}{E}+\frac{h}{\mu}\varphi_x\eta_z & \frac{h}{\mu}\varphi_x 2\eta_{xz} \\ -\frac{\nu}{E}+\frac{h}{\mu}\varphi_z\eta_x & \frac{1}{E}+\frac{h}{\mu}\varphi_z\eta_z & \frac{h}{\mu}\varphi_z 2\eta_{xz} \\ \frac{h}{\mu}\varphi_{xz}\eta_x & \frac{h}{\mu}\varphi_{xz}\eta_z & \frac{1}{2G}+\frac{h}{\mu}\varphi_{xz}2\eta_{xz} \end{bmatrix} \begin{bmatrix} d\sigma_x \\ d\sigma_z \\ d\tau_{xz} \end{bmatrix} \tag{5.35}$$

For the reason of convenience the above matrix can be rewritten as:

$$\begin{bmatrix} d\varepsilon_x \\ d\varepsilon_z \\ d\varepsilon_{xz} \end{bmatrix} = \begin{bmatrix} a_{11} & a_{12} & a_{13} \\ a_{21} & a_{22} & a_{23} \\ a_{31} & a_{32} & a_{33} \end{bmatrix} \begin{bmatrix} d\sigma_x \\ d\sigma_z \\ d\tau_{xz} \end{bmatrix} \tag{5.36}$$

In the original work by Poorooshasb et al. (1996), one of the fundamentals assumptions of the integro-differential (ID) technique is that in certain type of problems one component of the displacement is taken to be equal to zero. In this present study, the lateral strain component, which is along the x direction (Figure 5.1), is zero and it leads to the following:

$$d\varepsilon_x = 0 \Rightarrow a_{11}d\sigma_x + a_{12}d\sigma_z + a_{13}d\tau_{xz} = 0 \text{ or;} \tag{5.37}$$

$$d\sigma_x = -\frac{a_{12}}{a_{11}}d\sigma_z - \frac{a_{13}}{a_{11}}d\tau_{xz} \tag{5.38}$$

substituting the above relation in equation 5.36 will result in a reduced form matrix to:

$$\begin{bmatrix} d\varepsilon_z \\ d\varepsilon_{xz} \end{bmatrix} = \begin{bmatrix} \lambda_{11} & \lambda_{12} \\ \lambda_{21} & \lambda_{22} \end{bmatrix} \begin{bmatrix} d\sigma_z \\ d\tau_{xz} \end{bmatrix} \tag{5.39}$$

where the coefficients are described below as:

$$\lambda_{11} = a_{22} - \frac{a_{21}a_{12}}{a_{11}} \tag{5.40}$$

$$\lambda_{12} = a_{23} - \frac{a_{21}a_{13}}{a_{11}} \tag{5.41}$$

$$\lambda_{21} = a_{32} - \frac{a_{31}a_{12}}{a_{11}} \tag{5.42}$$

$$\lambda_{22} = a_{33} - \frac{a_{31}a_{13}}{a_{11}} \tag{5.43}$$

Finally, the matrix in equation 5.39 needs to be inverted to read as:

$$\begin{bmatrix} d\sigma_z \\ d\tau_{xz} \end{bmatrix} = \begin{bmatrix} c_{11} & c_{12} \\ c_{21} & c_{22} \end{bmatrix} \begin{bmatrix} d\varepsilon_z \\ d\varepsilon_{xz} \end{bmatrix} \tag{5.44}$$

where the coefficients are as follows:

$$c_{11} = \frac{\lambda_{22}}{\Delta} \tag{5.45}$$

$$c_{12} = -\frac{\lambda_{21}}{\Delta} \tag{5.46}$$

$$c_{21} = -\frac{\lambda_{12}}{\Delta} \tag{5.47}$$

$$c_{22} = \frac{\lambda_{11}}{\Delta} \text{ and;} \tag{5.48}$$

$$\Delta = \lambda_{11}\lambda_{22} - \lambda_{12}\lambda_{21} \tag{5.49}$$

The inversion of equation 5.39 helped in obtaining the stress increments in function of the strain increments and will be useful in the next section where the substitution of these stress increments will occur in the incremental equation of equilibrium of an element within the reinforced granular layer. In addition to that, the inversion will facilitate the use of the integro-differential technique to determine the incremental displacement fields, which is discussed in the coming section, and make it practical in the analysis.

5.3 THE INTEGRO-DIFFERENTIAL (ID) TECHNIQUE

The integro-differential (ID) technique is a simple numerical procedure developed jointly by the researchers at Concordia University, Canada and the Institute of Lowland Technology, Saga University, Japan to analyze certain types of geotechnical engineering problems. It is called the ID technique because it evaluates an integro-differential equation depending on the type of the problem. Its analysis follows the route proposed by Hill (1963) the central feature of which was to satisfy *"as many overall conditions of equilibrium as possible"* in order to achieve an adequate and accurate solution. At the time, the work proposed by Hill did not attract much attention mainly because the evaluation of the basic equation was obtained in a closed form and essentially dealt with a very simple soil model. With the advance and the availability of computers it is now possible to obtain a numerical solution of the central equation.

The technique was applied to different types of problems encountered in geotechnical engineering such as axi-symmetric one, e.g. the analysis of pile-raft foundations (Poorooshasb et al., 1995), the nature of the negative skin friction acting on a single rigid pile to bedrock (Poorooshasb et al., 1996), the design of inclined piles (Poorooshasb et al., 1998), and plain strain problems such as ground subsidence caused by earthquake excitation (Poorooshasb, 1998) and heavily reinforced earth (Poorooshasb, 2002).

The ID technique was tested against some other numerical techniques which use finite element method (FEM) and the results between the two techniques were judged to be satisfactory and acceptable in geomechanics. The ID technique appeared to be a

powerful method of analysis and it is simple to understand. The computational requirements in applying this technique are minimal in comparison to other numerical methods. In addition to that, the value of this technique appears to be very solid and capable of handling complex elastic-plastic constitutive models that uses a non-associated flow rule such as the one encountered in reinforced earth problems.

5.4 MATHEMATICAL FORMULATION OF THE PROBLEM

An element within the reinforced granular layer shown in Figure 5.1 is considered with the stress components acting on it and is illustrated in the Figure below.

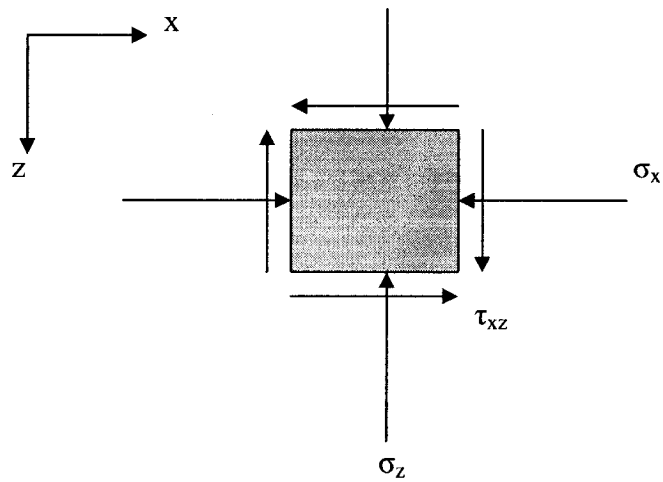

Figure 5.3 Stress components on an element within the reinforced granular layer

In the absence of body or dynamic forces the incremental equation of equilibrium along the vertical component, i.e. along the z axis shown in Figure 5.1, requires that:

$$\frac{\partial(d\sigma_z)}{\partial z}+\frac{\partial(d\tau_{xz})}{\partial x}=0 \tag{5.50}$$

Integrating equation 5.50 with respect to z leads to:

$$d\sigma_z + \int_0^z \frac{\partial}{\partial x}(d\tau_{x\xi})d\xi = 0 \tag{5.51}$$

Substituting from equation 5.44 for $d\sigma_z$ and $d\tau_{xz}$ yields the following equation:

$$c_{11}d\varepsilon_z + c_{12}d\varepsilon_{xz} + \int_0^z \frac{\partial}{\partial x}[c_{21}(x,\xi)d\varepsilon_\xi + c_{22}(x,\xi)d\varepsilon_{x\xi}]d\xi = 0 \tag{5.52}$$

Let the parameter *du* be the incremental vertical movement of the soil particles or in other words the velocity field along the z axis. The horizontal component along the x axis is by assumption zero. The strain components are deduced from the displacement field using the law of kinematics by the following equation:

$$\varepsilon_{ij} = \frac{1}{2}\left(\frac{\partial u_i}{\partial x_j} + \frac{\partial u_j}{\partial x_i}\right) \tag{5.53}$$

and therefore the strain components are as follows:

$$d\varepsilon_z = \frac{\partial}{\partial z}(du_z) \tag{5.54}$$

$$d\varepsilon_{xz} = \frac{1}{2}\frac{\partial}{\partial x}(du_z) \tag{5.55}$$

$$d\varepsilon_\xi = \frac{\partial}{\partial \xi}(du_\xi) \tag{5.56}$$

$$d\varepsilon_{x\xi} = \frac{1}{2}\frac{\partial}{\partial x}(du_\xi) \tag{5.57}$$

The above strain increments, equations 5.53 to 5.56, are to be inserted in equation 5.52 where the outcome is:

$$c_{11}\frac{\partial(du_z)}{\partial z} + c_{12}\frac{1}{2}\frac{\partial(du_z)}{\partial x} + \int_0^z [\frac{\partial}{\partial x}(c_{21}\frac{\partial(du_\xi)}{\partial \xi}) + \frac{\partial}{\partial x}(c_{22}\frac{1}{2}\frac{\partial(du_\xi)}{\partial x})]d\xi = 0 \tag{5.58}$$

Rearranging the terms in equation 5.58 and rewriting it as:

$$c_{11}\frac{\partial(du_z)}{\partial z}+c_{12}\frac{1}{2}\frac{\partial(du_z)}{\partial x}+\int_0^z[\frac{\partial c_{21}}{\partial x}\frac{\partial(du_\xi)}{\partial \xi}+c_{21}\frac{\partial^2(du_\xi)}{\partial x\partial \xi}+\frac{\partial c_{22}}{\partial x}\frac{\partial(du_\xi)}{\partial x}+c_{22}\frac{\partial^2(du_\xi)}{\partial x^2}]d\xi=0$$

(5.58a)

The following second order terms are considered to be very small and can be neglected in numerical evaluations:

$$\frac{\partial c_{21}}{\partial x}\frac{\partial(du_\xi)}{\partial \xi} \text{ and } \frac{\partial c_{22}}{\partial x}\frac{\partial(du_\xi)}{\partial x}$$

Hence, the last equation is reduced to:

$$c_{11}\frac{\partial(du_z)}{\partial z}+c_{12}\frac{1}{2}\frac{\partial(du_z)}{\partial x}+\int_0^z[c_{21}\frac{\partial^2(du_\xi)}{\partial x\partial \xi}+c_{22}\frac{\partial^2(du_\xi)}{\partial x^2}]d\xi=0 \qquad (5.59)$$

The developed formulation is intended to serve as the basis of numerical procedure proposed in the next section. In order to evaluate equation 5.59, the integral sign needs to be replaced by the sum sign ($\sum$) and it has to be written in its finite difference form. The result should be a number of linear simultaneous equations that can be solved to obtain the incremental displacement fields. The total displacement field of the system under study is estimated by adding up the incremental values. Note that the governing equation must be solved with the appropriate boundary conditions that must be satisfied and which will be presented in the subsequent section.

The governing equations developed in this chapter are not sufficient to solve the problem in soil mechanics. Therefore, the constitutive equations play an essential role and are necessary to complete the solution of the problem under study. Constitutive equations have a major impact on the solution by presenting a realistic and practical model of the soil behavior. In the last governing equation, the coefficients were based on the elastic-plastic formulation described earlier and which were necessary to be incorporated in the model to give the complete description of the soil behavior.

Constitutive models based on plasticity have contributed extensively to the development of analytical procedures. The CANAsand model, which is based on the theory of plasticity, using a non-associated flow rule has been proven in recent studies to be capable of modeling the response of sandy soils. The model can be applicable for both loose and dense sands. In the present study, CANAsand model with its developed equations is used to represent the stress-strain behavior of the granular fill spread between the embankment fingers of the system shown in Figure 5.1.

5.5 THE NUMERICAL SCHEME

In order to solve the governing equation 5.59, a finite difference mesh needs to be considered. The solution region will be covered by a network with a number of nodal points distributed at equal intervals along the x and z direction. At node *j*, the increment of vertical displacement is denoted by *x(j)*, at node *i* by *x(i)* and at node *ne* by *x(ne)*. The objective of the analysis is to evaluate the magnitude of du_z, the incremental vertical movement of the soil particles, at each and every point of the network. Following this route of reasoning, the incremental displacement field should be obtained and the total displacement field would be evaluated by adding up these incremental values. The governing equation must be solved and subjected to the appropriate boundary conditions which be must be satisfied.

The network used to evaluate the governing equation is simple and demonstrated in Figure 5.4 where the mesh has i_{max} columns, spaced regularly at Δx intervals, and j_{max} rows, spaced regularly at Δz intervals.

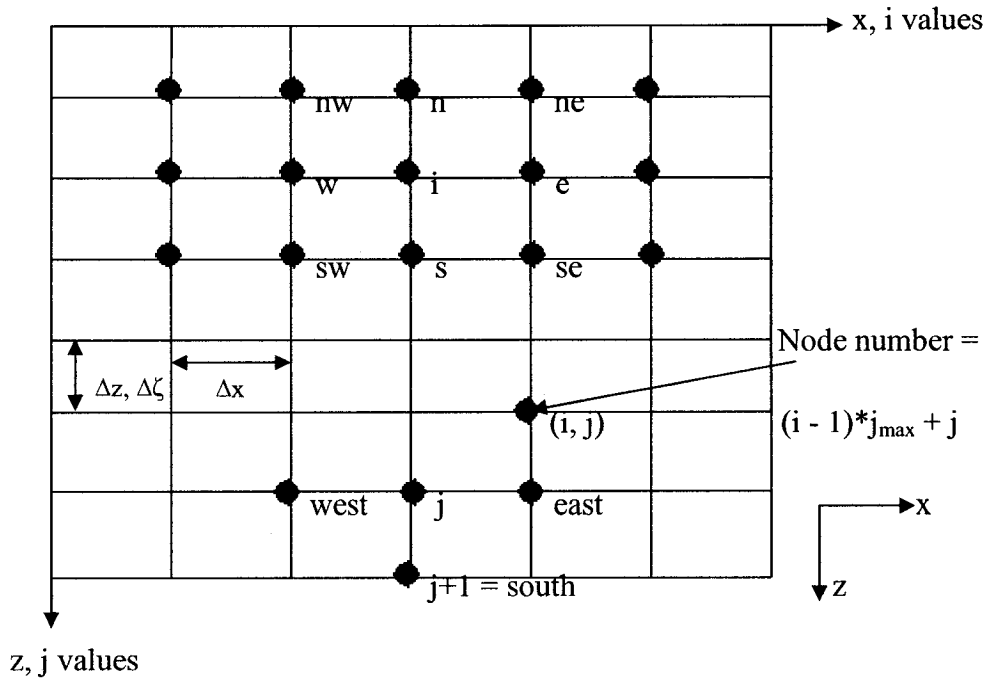

Figure 5.4 Network used in this study

Referring to Figure 5.4, it is assumed that every node has eight neighboring nodes of the net made up of horizontal and vertical lines and which are given compass abbreviations. Each node has an identification number of $n = (i - 1)*j_{max} + j$. Let Δz be kept constant therefore $\Delta\zeta = \Delta z$. In order to determine the magnitude of du_z at each and every node of the mesh, the coefficients of a set of linear simultaneous equations for $du(1)$, $du(2),\ldots du(n_{max})$ are first derived where $n_{max} = (i_{max} - 1)*j_{max} + j = i_{max} * j_{max}$ is the total number of unknown to be determined. Consider the situation at node (i, j) where the objective is to find the values of constants $a(n, 1), a(n, 2), a(n, 3),\ldots a(n, n),\ldots a(n, n_{max}+1)$ so that one of the equations of the set corresponding to the node n may be formed as:

$$a(n, 1)du(1) + a(n, 2)du(2) +\ldots a(n, n)du(n) + a(n, n+1)du(n + 1) +\ldots = a(n, n_{max} +1) \quad (5.60)$$

Equation 5.60 may be written in a matrix form as follows:

$$\begin{bmatrix} a_{11} & a_{12} & .... & a_{1n_{\max}} \\ a_{21} & a_{22} & .... & a_{2n_{\max}} \\ : & : & : & : \\ a_{n1} & a_{nn} & a_{nn+1} & a_{nn_{\max}} \end{bmatrix} \cdot \begin{bmatrix} du_1 \\ du_2 \\ du_{n+1} \\ du_{n_{\max}} \end{bmatrix} = \begin{bmatrix} a_{1,n_{\max}+1} \\ a_{2,n_{\max}+1} \\ a_{n+1,n_{\max}+1} \\ a_{n_{\max},n_{\max}+1} \end{bmatrix} \tag{5.61}$$

and therefore to find the displacement matrix *du* one can write:

$$\begin{bmatrix} du_1 \\ du_2 \\ du_{n+1} \\ du_{n_{\max}} \end{bmatrix} = \begin{bmatrix} a_{11} & a_{12} & .... & a_{1n_{\max}} \\ a_{21} & a_{22} & .... & a_{2n_{\max}} \\ : & : & : & : \\ a_{n1} & a_{nn} & a_{nn+1} & a_{nn_{\max}} \end{bmatrix}^{-1} \cdot \begin{bmatrix} a_{1,n_{\max}+1} \\ a_{2,n_{\max}+1} \\ a_{n+1,n_{\max}+1} \\ a_{n_{\max},n_{\max}+1} \end{bmatrix} \tag{5.62}$$

Note that *du* is the incremental displacement field at each and every node and the total displacement field at each node is the sum of these incremental values.

Recalling equation 5.59 and with the aid of Figure 5.4, the equation may be written in its finite difference form:

$$c_{11}\frac{\partial(du_z)}{\partial z} + c_{12}\frac{1}{2}\frac{\partial(du_z)}{\partial x} + \int_0^z [c_{21}\frac{\partial^2(du_\xi)}{\partial x \partial \xi} + c_{22}\frac{1}{2}\frac{\partial^2(du_\xi)}{\partial x^2}]d\xi = 0 \tag{5.59}$$

The first and second term on the left hand side of the equation are written as follows:

$$c_{11}\frac{\partial(du_z)}{\partial z} = c_{11}\left(\frac{x(j+1)-x(j)}{\Delta z}\right) \tag{5.63}$$

$$c_{12}\frac{1}{2}\frac{\partial(du_z)}{\partial x} = c_{12}\frac{1}{2}\left(\frac{x(e)-x(w)}{2\Delta x}\right) = c_{12}\left(\frac{x(e)-x(w)}{4\Delta x}\right) \tag{5.64}$$

The first term within the bracket under the integral is written along these lines and as mentioned earlier $\Delta\zeta = \Delta z$. With respect to the x axis, the two equations are:

$$x(n) = \left(\frac{x(ne)-x(nw)}{2\Delta x}\right) \tag{5.65}$$

and;

$$x(s)=\left(\frac{x(se)-x(sw)}{2\Delta x}\right) \tag{5.66}$$

Now with respect to z axis at a node *i* on the network the following is in place:

$x(i)=\left(\frac{x(s)-x(n)}{2\Delta x}\right)$ and replacing x(s) and x(n) by the above equations:

$$x(i)=\frac{\left(\frac{x(se)-x(sw)}{2\Delta x}-\frac{x(ne)-x(nw)}{2\Delta x}\right)}{2\Delta z}=\left(\frac{x(se)-x(sw)-x(ne)+x(nw)}{4\Delta x\Delta z}\right) \tag{5.67}$$

hence;

$$c_{21}\frac{\partial^2(du_\xi)}{\partial x\partial\xi}=c_{21}(i)\left(\frac{x(se)-x(sw)-x(ne)+x(nw)}{4\Delta x\Delta z}\right) \tag{5.68}$$

Finally, the second term within the bracket under the integral is written with respect to the x axis at a node *i* on the mesh:

$$c_{22}\frac{1}{2}\frac{\partial^2(du_\xi)}{\partial x^2}=c_{22}\frac{1}{2}\left(\frac{\frac{x(e)-x(i)}{\Delta x}-\frac{x(i)-x(w)}{\Delta x}}{\Delta x}\right)=c_{22}(i)\left(\frac{x(e)-2x(i)+x(w)}{2\Delta x^2}\right) \tag{5.69}$$

Therefore, for a typical node the corresponding ID equation is:

$$\begin{aligned}&c_{11}(j)\left(\frac{x(j+1)-x(j)}{\Delta z}\right)+c_{12}(j)\left(\frac{x(e)-x(w)}{4\Delta x}\right)+\\&\sum_{i=1}^{i=node}c_{21}(i)\left(\frac{x(se)-x(sw)-x(ne)+x(nw)}{4\Delta x\Delta z}\right)\Delta z+\\&\sum_{i=1}^{i=node}c_{22}(i)\left(\frac{x(e)-2x(i)+x(w)}{2\Delta x^2}\right)\Delta z=0\end{aligned} \tag{5.70}$$

Equation 5.70 can be expressed in a simplified form suitable for coding that is:

$$\begin{aligned}&\alpha\left(x(j+1)-x(j)\right)+\beta\left(x(e)-x(w)\right)+\\&\sum_{i=1}^{i=node}\alpha'\left(x(e)-2x(i)+x(w)\right)+\sum_{i=1}^{i=node}\beta'\left(x(se)-x(sw)-x(ne)+x(nw)\right)=0\end{aligned} \tag{5.71}$$

where the coefficients α, β, α' and β' are defined as:

$$\alpha = \frac{c_{11}}{\Delta z} \tag{5.72}$$

$$\beta = \frac{c_{12}}{4\Delta x} \tag{5.73}$$

$$\alpha' = \frac{c_{22}}{2\Delta x^2}\Delta z \tag{5.74}$$

$$\beta' = \frac{c_{21}}{4\Delta x \Delta z}\Delta z \tag{5.75}$$

The numerical scheme is complete and fully explicit. However, the governing equation (equation 5.71) must be solved and subjected to the appropriate boundary conditions which must be satisfied:

- The z axis in Figure 5.4 is a line of symmetry. Therefore at x = 0, all the labels indicating west are replaced by east. To impose this condition, it is sufficient to specify that at x = 0, nw = ne, sw = se and west = east.
- At the surface of the system, the vertical stress component σ_z must be equal to zero. This condition is satisfied by using an upper limit of the integral (at z = 0, $d\sigma_z = 0$) in equation 5.51 which is the following: $d\sigma_z + \int_0^z \frac{\partial}{\partial x}(d\tau_{x\xi})d\xi = 0$.
- At the base, the vertical stress is γD where D is the depth of the system and γ is the unit weight of the fill.
- At the vertical line, between the granular fill and the embankment fingers, the boundary of the solution region is full of shearing stress. The shearing stress at

this location is τ_{xz} and the friction based on the horizontal stress is $\sigma_{xx}\tan(\phi_{wall})$ where ϕ_{wall} is $(2/3)\phi_{fill}$.

The calculations are to take place in n stages where at each stage evaluations are performed and are added to the next stage. The material properties are then evaluated and reevaluated. Increments of stress are generated at each stage and are added at each step. The number of stages reported in this study is 10. At the base, the vertical stress is being decreased at each level by the difference of the initial pressure assumed to act at the base and the final pressure on the soil.

5.6 STRESS LOADING THE REINFORCEMENT

The reinforced layer enhances the performance of the system in reducing its settlement. Therefore, the reinforced granular layer increases the value of the stress component and as a result it increases the stiffness of the soil. The tension created in the geotextile reinforcement needs to be evaluated to be able to obtain the increase in lateral stress, $\Delta\sigma_x$. Figure 5.5 shows the position of the reinforcement at rest and the position as a result of loading.

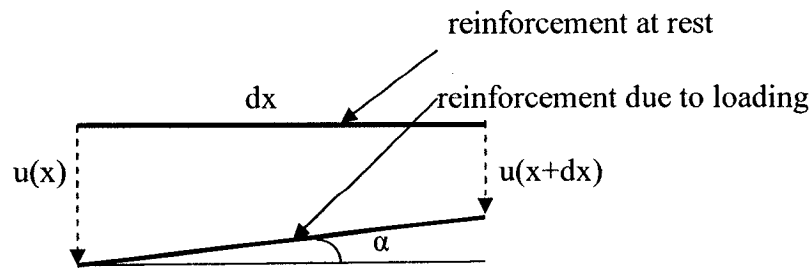

Figure 5.5 Loading of the geotextile reinforcement

At rest, the length of the reinforcement strip is dx and due to loading the length is dx/cosα. The displacements of the reinforcement due to the stress loading are shown in Figure 5.5 as u(x) and u(x+dx). The angle α is computed from Figure 5.5 as follows:

$$\tan\alpha = \frac{u(x) - u(x+dx)}{dx} \text{ and;}$$

$$\alpha = \tan^{-1}\left(\frac{u(x) - u(x+dx)}{dx}\right) \tag{5.76}$$

The change in shape of the geotextile is determined as:

$$\left(\frac{dx}{\cos\alpha} - dx\right)/dx \text{ ; Or;}$$

$$\left(\frac{1}{\cos\alpha} - 1\right) \tag{5.77}$$

And therefore the tension in the reinforcement is given by the equation:

$$T = J\left(\frac{1}{\cos\alpha} - 1\right) \tag{5.78}$$

where the parameter J denotes the stiffness modulus of the reinforcement.

Let d represents the vertical distance or the depth of the system under study. Hence, the increase in lateral stress due to the reinforcement is:

$$\Delta\sigma_x = \frac{J}{d}\left(\frac{1}{\cos\alpha} - 1\right) \tag{5.79}$$

Then, the increase in lateral stress needs to be added to the value of the horizontal component of the stress tensor in equation 5.36. In that way, the contribution from the reinforced granular layer has been taken into account in reducing the soil deformation.

5.7 CHARACTERISTICS OF THE ELASTIC-PLASTIC RESPONSE

To characterize the elastic-plastic response of the granular fill, model parameters are needed to calibrate the constitutive equations. Due to lack of experimental data necessary for the model, some index parameters and empirical coefficients are considered to obtain a plausible stress-strain relationship. As determined earlier in chapter 3, the angle of friction is in function of the void ratio by the equation:

$$\phi = \phi_{critical} + (\phi_{compact} - \phi_{critical}) \frac{(e_{critical} - e)}{c} \tag{5.80}$$

where e is the void ratio, $\phi_{compact}$ and $\phi_{critical}$ are the angles of friction at the compact state and the critical state which are respectively assumed to be 45^{o} and 25^{o}. c is the vertical distance between $e_{critical}$ and $e_{compact}$ in the *e-log p* graph shown in Figure 3.11 and in this study may be chosen as 0.5. The elastic young modulus is assumed to be in function of the current state of stress and some index parameters identifying the current state of sand such as the void ratio. In the present model, the relationship chosen to characterize the variation of the young modulus with stress and void ratio:

$$E = 1 + E_o \sigma \frac{(e_{base} - e)}{(e - e_{compact})} \tag{5.81}$$

where E_o is the initial young modulus and is estimated by the function:

$$E_o = 2G(1+\nu) \tag{5.82}$$

and G, the shear modulus:

$$G = \frac{E}{2(1+\nu)} \tag{5.83}$$

The Poisson's ratio, ν, is assumed to have a value of 0.15 for the material used.

e_{base} and $e_{compact}$ are the void ratios at the baseline and at the compact state. In the complete representation of the state boundary surface for two-dimensional stress cases, the baseline designates the loosest possible state a sample may have. "Void ratios higher than the one indicated by the baseline cannot be experienced by an element" (Poorooshasb 2002). e_{base} and $e_{compact}$ are written as:

$$e_{base} = ehbase - \lambda \ln \sigma \tag{5.84}$$

and at the compact state:

$$e_{compact} = ehcompact - \lambda \ln \sigma \tag{5.85}$$

The value of *ehbase* and *ehcompact* are considered to be 1.1 and 0.4 respectively and λ is assumed to be very small as discussed earlier in section 3.4.2 of chapter 3.

The form of the plastic strain hardening function, h, was derived earlier from the plastic strain curve expressed by hyperbolic stress-strain relation (equation 5.9) as:

$$h = \frac{a\mu\eta_{SBS}}{(\eta_{SBS} - \eta)^2 \exp(\eta / \mu)} \tag{5.86}$$

The dependence of h on the void ratio is through the parameter a. The parameter a in the model formulation describes the hardening law for the plastic moduli. This empirical coefficient may have other forms but as long as it is in function of the void ratio e the analysis remains valid (Poorooshasb 1991). In this study, it has the following form:

$$a = a_0 \frac{(e - e_{compact})}{(e_{base} - e)} \tag{5.87}$$

where a_0 is assumed to have the value of 0.1 and e is the void ratio. η_{SBS} is the maximum value η the sample may attain for a given value of e. The stress ratio at the state boundary surface, η_{SBS}, by following the form of equation 5.80 is expressed as:

$$\eta_{SBS} = \eta_{critical} + (\eta_{compact} - \eta_{critical}) \frac{(e_{critical} - e)}{c} \tag{5.88}$$

where $\eta_{compact}$ and $\eta_{critical}$ are related to $\phi_{compact}$ and $\phi_{critical}$. The above constitutive assumption may also be written as the form used in the present study which is:

$$\eta_{SBS} = \mu + (\mu_{compact} - \mu) \frac{(e_{critical} - e)}{c} \tag{5.89}$$

where μ is the slope of the normal projection of the critical state line and $\mu_{compact}$ is the slope of the normal projection of the compact state line in the (τ, σ) space and which are also related to $\phi_{compact}$ and $\phi_{critical}$. η is the stress ratio (τ / σ) and ϕ is the angle of friction of the material. $e_{critical}$ is the void ratio at the critical state and is written as:

$$e_{critical} = eh - \lambda \ln \sigma \tag{5.90}$$

where eh is considered to have the value of 0.9 and λ has a very low magnitude. Similarly, the other constitutive assumption used in this study for a void ratio higher than the void ratio at the critical state and closer to the void ratio at the baseline, is expressed by:

$$\eta_{SBS} = \mu \frac{(e_{base} - e)}{b} \tag{5.91}$$

where b is the vertical distance between e_{base} and $e_{critical}$ in the *e-log p* graph and in this study may be chosen as 0.2.

In order to have a final stress-strain relationship reasonable for the model under study, the strain increments have to be determined. Since the total shear strain is the sum of the plastic strain and the elastic strain, hence;

$$d\varepsilon = d\varepsilon^p + d\varepsilon^e$$

The plastic strain increments are evaluated by the following equations developed previously as:

$$d\varepsilon_{zz}^{p} = d\varepsilon_{zz} - \frac{d\sigma_{zz}}{E} \tag{5.92}$$

$$d\varepsilon_{xz}^{p} = d\varepsilon_{xz} - \frac{d\tau_{xz}}{G} \tag{5.93}$$

where E and G are the young modulus and the shear modulus respectively. Therefore, the total plastic strain is estimated by the following:

$$d\varepsilon^{p} = \sqrt{(d\varepsilon_{zz}^{p})^{2} + (d\varepsilon_{xz}^{P})^{2}} \tag{5.94}$$

The strain increments $d\varepsilon_{zz}$ and $d\varepsilon_{xz}$ are estimated from the strain-displacement relation as follows:

$$d\varepsilon_{zz} = \frac{\partial}{\partial z}(du_{z}) \text{ ; and;}$$

$$d\varepsilon_{xz} = \frac{1}{2}\frac{\partial}{\partial x}(du_{z})$$

where the above equations may be written in their finite difference form using the mesh described in Figure 5.4:

$$d\varepsilon_{zz} = \left(\frac{x(j+1) - x(j)}{\Delta z}\right) \tag{5.95}$$

$$d\varepsilon_{xz} = \left(\frac{x(e) - x(w)}{2\Delta x}\right) \tag{5.96}$$

The stress increments $d\sigma_{zz}$ and $d\tau_{xz}$ in equations 5.92 and 5.93 are determined from the developed relation in 5.44 as:

$$d\sigma_{zz} = c_{11}d\varepsilon_{zz} + c_{12}d\varepsilon_{xz} \tag{5.97}$$

$$d\tau_{xz} = c_{21}d\varepsilon_{zz} + c_{22}d\varepsilon_{xz} \tag{5.98}$$

where c_{11}, c_{12}, c_{21} and c_{22} are the coefficients relating stress to strain and defined in equations 5.45 to 5.49. Recalling equation 5.38, the horizontal stress increment is in function of $d\sigma_{zz}$ and $d\tau_{xz}$:

$$d\sigma_{xx} = -\frac{a_{12}}{a_{11}} d\sigma_{zz} - \frac{a_{13}}{a_{11}} d\tau_{xz}$$

where a_{11}, a_{12} and a_{13} are the elastic-plastic coefficients relating stress and strain and are defined in equation 5.35 and 5.36. The volumetric strain is related to the void ratio and the strain increments through the following equation:

$$d\varepsilon_{ii} = -\frac{de}{1+e} \tag{5.99}$$

Since the lateral strain $d\varepsilon_{xx}$ is assumed to be zero in this analysis, therefore the relation would be:

$$d\varepsilon_{zz} = -\frac{de}{1+e} \text{ and;}$$

$$de = -d\varepsilon_{zz}(1+e) \tag{5.100}$$

where e is the void ratio and the minus sign is used in conformity with soil mechanics conventions. Note that a decrease in *de* would indicate a positive strain.

Since this is an incremental analysis, all the stress increments defined above are to be added to the stresses at each stage of calculations. They would be added to the previous values of stress in the following way:

$$\sigma_{zz} = \sigma_{zz}^{old} + d\sigma_{zz} \tag{5.101}$$

$$\sigma_{xx} = \sigma_{xx}^{old} + d\sigma_{xx} \tag{5.102}$$

$$\tau_{xz} = \tau_{xz}^{old} + d\tau_{xz} \tag{5.103}$$

In addition to that, the incremental volume increase/decrease or the change in volume will be added to the void ratio of the material by this relation:

$$e = e^{old} + de \tag{5.104}$$

where e is the void ratio of the fill and de is the incremental change in volume.

Note that when the system is at rest the coefficient of earth pressure is chosen to be $(1-\sin\phi)$. Therefore the vertical and the horizontal stresses are:

$$\sigma_{zz} = \gamma z \tag{5.105}$$

$$\sigma_{xx} = (1-\sin\phi)\sigma_{zz} \tag{5.106}$$

At rest, the normal stress and the shear are defined from the Mohr's circle of stress respectively:

$$\sigma = \frac{1}{2}(\sigma_{xx} + \sigma_{zz}) \tag{5.107}$$

$$\tau = \frac{1}{2}(\sigma_{zz} - \sigma_{xx}) \tag{5.108}$$

5.8 RESULTS AND DISCUSSION

Reinforced granular systems may induce settlements over very soft soils. The use of geosynthetic reinforcement is efficient in reducing these settlements and in stabilizing the system. The maximum surface settlement of non-cohesive soils can be estimated using the proposed model. The immediate surface settlement is due to the self-weight of the fill overlaying the soft soil. As discussed in the previous chapter, the system will undergo two settlements. The primary settlement will take place before the spreading of the granular fill and the final immediate settlement is determined after the dispersal of the

fill between the embankment fingers. It is assumed that the fill will be spread in one stage and compacted to the specified degree of compaction. Figure 5.6 shows the ground deformation of the system before the spreading of the fill and the profile the fill will take when the dispersion takes place. In order to level the ground at the surface, a surcharge has been assumed to act on the surface. The assumed surface loading will be of small values on the sides and zero at the center.

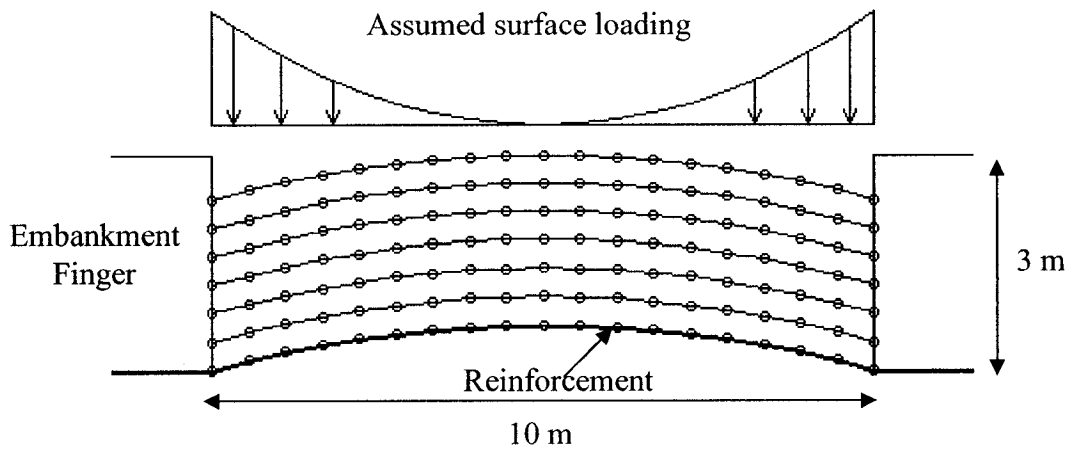

Figure 5.6 Profile before the immediate settlement

The upward deflection at the bottom of the system is measured vertically at the center and is 0.635 meter for this case with the material properties described below. The ground deformation at the bottom was determined and discussed in depth in the previous chapter with the developed equations related to it. This deflection is mainly due to the pressure caused by the embankment fingers on the soft soil. In this study, the computer simulations correspond to the immediate settlement of the reinforced fill layer with a depth of 3 meter overlaying very soft soil with a cohesion value of 10 kPa. The distance

between the embankment fingers is 10 m with a height of 3 m and their unit weight is assumed to be 20 kN/m^3. The embankment fingers are assumed to be made of very high quality dense material to stand vertically. This is a simplified assumption because the maximum surface settlement is expected at the center far away from the fingers where there is a minimal settlement and only the vertical settlement of the fingers is taken into consideration. Otherwise, inclined edges would complicate the formulations involved making it quite unusable in this study. The geotextile reinforcement has a stiffness modulus, J, of 4000 kN/m. The immediate settlement of the system is determined by the superposition of the bulge due to the loading of the embankment fingers and the settlement due to the self-weight of the fill. Figure 5.7 shows the superposition of these two settlements. The bulge is represented by dotted lines and the fill settlement by solid lines.

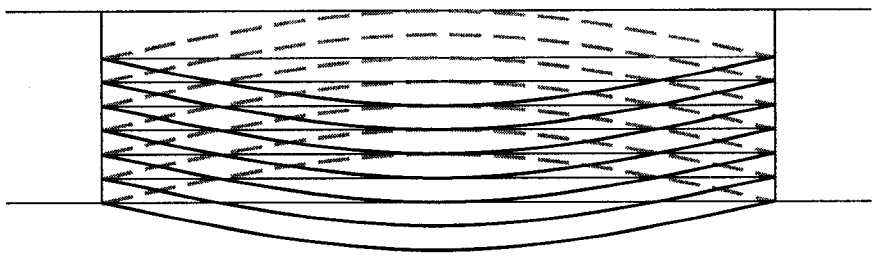

Figure 5.7 The superposition of settlements

In order to evaluate the performance of the model, the fill is considered with a wide range of void ratio varying from 0.5 - 0.9 from very dense to very loose sand. The first simulation is related to a very dense fill with a void ratio of 0.5. Figure 5.8 shows the surface profile after the immediate settlement of a very dense granular fill.

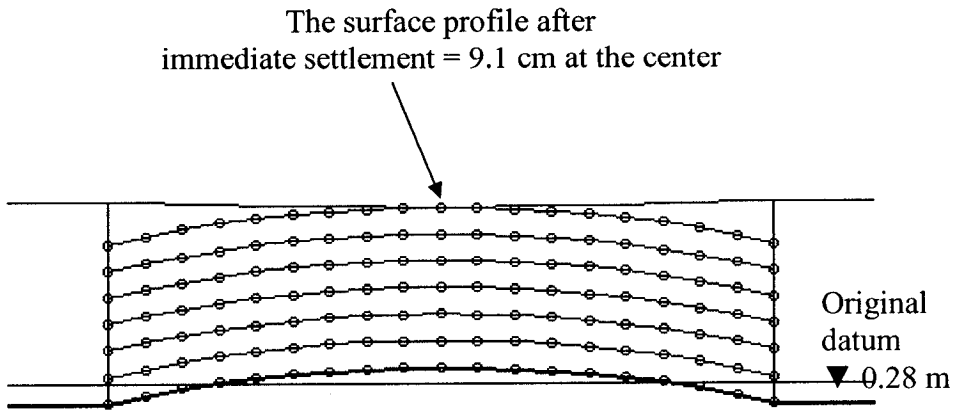

Figure 5.8 Settlement of a very dense fill

It can be seen that after the immediate settlement, the surface has settled 9.1 cm. This is the maximum surface settlement that occurs in the middle of the system. The angle of friction and the unit weight of the fill depend on the void ratio and therefore they have the values of 41° and 17.65 kN/m^3 respectively. It is important to note that the void ratio is close to the void ratio at the compact state, therefore the soil behavior is more elastic than elastic-plastic. Since the system is overlaying soft soil, then the embankment fingers along with the fill will settle as well. In this case, the fingers have settled 0.28 m. The more compact the soil is the higher pressure is on the soft soil and the more the fingers will settle. This settlement is being measured vertically at the bottom from the original position of the datum shown in Figure 5.8.

For the next fill profile the value of the void ratio is increased to 0.6. Again the soil behavior is elastic but there are some plastic strains. The soil is looser than the previous case and the settlement has increased about the double of the previous one and is 18.3 cm as shown in Figure 5.9.

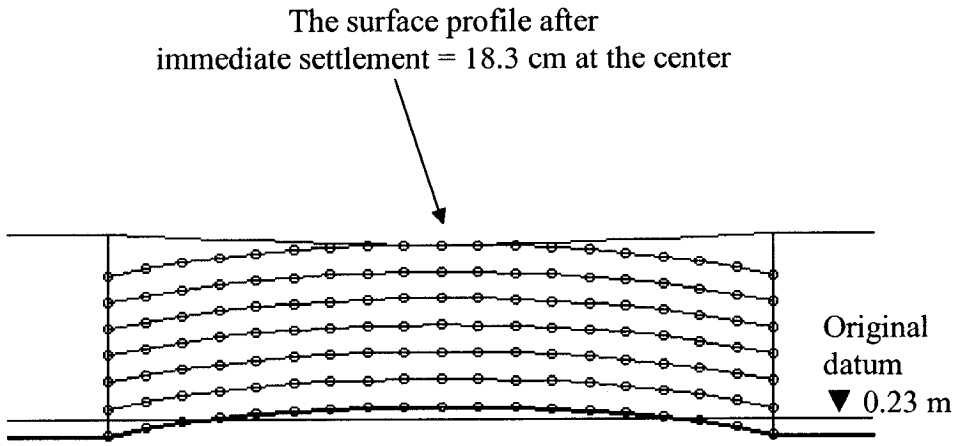

Figure 5.9 Settlement of a dense to medium fill

The friction angle of the fill, ϕ_{fill}, is 37° and the unit weight, γ_{fill}, is 16.55 kN/m^3. The embankment fingers have settled 0.23 m from their original position. The fingers here have settled less than the previous case since the fill is becoming looser and the pressure is decreasing.

It is emphasized here that the degree of compaction of a fill varies from one material to another. Therefore, the degree of compaction, measured by the void ratio, of this particular medium is classified with reference to its critical and compact void ratios.

The result of the test on medium to loose fill is presented in Figure 5.10. The void ratio has been increased to 0.7. It is obvious that as the void ratio is increased the soil behaves as an elastic-plastic material rather than an elastic one. In this case, the settlement becomes 25.4 cm which is about 39% more than the case when the void ratio, *e*, was equal to 0.6. The fingers have settled 0.19 m which 20% less than the preceding test and that is due to the fact that the soil is becoming looser.

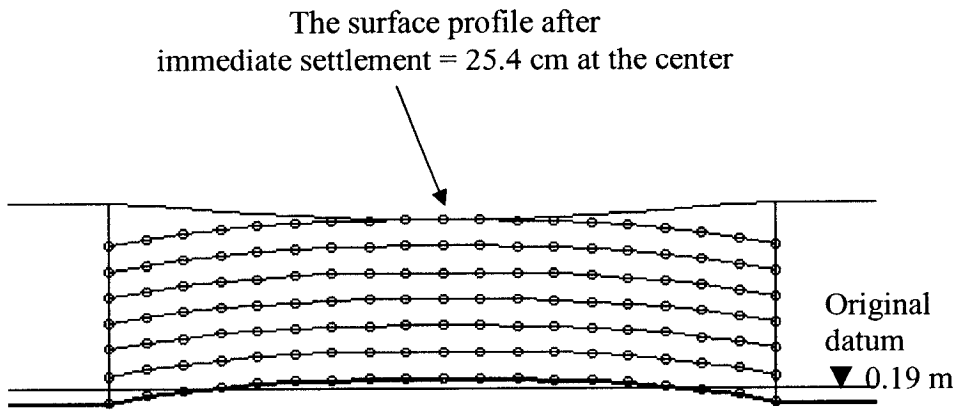

Figure 5.10 Settlement of a medium to loose fill

The angle of friction and the unit weight of the fill were determined as 33° and 15.58 kN/m^3 respectively. It is essential to notice that the unit weight of the fill and the angle of friction are decreasing as the void ratio is increasing. The angle of friction of the fill is leaning towards to the angle of friction at the critical state, $\phi_{critical}$ which is equal to 25°.

The response of the loose to very loose sand with a void ratio of 0.8 is illustrated in Figure 5.11. As expected by increasing the void ratio the settlement of the fill layer increases as well. The surface settlement has increased another 16% than the preceding test and reaches 29.4 cm. This is due to the fact that the void ratio here is close to the critical void ratio denoted by $e_{critical}$ and which was previously set to 0.9. The angle of friction of the fill is 29° and the unit weight is 14.71 kN/m^3. In this test the embankment fingers have settled 0.18 m from their original grade. It is observed here that as the void ratio is increasing the embankment fingers are settling less than before since the unit weight of the soil has been decreasing.

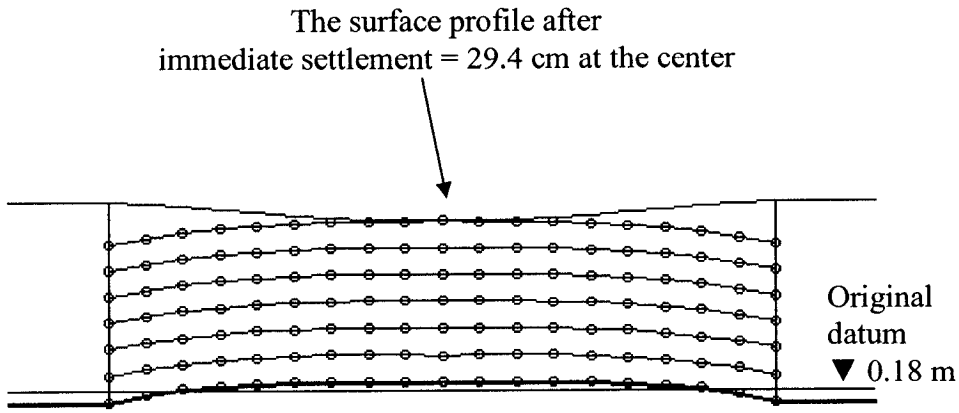

Figure 5.11 Settlement of a loose to very loose fill

The last test was performed on a very loose soil with a void ratio of 0.9. The distorted shape of the fill layer is presented in Figure 5.12. The surface settlement corresponds to the most critical void ratio of the soil. The maximum surface settlement was estimated at 33.3 cm, another increase of 13.5%. The angle of friction corresponds to the critical angle of friction and has the value of 25° and the reinforced fill layer has a unit weight of 13.94 kN/m^3.

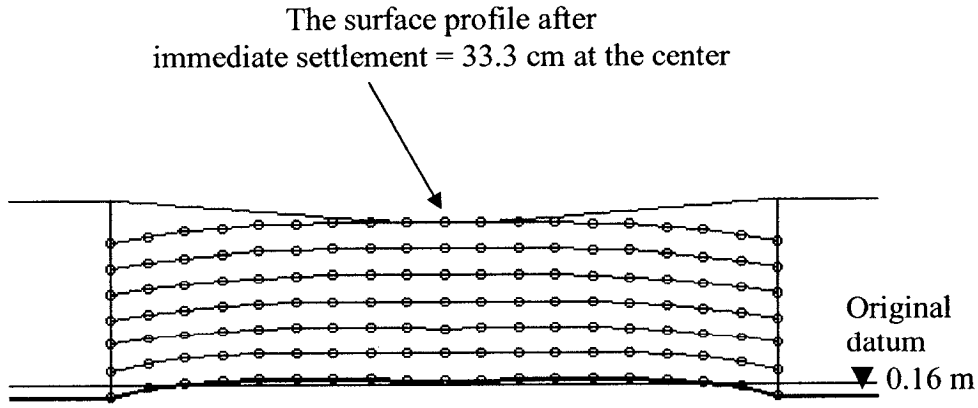

Figure 5.12 Settlement of a very loose fill

In this last computer-generated test, the embankment fingers have a settlement of 0.16 m, 14% less compared to the previous result, and is the lowest settlement among all the other tests carried out in this study.

The points settling below the maximum surface settlement (centerline) of the system were analyzed with respect to depth as well. Table 5.1 presents the settlements with respect to the depth of the fill layer at void ratios ranging from 0.5 – 0.9.

	e = 0.5	**e = 0.6**	**e = 0.7**	**e = 0.8**	**e = 0.9**
Depth (m)	**ΔS (m)**	**ΔS (m)**	**ΔS (m)**	**ΔS (m)**	**ΔS (m)**
0	0.091	0.183	0.254	0.294	0.333
0.394	0.091	0.183	0.254	0.294	0.333
0.788	0.0918	0.186	0.258	0.299	0.34
1.182	0.0934	0.189	0.264	0.308	0.351
1.576	0.0955	0.194	0.272	0.319	0.367
1.97	0.0984	0.201	0.282	0.334	0.387
2.365	0.102	0.209	0.296	0.354	0.413

Table 5.1 Settlement with respect to depth

The results presented above are the settling points located at the middle of the system beneath the maximum surface settlement. These settling points were chosen to study the deformation with respect to depth. ΔS is the settlement and zero meter depth indicates the surface of the fill layer. At the depth of zero m, ΔS shows the surface settlements illustrated earlier in this chapter and as the depth increases ΔS shows the settlement of the nodes located underneath these surface settlements. It is noted here that as the depth increases the settlements are increasing as well. The settlement of these nodes is larger than the surface settlements due to the fact that the stresses are higher at these locations.

Larger settlements are expected at nodes situated at the base of the system since the base is directly located on the very soft soil i.e. these nodes are positioned right on the reinforcement overlaying the soft soil. Figure 5.13 shows the settlements presented in Table 5.1 with respect to the depth of the fill layer for e = 0.5 – 0.9.

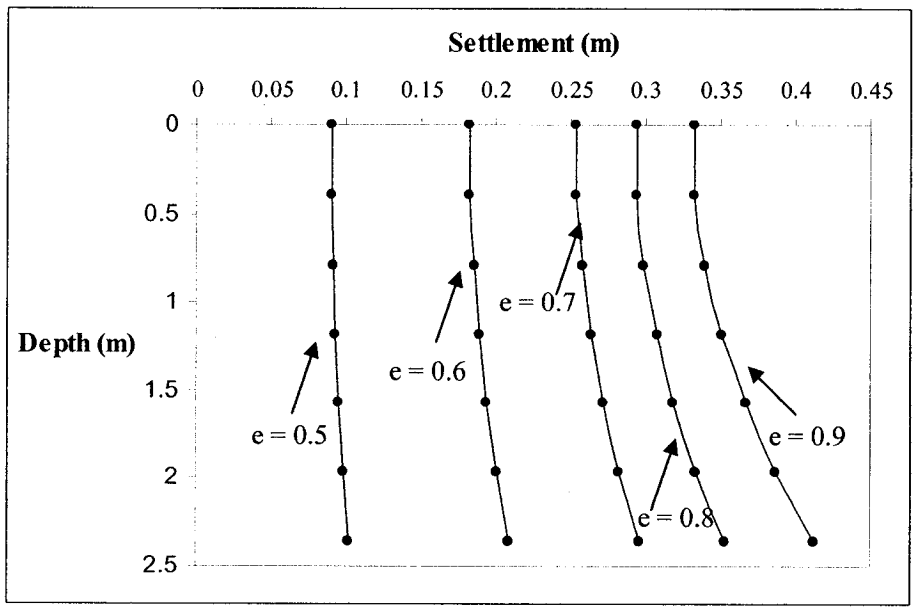

Figure 5.13 Settlement vs. depth (e = 0.5 – 0.9)

It is clearly shown in Figure 5.13 that the nodes located beneath the surface have higher settlements and that the deeper the nodes are in the fill layer the larger the settlements are for these nodes. Higher stresses are encountered at deeper nodes and especially at the ones resting on the soft soil. For the case of the very loose fill where the void ratio is equal to 0.9, the surface settlement was estimated at 0.33 m and at the base the settlement was determined to be 0.41 m and that is 8 cm more than the surface one. For the case of the very dense fill, at a void ratio equal to 0.5, the computed surface settlement was 9.1 cm whereas at the base of the system the node settled 10.2 cm. It is pointed out here that

the difference between these last two deformations (at e = 0.5) is very small compared to that of the former case where the soil is looser. When the soil was well compacted the soil settled less whereas looser soil settled more.

It was shown that the elastic-plastic model developed in this chapter is capable of estimating the immediate surface settlement of a cohesionless media. The results illustrated the importance of the void ratio and its effect on the behavior of the reinforced granular layer. Small settlements were associated with lower void ratios whereas large deformations were associated with higher void ratios and the evaluated surface settlements were in the range of 0.09 – 0.34 m.

5.8.1 RESULTS AND DISCUSSION OF THE FINITE ELEMENT MODEL

Since no similar studies were found on this type of model to compare the results of the immediate settlements, the other alternative was to use a finite element program to model the system. Phase^2 from rocscience is a powerful elastic-plastic finite element stress analysis program designed for geotechnical engineering purposes. This software was used for many researches and projects and referenced in numerous published papers.

In order to have a complete and accurate analysis of the finite element model several elastic properties and strength parameters had to be assumed. Note that these assumptions were not incorporated in the modeling of the system described in the previous section since they were not required in the analysis. However, they are very

essential to this analysis in obtaining a reasonably accurate behavior comparable to the original model. In addition to that another important point which needs to be noted here is that the void ratio *e* of the reinforced granular layer does not change with depth when the compaction proceeds.

The system under study was modeled using finite element analysis with the same geometry prescribed in the earlier section. The depth of the fill layer is set to 3 m same as the height of the embankment fingers which have a unit weight of 20 kN/m^3. The spacing between the embankment fingers is unchanged with a 10 m distance. Geosynthetic reinforcement was used to reinforce the system at the base and to separate the fill from the soft soil with a stiffness modulus of 4000 kN/m. The soft soil requires a depth in this model and is chosen to be 8 m with cohesion strength of 10 kPa. The upward ground deformation caused by the embankment fingers before the spreading of the granular fill was estimated before at 0.635 m and which is taken into consideration when modeling the system.

For the soft soil, a unit weight of 14 kN/m^3 has been assumed with a Poisson's ratio of 0.25 since according to Das (2000) the range of the Poisson's ratio for soft soil is between 0.15 – 0.25. The angle of friction used for the soft soil is 20° with a residual value of 10° and where it is considered a medium plastic soil. The embankment fingers were considered to be very dense materials having a Poisson's ratio of 0.35, an angle of friction of 47° and a Young's modulus of 45 MPa. It is important to state that the above elastic properties and strength parameters have been chosen according to the ranges

described by Das (1998, 2000). Figure 5.14 shows the finite element model of the system under study with its mesh using Phase^2. The mesh type used in this study is a uniform one with six noded triangles for the element type.

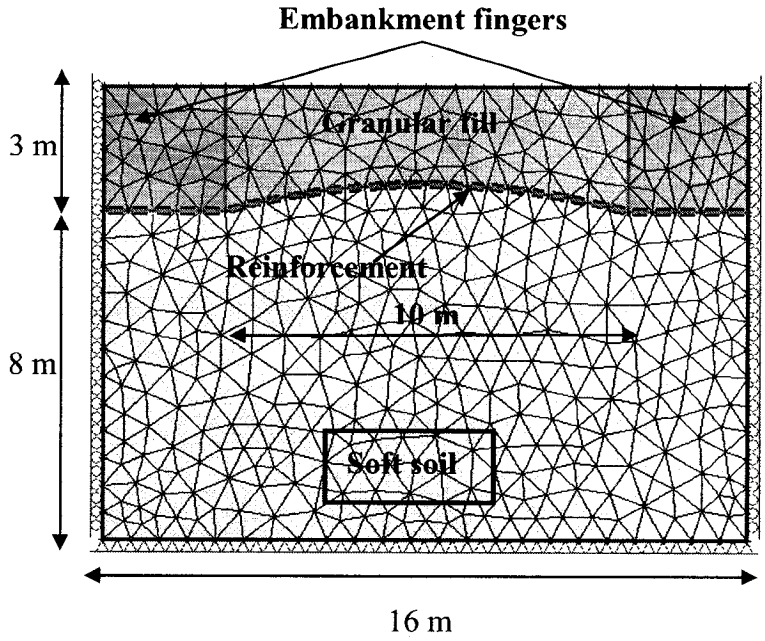

Figure 5.14 FEM model

For the case of a very dense fill, the angle of friction is set to 41° with a unit weight of 17.55 kN/m^3. The material is assumed to have isotropic elastic properties where the elastic properties are not dependent on directionality, and are defined by a single value of Young's modulus and a single value of Poisson's ratio. The strength model chosen to describe the behavior of the fill is the Mohr-Coulomb plastic model where the material can yield and exhibit non-linear stress-strain behavior. Since dense sands expands under shearing then there is a need to specify a dilation angle and in this case is equal to 16°. The angle of dilation is defined here as the difference between the angle of

friction of the fill and the angle of friction at the critical state which is equal to 25°. The initial element loading is set to body force only where the model will settle under its own weight to determine the immediate surface settlement. Figure 5.15 presents the surface profile for a very dense fill.

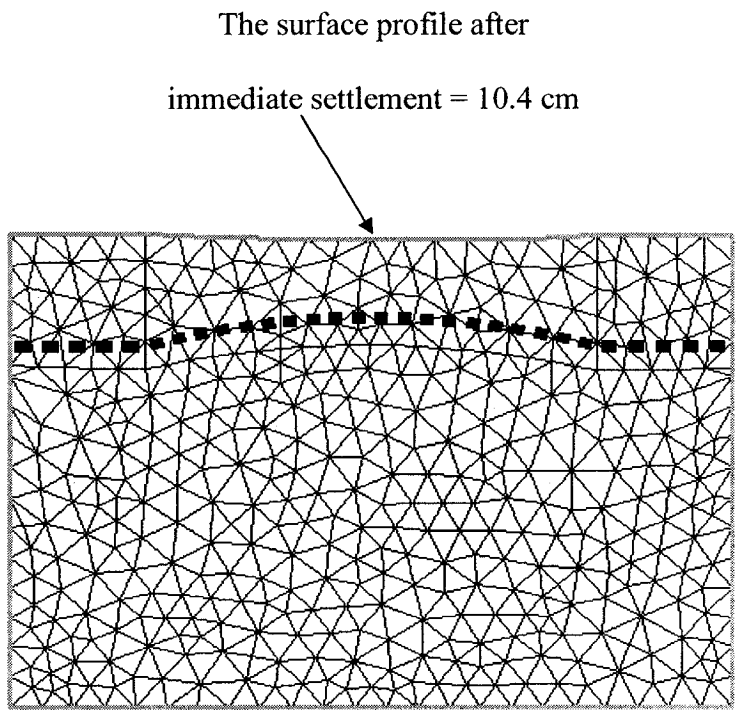

Figure 5.15 Settlement of a very dense fill

The surface settlement was computed to be 10.4 cm for this case as compared to 9.1 cm from the proposed model. The settlement here has an increase of 14% and that is 1.3 cm more. The relative percentage of errors between the two settlements is estimated at 12.5%.

The response of a dense to medium fill is illustrated in Figure 5.16. The fill in this test has an angle of friction of 37°, a unit weight of 16.55 kN/m^3 and a dilation angle equal to 12°. The dotted line represents the original position of the reinforcement which settled along with the system. The reinforcement has been given a value of 0.35 for its Poisson's ratio. The system has a surface settlement of 20.7 cm and which is found to be 13% higher than the one determined earlier at 18.3 cm.

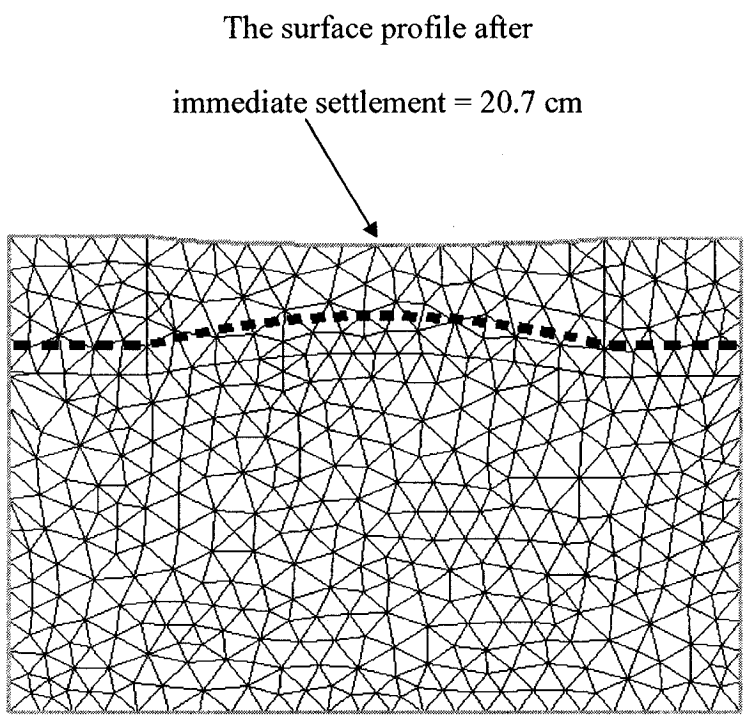

Figure 5.16 Settlement of a dense to medium fill

In the test carried out on the medium to loose fill, the fill has an angle of friction of 33° and a unit weight of 15.58 kN/m^3. In this analysis, the degree of compaction of the fill is measured according to the angle of friction as opposed to the original model where the degree of compaction was measured according to the void ratio. The angle of friction

was derived previously as a function of the void ratio. Figure 5.17 illustrates the settlement profile for a medium to loose fill. The angle of dilation here has been equal to 8^{o} for the granular fill. The fill settled 27 cm in this case with 6% higher than the one evaluated originally. It is important to note that the fingers settlements are not studied in this analysis due to the complexity of the soil behavior and the lack of data parameters.

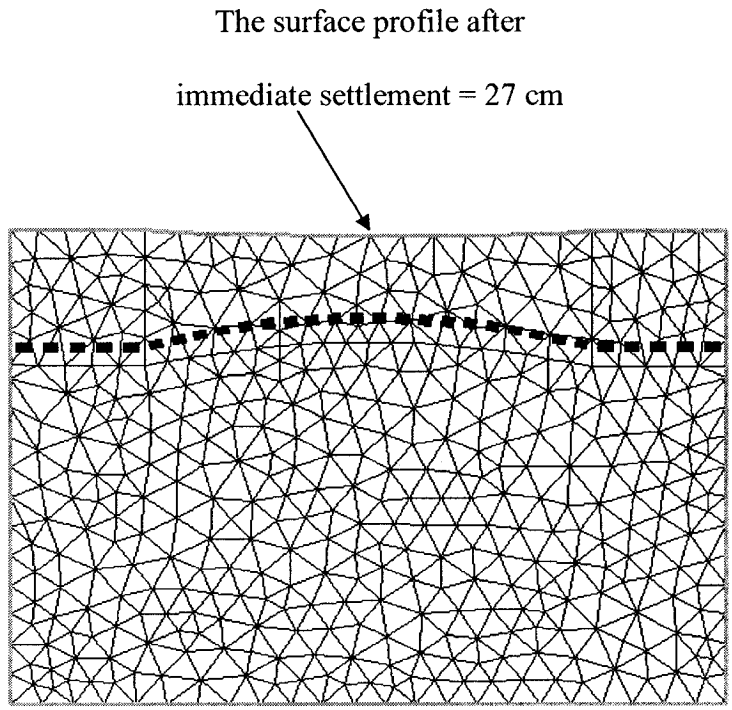

Figure 5.17 Settlement of a medium to loose fill

In the next test, loose to very loose fill is analyzed with an angle of friction of 29^{o} and a unit weight of 14.71 kN/m^3. The soil is becoming looser as these last two parameters are decreasing and the surface profile for this case is shown in Figure 5.18. In the figure below, the deformed mesh of the system under study is shown along with its surface settlement. The evaluated settlement here is 33 cm with an increase of 12% as

compared to the original one with 29.4 cm. A 12% increase in this case is only equivalent to 3.6 cm and a 10% margin of error.

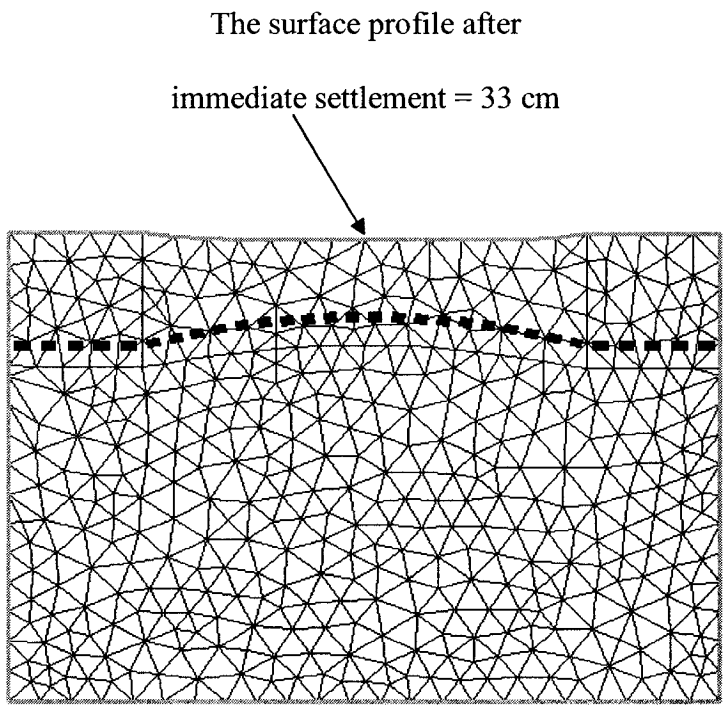

Figure 5.18 Settlement of a loose to very loose fill

The last analysis was performed on a very loose fill with an angle of friction of 25° and a unit weight of 13.94 kN/m^3. In this test, the angle of friction is equal to the critical angle of friction defined for the fill in this study. Figure 5.19 presents the surface profile due to the immediate settlement. The settlement of a very loose soil is evaluated at 40 cm as compared to 33.3 cm in the proposed model. In this case, the settlement computed from the FEM model has an increase of 6.7 cm to the original one.

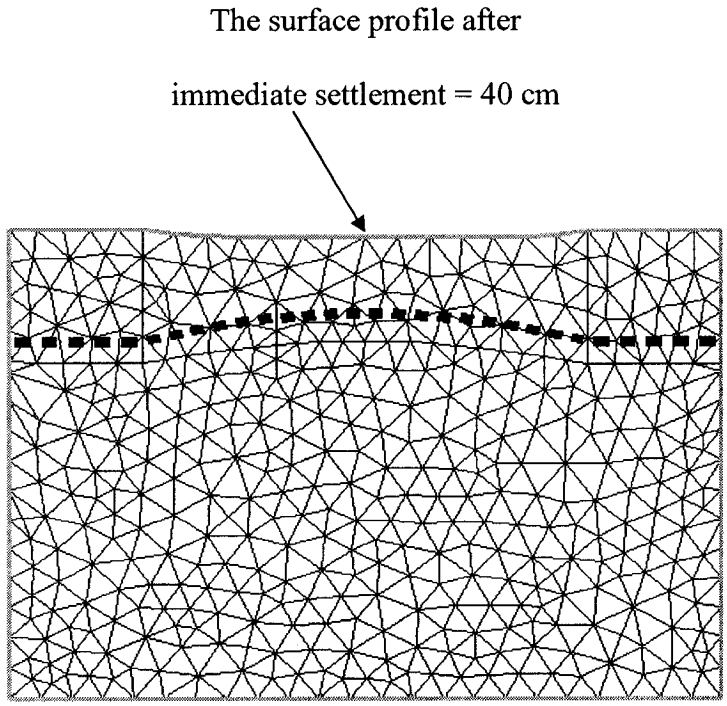

Figure 5.19 Settlement of a very loose fill

The FEM model was also analyzed using a refined mesh to determine the surface settlement and is shown in Figure 5.20.

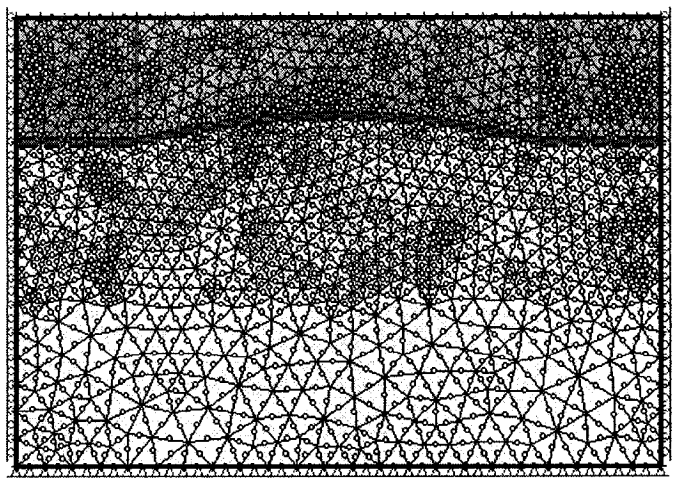

Figure 5.20 FEM model with a refined mesh

The results of the refined mesh are compared to the previous mesh and are tabulated in table 5.2.

Degree of compaction	Very dense fill	Dense to medium fill	Medium to loose fill	Loose to very loose fill	Very loose fill
FEM model (cm)	10.4	20.7	27	33	40
FEM model with refined mesh (cm)	11	21.6	28.5	33	42

Table 5.2 Results of refined FEM model

The settlements were determined to be very close to the previous ones with less than 5% margin of errors.

5.9 FINAL REMARKS

The settlements obtained from the finite element model are higher than the estimated one and in the worst case the errors involved are about 16%. This margin of errors is considered quite acceptable in geotechnical engineering. It is very important to note that the FEM results presented in this section were determined under the assumption that the elastic properties and strength parameters described earlier are the soil condition of the proposed model. However, if a parameter does not match the soil condition under which the study is based the values of the surface settlements could vary. For instance if the angle of friction of the soft soil beneath the reinforced layer is highly plastic with a value of 17^{o} and a residual one of 6^{o}, the range of the immediate settlement would be between 0.094 – 0.36 m as compared to 0.104 – 0.4 m. The objective here was to show that the surface settlements obtained from the integro-differential technique can be

experienced by such a system. However, the fact that several parameters had to be assumed and that no other studies were available made this present study open for one alternative which is to try to reproduce similar behavior by a finite element model. It is added here that the intention of using a finite element model was to demonstrate that the estimated surface settlements are very reasonable.

In this study, the constitutive formulations and the behavior of the cohesionless granular media when subjected to shearing are based on a non-associative flow rule. The material undergoes plastic deformation when the state of stress reaches the yield surface and the direction of the plastic strain increment is independent of the direction of the stress increment. The direction of the plastic strain vectors is defined through a flow rule by assuming the existence of a constant curve called the plastic potential function and to which the plastic strain vectors are orthogonal. This is referred to as the normality rule. Since this is a non-associative flow rule then for the reinforced granular layer the plastic potential and the yield function are different. The yield functions are lines of constant stress ratio or simply straight rays passing through the origin of the stress space. Having stated that, the plastic strain vectors are only perpendicular to the plastic potential and not to the yield functions where these last ones do not serve as the plastic potentials. As a result, the difference in the surface settlements between the model under study and the finite element model could have been affected by the explanation described above on the theory that follows non-associative flow rule and the theory of plasticity interpreted by the finite element model. The difference in interpreting the theory may have an impact on the results and adding to it that the normality rule does not hold.

Another important characteristic is the work hardening of the material which occurs between the points of yielding and the points of failure. The concept of the work hardening can be expressed in terms of the work done by the additional stress increments to produce given plastic strain increments and that for all such added stresses the material remains stable. The value of the scalar representing the plastic strain hardening depends whether the element is loading, unloading or reloading. In a loading process, the form of the plastic strain hardening function is derived from the plastic strain curve which is expressed by hyperbolic stress-strain relation. The dependence of this last function on the void ratio of the material is through an empirical coefficient which describes the hardening law for the plastic moduli. In the model formulation this empirical coefficient may have different forms but it should always be in function of the void ratio for the analysis to remain valid. The characteristics of the plastic strain hardening adopted in this study and the way it is formulated in the model may affect the final results obtained from the two compared analyses since the other analysis does not use the same formulation.

Since a slight curvature is always present in the yield function then a very small value of the slope of the Casagrande line is assumed in this study. The choice regarding this assumption is a matter of convenience to avoid the complexity in the formulation of the stress-strain behavior causing it to be impractical. Again this is another assumption which could not be taken into consideration when using the finite element program. All the characteristics mentioned in this last section may have a significant impact on the surface settlements obtained and could justify the errors occurred.

6. CONCLUSION

6.1 CONCLUDING REMARKS

Recently, the issues of disaster prevention in geotechnical engineering have become very important and earth reinforcement technique could be one of the effective solutions. The stability of geotechnical systems containing cohesionless granular media cannot be easy modeled due to its complex mechanical behavior. In addition to that the major difficulty arises from the irregular behavior of granular material when settling under its own weight. Therefore an incremental stress-strain analysis used to analyze the behavior of reinforced granular layer overlaying very soft soil is postulated.

The non-linear behavior of the fill and the stress-strain relationship has been described. Furthermore, the constitutive equations have been derived for the analysis and modeling of the elastic-plastic behavior of the granular layer. The formulation of the constitutive equations has been developed based on the compact state, the critical state and the state boundary surface. The model is capable of simulating the immediate settlement of both loose and dense fill behavior.

The mathematical formulation of the problem is presented along with the mesh used to cover the solution region. The elastic-plastic model is developed to analyze the behavior of the reinforced layer by relating stress increments to strain increments in a matrix representation. The characteristics of the elastic-plastic response have been proved

to be very efficient in the analysis by calibrating the constitutive equations using some index parameters and empirical coefficients to obtain a plausible stress-strain relationship.

An integro-differential equation is applied to investigate this type of problem in the field of geotechnical engineering. With the aid of this equation, which lead to a governing equation written in finite difference form, the total displacement field of the system was estimated. However, the emphasis in this research is placed on developing the equation and the numerical technique used in the evaluation of the settlements experienced by the system under study. The application of this technique is simple and requires minimal computational efforts as opposed to other numerical models.

In the proposed method by Lawson (1999) for the reclamation of soft soil using geosynthetic reinforcement, one of the steps was to construct embankment fingers over the soft soil to stress the geosynthetic. It was not taken into account that the reinforcement will undergo deformation before placing the fill. Therefore, in this study a primary ground deformation has been evaluated prior to the spreading of the granular layer between the embankment fingers. The settlement was in function of the pressure from the soft soil underneath the system and the loading from the fingers. The performance of the system was dependant on several parameters such as the loading acting on the system derived from the height of the embankment fingers, the stiffness modulus of the reinforcement, the cohesion or the undrained strength of the soft soil and the spacing between the embankment fingers. These variables helped in estimating the

settlement of such a model and affected the system in many direct ways. Moreover, the ground deflection was able to give the structure the profile the fill will take after the dispersion of the fill and the lines forming the profile are referred to as contour lines.

The immediate settlements were computed for a wide range of void ratio going from very dense to very loose fill. The numerical simulations showed that small surface settlements were associated with lower void ratio whereas large surface settlements were associated with higher void ratio. The parameters characterizing the settlement are the thickness of the reinforced layer, the unit weight and the angle of friction of the fill, the stiffness of the reinforcement and the cohesion of the soft soil. Among the parameters involved, the void ratio plays a paramount role in determining the settlement of sandy soil layer. The degree of compaction is measured according to the void ratio of the medium with reference to its critical and compact void ratio. If the representation of the void ratio is near the compact state or the compact void ratio then the soil is very dense and if it falls close to the critical void ratio then the soil is referred to as very loose. The model was able to predict the surface profile due to the immediate settlement of a reinforced granular layer settling under its own weight.

In the present research it was attempted to model the system under study using finite element analysis. Several parameters were assumed to have a complete and accurate analysis of the model. Medium and low plasticity soils were used to study the undergoing settlements and the errors involved were quite acceptable for this type of analysis.

6.2 RECOMMENDATIONS FOR FURTHER RESEARCH

The proposed model, which uses an integro-differential method, has a strong potential in the analysis of certain types of geotechnical problems. However, it is recommended to further investigate the model with well documented case studies before relying on the results. In order to use the model for practical purposes, the computational results should be validated in a different method such as using the technique to solve other types of encountered problems in geotechnical engineering.

The proposed analysis may be applied to other types of reinforced mats such as cohesive fills provided that the fill material will follow the same constitutive law outlined in this research. Loading on the surface is another problem which could be investigated when the system is used for constructing means of transportation such as highways, railways and airports.

LIST OF REFERENCES

1. **Altaee, A. and Fellenius, B.H.** (1994), "Physical modeling in sand", Canadian Geotechnical Journal, Vol. 31, pp. 420-431.
2. **Andrawes, K.Z., Mcgown, A. and Al-Hasani, M.M.** (1978), "Alteration of soil behavior by the inclusion of materials with different properties", Symposium on Reinforced Earth and Other Composites Soil Techniques, TRRL, Heriot-Watt University, TRRL suppl., report 457.
3. **Andrawes, K.Z., Mcgown, A. and Wilson-Fahmy, R.F.** (1983). "The behavior geotextile reinforced sand loaded by s strip footing", Proc. of the 8th European Conference on Soil Mechanics and Foundation Engineering, Helsinki, Vol. 1, pp. 329-334.
4. **Azaraih, I., Dhat, N.R., Gupta, R.P. and Chatre, M.V.** (1999), "Foundation Problems in Soft Marine Clays and Breakwaters", Geoshore, International Conference on Offshore and Nearshore Geotechnical Engineering, Mumbai, pp. 371-376.
5. **Basset, R.H. and Last, N.C.** (1978), "reinforcing earth below footings and embankments", Proc. Sym. Earth Reinforcement, ASCE, Vol. 101, pp. 1241-1255.
6. **Bauer, A. and Preissner, H.** (1986), "Studies on the stability of geotextile reinforced two layer system", Proc, of the 3rd International Conference on Geotextiles, Vienna, Vol. 4, pp. 1079-1084.

7. **Been, K. and Jeffries, M.G.** (1985), "A state parameter for sands", Geotechnique, Vol. 35, No. 2, pp. 99-112.

8. **Bell, J.R. and Hicks, R.G.** (1980), "Evaluation of test methods and use criteria for geotechnical fabrics in highway applications", Interim Report No. FHWA/Rd-80/021, Federal Highway Administration, Offices of Research and Development, Structures & Applied Mechanics Division, Washington, D.C

9. **Binquet, J. and Lee, K.L.** (1975, a), "Bearing capacity analysis of reinforced earth slabs", Journal of Geotechnical Engineering Division, ASCE, Vol. 101, No. GT12, pp. 1241-1255.

10. **Binquet, J. and Lee, K.L.** (1975, b), "Bearing capacity tests on reinforced earth slabs", Journal of Geotechnical Engineering Division, ASCE, Vol. 101, No. GT12, pp. 1257-1276.

11. **Blight, G.E.** (1988), "Some Less Familiar Aspects of Hydraulic Fill Construction", In Hydraulic Fill Structures, Geotechnical Special Publication, No. 21, ASCE, pp. 1000-1027.

12. **Bourdeau, P.L., Harr, M.E. and Holtz, R.D.** (1982). "Soil fabric interaction – An analytical model", Proc. Of 2nd International Conference on Geotextiles, Las Vegas, USA, Vol. 1, pp. 387-392.

13. **Broms, B.B. and Massarsch, K.R.** (1977), "Grid mats – A new foundation method", Proceedings of the 9th International Conference on Soil Mechanics and Foundation Engineering, Tokyo, Vol. 2, pp. 433-438.

14. **Broms, B.B. and Shirlaw, J.N.** (1987), "Stabilization of waste ponds at Changi depot", Proceedings of the 9th South East Asian Geotechnical Conference, Bangkok.

15. **Brown, B.S. and Poulos, H.G.** (1981), "Analysis of foundation on reinforced soil", Proc. of the 10th International Conference Soil Mechanics and Foundation Engineering, Stockholm, Vol. 3, pp. 595-598.

16. **Casagrande, A.** (1936), "Characteristics of cohesionless soils affecting the stability of earth fills", Journal of the Boston Society of Civil Engineers, Vol. 23, No. 1, pp.13-32.

17. **Castro, G.** (1969), "Liquefaction of sands", Harvard University, Cambridge, Harvard Soil Mechanics Series, No. 81.

18. **Castro, G. and Poulos, S.J.** (1977), "Factors affecting liquefaction and cyclic mobility", Journal of the Geotechnical Engineering Division, ASCE, Vol. 103, No. GT 6, pp. 501-516.

19. **Chandra, S.** (1979), "Analysis of beams and plates on nonlinear foundation", Ph.D. thesis, Indian Institute of Technology, Kanpur, India.

20. **Coulomb, C.A.** (1773), "Essai sur une application des règles de maximis et minimis a quelques problèmes de statiques, relatifs a l'architecture", Mémoires de Mathématiques de l'académie royal des sciences, Paris, Vol. 7, pp. 343-382.

21. **Dafalias, Y.F. and Popov, E.P.** (1975), "A model of nonlinearity hardening materials for complex loading", Acta Mechanica, Vol. 21, pp. 173-192.

22. **Das, B.M.** (1989), "Foundation on sand underlain by soft clay with geotextile at sand –clay interface", In Geosynthetics Conference, San Diego, USA, Vol. 1, pp. 203-214.

23. **Das, B.M.** (1998), "Principles of geotechnical engineering", 4th Edition, PWS Publishing Company, A division of International Thomson Publishing Inc., California State University, Sacramento, USA, pp. 352-353.

24. **Das, B.M.** (2000), "Fundamentals of geotechnical engineering", Brooks/Cole, A division of Thomson Learning, California State University, USA, pp. 416-417.

25. **De Saint-Venant, B.** (1870), "Mémoire sur l'établissement des équations diferentiellels mouvements intérieurs opère dans les corps solides ductiles au delà des limites ou l'élasticité pourrait les ramener a leur premier état", Comptes Rendus, Acad. Sci. Paris, Vol. 70, pp. 1323-1325.

26. **Desrues, J., Chambon, R., Mokni, M., and Mazerolle, F.** (1996), "Void ratio evolution inside shear bands in triaxial sand specimens studied by computed tomography", Géotechnique, Vol. 46, No. 3, pp. 529–546.

27. **Drucker, D.C. and Prager, W.** (1952), "Soil mechanics and plastic analysis or limit design", Quarterly of applied Mathematics, Vol. 10. No. 2, pp. 157-165.

28. **Duncan, J.M. and Chang, C.Y.** (1970), "Non-linear analysis of stress and strain in soils", Journal of Soil Mechanics and Foundations Division, ASCE, Vol. 96, No, SM5, pp. 1629-1653.

29. **Feld, J.** (1971), "Discussion on Hydraulics Fills to Support Structural Loads", J.S Soil Mechanics and Foundation Division, ASCE, Vol. 96, No. SM1, pp. 194-195.

30. **Floss, F. and Gold, G.** (1990), "Use of the FEM for the single reinforced two-layer system", Geotextiles and Geomembranes and Related Products, Den Hoedt (ed.), Balkema, Rotterdam, pp. 248.

31. **Gosh, C. and Madhav, M.R.** (1994, a), "Settlement response of reinforced shallow earth bed", Geotextiles and Geomembranes, Vol. 13, No. 5, pp. 643-656.

32. **Gosh, C. and Madhav, M.R.** (1994, b), "Reinforced granular fill - Soft soil system: confinement effect", Geotextiles and Geomembranes, Vol. 13, No. 5, pp. 742-759.

33. **Gosh, C. and Madhav, M.R.** (1994, c), "Reinforced granular fill - Soft soil system: confinement effect", Geotextiles and Geomembranes, Vol. 13, No. 5, pp. 727-741.

34. **Hill, R.** (1963), "The mathematical theory of plasticity", Oxford University Press, pp. 355.

35. **Hill, R.** (1963), "A general method of analysis for metal working processes", J, Mech. Phys. Solids, Vol. 11, pp. 305-326.

36. **Hufenus, R., Rueegger, R., Banjac, R., Mayor, P., Springman, S.M. and Bronnimann, R.** (2006), "Full-scale field tests on geosynthetic reinforced unpaved roads on soft subgrade", Geotextiles and geomembranes, Vol. 24, pp. 21-37.

37. **Imanishi, H., Ochiai, H., Omine, K. and Yamauchi, M.** (1998), "Mechanical behavior of geonet in ground replacement method", Proceedings of the International Symposium on Lowlands Technology, Saga University, Japan, pp. 301-308.

38. **Ishihara, K., Tatsuoka, F. and Yasuda, S.** (1975), "Undrained deformation and liquefaction of sand under cyclic stresses", Soils and Foundations, Vol. 15, No. 1, pp. 29-44.

39. **Kerr, A.D.** (1964), "Elastic and viscoelastic foundation models", Journal of Applied Mechanics, ASME, Vol. 31, pp. 491-498.

40. **Koerner, R.M. and Welch, J.P.** (1980), "Construction and geotechnical engineering using synthetic fabric", John Wiley & Sons, New York.

41. **Koerner, R.M.** (1994), "Designing with geosynthetic", Prentice Hill, A paramount communications company, Drexel University, USA, pp. 2-6.

42. **Kondner, R.L.** (1963), "Hyperbolic stress-strain response: cohesive soils", Journal of Soil Mechanics and Foundations Division, ASCE, Vol. 89, No, SM1, pp. 115-143.

43. **Lambe, T.W.** (1964), "Methods of Estimating Settlement", Journal of Soil Mechanics and Foundations Division, ASCE, Vol. 90, No. SM5, pp. 43-67.

44. **Lambe, T.W.** (1967), "Stress Path Method", Journal of Soil Mechanics and Foundations Division, ASCE, Vol. 93, No, SM6, pp. 117-141.

45. **Lawson, C.R.** (1999), "Earth Reinforcement Technique with geosynthetics in Asian Region", Proc. Of the 11th Asian Regional Conference on Soil Mechanics and Geotechnical Engineering, Seoul, Korea, pp. 25-36.

46. **Lee, K.L.** (1965), "Triaxial compressive strength of saturated sands under seismic loading conditions", Ph.D. dissertation, University of California at Berkley, U.S.A., pp. 521.

47. **Lee, K.M., Shen, C.K., Leung, D.H.K. and Mitchell, J.K.** (1999), "Effects of Placement Method on Geotechnical Behavior of Hydraulic Fill Sands", Geotechnical and Geoenvironmental Engineering, ASCE, Vol. 1256, No. 10, pp. 832-846.

48. **Levy, M.** (1871), "Extrait du mémoire sur les équations générales des mouvements intérieurs des corps solides ductiles au delà des limites ou l'élasticité pourrait les ramener a leur premier état", Journal Math. Pure appl., Vol 16, pp.369.

49. **Madhav, M.R. and Poorooshasb, H.B.** (1988), "A new model for geosynthetic reinforced soil", Computers and Geotechnics, Vol. 6, No. 4, pp. 277-290.

50. **Madhav, M.R. and Poorooshasb, H.B.** (1989), "Modified Pasternak model for the reinforced soil", Math. And Comp. Modeling, An Int. J., Vol. 12, No. 12, pp. 1505-1509.

51. **Martin, J.P., Crawford, R.B., Swan, R.H. and DePaul, A.J.** (1988), "Modeling of Geotextile Reinforced Mat Placed on soft dredgings", In Hydraulic Fill Structures, Geotechnical Special Publication, No. 21, ASCE, pp. 763-777.

52. **Meyerhof, G.G.** (1951), "The ultimate bearing capacity of foundations", Geotechnique, Vol. 2, pp. 301-332.

53. **Meyerhof, G.G. and Adams, J.I.** (1968), "The ultimate uplift capacity of foundations", Canadian Geotechnical Journal, No. 5, pp. 225-244.

54. **Meyerhof, G.G.** (1974), "Ultimate bearing capacity of footings on sand overlying clay", Canadian Geotechnical Journal, No. 2, pp. 223-229.

55. **Miki, G.** (1985), "Soil Improvement Method in Japan", Proc. Of 3rd International Geotechnical Seminar, Soil Improvement Methods, Japan, pp. 229-236.

56. **Milligan, G.W.E., Fannin, J. and Farrar, D.M.** (1986), "Model and full scale tests of granular layers reinforced with a geogrid", Proc, of the 3rd International Conference on Geotextiles, Vienna, Austria, pp. 61-66.

57. **Mitchell, J.K.** (1988), "Densification and Improvement of Hydraulic Fills", In Hydraulic Fill Structures, Geotechnical Special Publication, No. 21, ASCE, pp. 606-633.

58. **Miura, N. and Madhav, M.R.** (1994), "General Description and Geotechnical Characteristics", Lowlands Development and Management, Brookfield, pp. 9-29.

59. **Miura, N. and Madhav, M.R.** (1994), "General Description and Geotechnical Characteristics", Lowlands Development and Management, Brookfield, pp. 30-39.

60. **Morgenstern, N.R. and Kupper, A.A.G.** (1988), "Hydraulic Fill Structures – A perspective", In Hydraulic Fill Structures, Geotechnical Special Publication, No. 21, ASCE, pp. 1-31.

61. **Nieuwenhuis, J.D.** (1977), "Membranes and the bearing capacity of road bases", Proc. of International Conference on the Use of Fabrics in Geotechnics, Paris, pp. 3-8.

62. **Nishigata, T. and Yamaouka, I.** (1990), "Bearing capacity of unpaved road reinforced by geotextile", Geotextiles and Geomembranes and Related Products, Den Hoedt (ed.), Balkema, Rotterdam, pp. 249.

63. **Noorzad, A.** (1998), "Cyclic behavior of cohesionless granular media using the compact state concept", Ph.D. thesis, Concordia University, Montreal, Canada.

64. **Pietruszczak, S. and Mroz, Z.** (1983), "On hardening anisotropy of K_0 consolidated clay", International Journal for Numerical and Analytical Methods in Geomechanics, Vol. 7, pp. 19-38.

65. **Pietruszczak, S. and Stolle, D.F.E.** (1987), "Modeling of sand behavior under earthquake excitation", International Journal for Numerical and Analytical Methods in Geomechanics", Vol. 11, No. 3, pp. 221-240.

66. **Poorooshasb, H.B.** (1961), "The properties of soils and other granular media in simple shear", Ph.D. thesis, University of Cambridge, U.K.

67. **Poorooshasb, H.B., Holubec, I. and Sherbourne, A.N.** (1966), "Yielding and flow of sand in triaxial compression", Canadian Geotechnical Journal, Vol. 3, No. 4, pp. 179-190.

68. **Poorooshasb, H.B., Holubec, I. and Sherbourne, A.N.** (1967), "Yielding and flow of sand in triaxial compression", Canadian Geotechnical Journal, Vol. 4, No. 4, Part II and III, pp. 376-399.

69. **Poorooshasb, H.B.** (1971), "Deformation of sand in triaxial compression", Proceedings of the 4th Asian Regional Conference on Soil Mechanics and Foundation Engineering, Bangkok, Vol. 1, pp. 63-66.

70. **Poorooshasb, H.B.** (1985), "An extension of the Pasternak foundation concept", Soils and Foundations, Vol. 25, No. 3, pp.31-40.

71. **Poorooshasb, H.B.** (1989), "Description of flow of sand using state parameters", Computers and Geotechnics, Vol. 8, pp. 195-215.

72. **Poorooshasb, H.B.** (1991), "On mechanics of heavily reinforced granular mats", Soils and Foundations, Vol. 31, No. 2, pp. 134-152.

73. **Poorooshasb, H.B.** (1995), "One gravity model testing", Soils and Foundations, Vol. 35, No. 3, pp. 35-59.

74. **Poorooshasb, H.B.** (1995), "Analysis of piled-raft foundation", Proceedings of the 5th International Symposium on Numerical Models in Geomechanics (NUMOG-V), Davos, Switzerland, pp. 213-241.

75. **Poorooshasb, H.B., Alamgir, M. and Miura, N.** (1996, a), "Negative skin friction on rigid and deformable piles", Computers and Geotechnics, Vol. 18, No. 2, pp. 109-126.

76. **Poorooshasb, H.B., Alamgir, M. and Miura, N.** (1996, b), "Application of an integro-differential equation to the analysis of geotechnical problems", Structural Engineering and Mechanics, Vol. 4, No. 3, pp. 227-242.

77. **Poorooshasb, H.B., Alamgir, M. and Miura, N.** (1996, c), "Refinement of a numerical technique for solution of geotechnical problems", Proceedings of the

3rd Asian-Pacific Conference on Computational Mechanics, Seoul, Korea, pp. 2145-2150.

78. **Poorooshasb, H.B.** (1998), "Analysis of inclined piles used to prevent downhill creep of unsaturated clay formation", Structural Engineering and Mechanics, Vol.6, No.3, pp. 245-257.

79. **Poorooshasb, H.B.** (1998), "Ground subsidence caused by earthquake type excitation", Proceedings of the International Symposium on Lowland Technology, Saga University, pp.11-22.

80. **Poorooshasb, H.B.** (2002), "Performance of reinforced fill placed over a level containing circular soft spot", Proceedings of the International Symposium on Lowlands Technology, Saga University, pp. 11-16.

81. **Poorooshasb, H.B.** (2002), "Subsidence evaluation of geotextile-reinforced gravel mats bridging a sinkhole", Geosynthetics International, Vol. 9, No. 3, pp. 259-282.

82. **Poorooshasb, H.B. and Noorzad, A.** (1996), "The compact state of the cohesionless granular media", International Journal of Science and Technology: Scientia Iranica, Vol. 3, Nos. 1, 2, 3, pp. 1-8.

83. **Poorooshasb, H.B. and Pietruszczak, S.** (1985), "On yielding and flow of sand: A generalized two-surface model", Computer and Geotechnics, Vol. 1, pp. 35-58.

84. **Poorooshasb, H.B. and Pietruszczak, S.** (1986), "A generalized flow theory for sand", Soils and Foundations, Vol. 26, No. 2, pp. 1-15.

85. **Poulos, S.J.** (1981), "The steady state of deformation", Journal of the Geotechnical Engineering, ASCE, Vol. 107, No. GT 5, pp. 553-562.

86. **Prandtl, L.** (1924), "Spannungsverteilung in plastischen korerpern", Proceedings of the first international congress on applied mechanics, Delft, pp. 43.

87. **Ramu, K., Madhav, M.R. and Poorooshasb, H.B.** (2000), "A study of reclamation of soft ground with geosynthetic and granular fill", Proceedings of the 2nd International Symposium on Lowlands Technology, Saga University, pp. 199-206.

88. **Ramu, K., Madhav, M.R., Poorooshasb, H.B. and Miura, N.** (2000), "Reclamation of soft ground with geosynthetic and granular fill", International Conference on Ground Improvement and Geosynthetic, Helsinski, Finland, pp. 397-40.

89. **Ramu, K.** (2001), "Modeling approaches for and analysis of reclamation process and response of reclaimed ground", Ph.D. thesis at The Indian Institute of Technology, Kanpur, India.

90. **Ramu, K. and Madhav, M.R.** (2002), "Modeling of reclamation based on extended cable theory", Proceedings of the International Symposium on Lowlands Technology, Saga University, pp. 211-216.

91. **Reuss, A.** (1930), "Berueecksichtigung der elastischen formaenderungen in der plastizitaets theorie", Z. Angen. Math. Mech., Vol. 10, pp. 266.

92. **Reynolds, O.** (1885), "On the dilatancy of media composed of rigid particles in contact, with experimental illustrations", Phil. Mag., Series 5, pp. 469-481.

93. **Rhines, P.B.** (1969), "Foundation models for continuously supported structures", Ph.D. Thesis, New York University.

94. **Risseeuw, P. and Voskamp, W.** (1993, b), "Geotextile reinforcement for a highway embankment across swamp land in Sedyatmo, Indonesia", In Geosynthetic Case Histories, pp. 216-217.

95. **Roscoe, K.H., Schofield, A.N. and Wroth, C.P.** (1958), "On yielding of soils", Geotechnique, Vol. 8, pp. 22-53.

96. **Roscoe, K.H. and Poorooshasb, H.B.** (1963), "A fundamental principle of similarity in model tests for earth pressure problems", Proceedings of the 2nd Asian Regional Conference on Soil Mechanics and Foundation Engineering, Bangkok, Thailand, Vol. 1, pp. 134-140.

97. **Schofield, A.N. and Wroth, C.P.** (1968), "Critical state soil mechanics", McGraw-Hill, New York, NY, pp. 310.

98. **Scott, R.F.** (1989), "Essais en centrifuge et technique et de la modélisation", Revenue Française de Géotechnique, Paris, No. 48, pp. 15-34.

99. **Selvadurai, A.P.S.** (1979), "Elastic analysis of soil foundation interaction", Elsiever Publications, Amsterdam.

100. **Shukla, S.K. and Chandra, S.** (1994, a), "The effect of prestressing on the settlement characteristics of geosynthetic reinforced soil", Geotextiles and Geomembranes, Vol. 13, pp. 531-543.

101. **Shukla, S.K. and Chandra, S.** (1994, b), "A generalized mechanical model for geosynthetic reinforced foundation soil", Geotextiles and Geomembranes, Vol. 13, pp. 813-825.

102. **Shukla, S.K. and Chandra, S.** (1995), "Modeling of geosynthetic - reinforced engineered granular fill on soft soil", Geosynthetic International, Vol. 2, No.3, pp. 603-618.

103. **Terzaghi, K. and Peck, R.B.** (1948), "Soil Mechanics in engineering practice" Wiley, New York.

104. **Tresca, H.** (1864), "Sur l'écoulement des corps solides soumis a de fortes pression". Comptes rendus Acad. Sci., Paris, vol. 59, pp. 574.

105. **Van Impe, W.F. and Madhav, M.R.** (1995), "Deep Dynamic Densification Method", Proc. Of 11th Regional Conference, Cairo, Vol.2.

106. **Vidal, H.** (1966), "La Terre Armée, un nouveau matériau pour les travaux publics", Annales D'ITBTP, pp.223-224.

107. **Von Mises, R.** (1913), "Mechanik der festen lorper in plastisch deformabllem zustand", Nachr. Gess. Wess. Gottingen, pp. 582.

108. **Von Mises, R.** (1928), "Mechanik der plastischen formanderung von kristallen", Z. Angen. Math. Mech., Vol. 8, pp. 161.

109. **Watari, Y., Higuchi, Y. and Aboshi, H.** (1986), "Field studies of the behavior of the geogrids and very soft ground", Proceedings of the 3rd International Conference on Geotextiles, Vienna, Vol.1, pp.187-191.

110. **Whitman, R.V.** (1971), "Hydraulic Fills to Support Structural Loads", J.S Soil Mechanics and Foundation Division, ASCE, Vol. 96, No. SM1, pp. 169-193.

111. **Yamanouchi, T. and Gotoh, K.** (1979), "A proposed practical formula of bearing capacity for earthwork method on soft clay ground using resinous mesh", Technical report of the Kyushu University, Vol. 52, No. 3, pp. 201-207.

112. **Yin, J.H.** (1997, a), "Modeling of geosynthetic reinforced granular fills over soft soil", Geosynthetics International, Vol. 4, No. 2, pp. 165-185.

113. **Yin, J.H.** (1997, b), "A non-linear model of geosynthetic reinforced granular fill over soft soil", Geosynthetics International, Vol. 4, No. 5, pp. 523-537.

114. **Yonezu, K., Kitamori, I. and Yamanouchi, T.** (1993), "Geosynthetic floating mat method and deep foundation improvement Osaka Land Reclamation", In Geosynthetic Case Histories, Japan, pp. 164-165.